Integration of non-traditional stable isotopes and synchrotron measurements

by

Heather Kayleigh Shrimpton

A thesis

presented to the University of Waterloo

in fulfillment of the

thesis requirement for the degree of

Doctor of Philosophy

in

Earth Sciences

Waterloo, Ontario, Canada, 2022

Examining Committee Membership

The following served on the Examination Committee for this thesis. The decision of the Examining Committee is by majority vote.

External Examiner   Matthew Leybourne

Professor, Queen's University, Geology

Supervisor(s)   David Blowes

Professor, University of Waterloo, Earth Sciences

Internal Member   Brian Kendall

Associate Professor, University of Waterloo, Earth Sciences

Internal-external Member   Marcel Nooijen

Professor, University of Waterloo, Chemistry

Other Member(s)   Carol Ptacek

Professor, University of Waterloo, Earth Sciences

Author's Declaration

This thesis consists of material all of which I authored or co-authored: see Statement of Contributions included in the thesis. This is a true copy of the thesis, including any required final revisions, as accepted by my examiners.

I understand that my thesis may be made electronically available to the public.

Statement of Contributions

Heather Shrimpton was the sole author of Chapters 1, 2, 3, 4, 6, and 7. These chapters were written under the supervision of Dr. David Blowes. Chapters 4 and 7 are not intended for publication. This thesis contains in part five manuscripts that are intended for publication. Exception to sole authorship of the material are as follows:

Research presented in Chapter 2

Work for this chapter was originally completed in fulfilment of credit for CHEM 740 at the University of Waterloo, under the supervision of Dr. Marcel Nooijen. Funding was provided by an NSERC Discovery Grant and Canada Research Chair grant awarded and an Ontario Research Fund−Research Excellence grant awarded to D. W. Blowes, and the NSERC TERRE-NET program. The research and writing of the chapter were completed by Heather Shrimpton.

Research presented in Chapter 5

This research was conducted at the Advanced Photon Source (APS) in Argonne, IL, USA, and at the University of Waterloo by Heather Shrimpton and Julia Jamieson-Hanes under the supervision of Dr. David Blowes. Julia Jamieson-Hanes designed the study with input from Heather Shrimpton and advice from Dr. David Blowes. Heather Shrimpton conducted all analytical measurements and data analysis. Heather Shrimpton drafted the manuscript, and all coauthors provided intellectual input on the manuscript drafts.

Citations:

Chapter 5: Shrimpton H. K., Jamieson-Hanes J. H., Ptacek C. J. and Blowes D. W. (2018) Real-time XANES measurement of Se reduction by zero-valent iron in a flow-through cell, and accompanying Se isotope measurements. *Environ. Sci. Technol.* **52**, 9304–9310.

As lead author of this chapter, I was responsible for data collection and analysis, and drafting and submitting manuscripts. My coauthors provided feedback on draft manuscripts, and guidance on conceptualizing study design.

Abstract

Selenium is well named after the moon, because statements about this element must often be qualified, making it feel ever changing; for instance, Se is a nutrient, but an excess of 400 μg per day is toxic for humans. High Se concentrations can cause reproductive decrease or complete failure in fish, aquatic birds, amphibians, and reptiles. These animals can also bioconcentrate Se, so high aqueous Se concentrations are not required to lead to toxic consequences. The problem of Se is not limited to wetlands; plants that uptake Se can cause selenosis to animals that forage on land, such as sheep and cattle. Remediating Se before it can reach a receptor is important in preventing the loss of the next generation of wildlife.

When treating Se in ground water, or measuring Se concentrations at contaminated sites, it can be difficult to determine where the Se is going unless extensive measurements are made, including solid sampling and speciation measurements. Non-traditional stable isotopes are an emerging tool in the remediation of groundwater contamination caused by anthropogenic activities. Taking Se stable isotope measurements in conjunction with information about removal mechanisms could produce a powerful predictive system to solve remediation problems.

A combination of theoretical calculations, laboratory experiments, and field measurements were used to evaluate Se stable isotopes as a remediation tool. Molecules for SeO_4^{2-}, SeO_3^{2-}, $HSeO_3^-$, $CaSeO_4$, and $CaSeO_3$ were all modeled using Gaussian 09 (Frisch et al. 2009). The vibrational energies from these models were then used to calculate the equilibrium fractionation between each pair of molecules. These equilibrium fractionation factors were found to be within 0.21 ‰ of other values from the literature, where available. Calculations were of the same magnitude as laboratory studies: 13.4 ‰ for reduction of SeO_4^{2-} to SeO_3^{2-}, and 0.8 ‰ for SeO_3^{2-} to $HSeO_3^-$, which is similar to the range for adsorption of 0 – 1.24 ‰. These theoretical values can be used to establish baseline values when no data is available from laboratory experiments, as is the case for the formation of $CaSeO_4$ and $CaSeO_3$. Calcium plays an important role in the sequestration of Se at pH above 7 (Goldberg and Glaubig 1988), making it relevant to the Se isotope literature.

Three separate laboratory experiments were conducted. Abiotic reduction of Se(IV) by $Na_2S_{(aq)}$ was investigated to determine whether isotopic fractionation can differentiate reduction by $H_2S_{(g)}$ and direct respiration or enzymatic reduction due to sulfur reducing bacteria (SRB) in the environment. A solid precipitate formed rapidly and was collected for PXRD analysis. The precipitate was either yellow, orange, or red depending on the starting pH and the Se:S ratio in solution. All three precipitate colors had different powder X-ray diffraction (PXRD) ring patterns. The yellow precipitate had no pattern, and may have been amorphous S(0), the orange precipitates were most similar to selenium sulfide, and the red precipitate was most similar to a mixture of Se(0) and S(0). The fractionation factor when samples were filtered at 3-4 hours was 7.9 ‰. When the solid was left in contact with solution for a longer duration, the fractionation factor increased to 10.9 ‰.

An experiment on biotic reduction of Se(IV) by a natural SRB consortium, including a comparison of results to the work of others, provides contrasting data for the abiotic experiment. Batch vessels were loaded with a mixture of lucerne hay (alfalfa), silica sand, and a small amount of zero valent iron (ZVI) before being transferred to an anaerobic chamber. A solution containing MgSO4, Na-lactate, and SRB culture was then added to each vessel, and they were crimp sealed. Samples were taken along a time series. Scanning electron microscope (SEM) images show microbes colonizing the sand crevices and much of the organic matter, but no Se precipitates are obvious. Initial fractionation in the reduction of Se(IV) was positive ($10‰ < \varepsilon \leq$ 19 ‰), followed by a decrease in $\delta^{82}Se$ in solution. Because a negative fractionation factor is unlikely, it is probable that multiple pools of reduced and organic Se species are entering solution, causing a final $\delta^{82}Se$ of -13.2 ‰ after three days, with the lowest $\delta^{82}Se$ of -16.7 ‰ seen at two days.

The final experiment used ZVI to reduce Se(VI) in a flow through cell system, while simultaneously collecting XANES data and isotope samples. A column with a transparent window packed with ZVI was placed in the hutch at a synchrotron (Sector 13, Advanced Photon Source (APS), Argonne, IL, USA), and a Na_2SeO_4, $CaCO_3$ solution was pumped through. The Na_2SeO_4 concentration was increased at 8 hour increments, and removed from influent solution

at the end of the experiment to observe the effect of rinsing the column with a $CaCO_3$ only solution. The linear combination fit (LCF) shows progressively reduced species of Se accumulating on the solid over time, with more Se present near the input of the cell than the output. The Se(VI) component decreased rapidly in the rinse phase of the LCF, suggesting most Se in solution was Se(VI). The $\delta^{82}Se$ could be fit with a straight line, yielding an isotopic discrimination of 9.6 ‰. The $\delta^{82}Se$ of the rinse solution could be fit with a Rayleigh type curve, with a fractionation factor of 2.4 ‰. This fractionation factor is between adsorption of Se onto iron minerals, and reduction of Se by ZVI in the presence of $CaCO_3$, as measured in an earlier batch experiment. Simultaneously obtaining isotope and solid phase data helps link removal mechanisms to fractionation factors. Isotope results from all three laboratory experiments suggest reductive processes are of the same magnitude as theoretical calculations, and Se reduction experiments conducted by others.

Samples for isotope and cation analysis were collected from along the length of an Se-bearing groundwater plume. Laboratory obtained Se isotope fractionation factors were then used to model the processes occurring in the plume. Geochemical and redox data were used to support the isotope modeling results. These modeling results, supported by redox data, allowed us to infer the processes occurring in the subsurface. The main processes within the plume include adsorption and dispersive dilution, as indicated by only small changes in $\delta^{82}Se$ values ($\delta^{82}Se$ = 1.5 – 3.4 ‰) and a large decrease in Se concentration (from 9770 to 774 $\mu g\ L^{-1}$). Reduction is occurring within the source area ($\delta^{82}Se$ = 1.3 – 3.8 ‰), and is the cause of the sharp increase in $\delta^{82}Se$ (8.7 ‰) under the wetland complex. Very low $\delta^{82}Se$ values behind the source area (-26 ‰) and at the distal end of the plume (-16 ‰) are likely due to the oxidation of low $\delta^{82}Se$ from local shales. Low concentration (< 900 $\mu g\ L^{-1}$), low $\delta^{82}Se$ values (-0.2 – 0.9 ‰) at the plume's edge are either the result of desorption/oxidation of previously reduced plume Se, or mixing of plume Se with background Se with a low $\delta^{82}Se$. The results from this field study demonstrate the potential use for Se stable isotope measurements in environmental samples.

Acknowledgements

Dedication

For my partner, Marten Pape, for his support during my career as a PhD student, and my daughter Leona, for the smiles and love of bugs. Also, this work is still for the baby ducks. And the baby crocodiles, too.

Table of Contents

List of Figures

List of Tables

Chapter 1: Introduction

1.1 Background

Selenium is a micronutrient; too little Se can result in health complications for both humans and livestock (Plant et al. 2003; Fordyce 2005). But Se is also toxic at higher concentrations, with the exact repercussions depending on the dosage, length and route of exposure, and species exposed. The speciation of the Se is also important, as some Se species are more bioavailable than others, or display more toxic effects (Spallholz and Hoffman 2002; Lenz and Lens 2009; Rigby et al. 2014). Humans can experience nail and hair loss, increased risk of diabetes, an unsteady gait, and paralysis at low, chronic dosages, and high concentration exposures can lead to nausea, vomiting, diarrhea, headaches, heart attacks, and lung problems including bronchial spasms, bronchitis, and chemical pneumonia (Plant et al. 2003; Levander and Burk 2006; Lenz and Lens 2009). Cattle have deformed hooves when their forage is elevated in Se ($5 - 50$ mg Kg^{-1} Se; Lenz and Lens 2009). Waterfowl and fish can have increased reproductive failure, as elevated aqueous Se can lead to embryo death and deformed young (Lemly 2002; Lenz and Lens 2009). Deformations of bird hatchlings can include twisted bills or limbs, eyes (e.g., glaucoma), and brain (e.g. hydrocephaly) (Janz et al. 2010). For fish hatchlings, deformations can be of the head, spine, mouth, and fins (Lemly 2002). Adult fish can experience swollen gill lamellae, anemia, corneal cataracts, bulging eyes, and organ problems (Lemly 2002). Amphibians can have deformed larval mouthparts, causing decreased swimming and eating capabilities and lower survival rates (Janz et al. 2010). There is also decreased crocodilian egg viability when exposed to elevated background Se (Roe et al. 2004).

Selenium can be released into the environment from natural sources, such as exposed black shales, and anthropogenic sources, such as agriculture, mining, coal power-plant fly-ash, metal smelting, and oil refining (Lemly 2004; Reyes et al. 2009; Winkel et al. 2015). The Canadian aquatic Se guidelines for protection of aquatic life is 1 µg L^{-1} (Canadian Council of Ministers of the Environment 2016). Because of the lethal effects on the offspring of sensitive species, it

makes sense to remediate Se contamination of groundwater promptly before it can discharge into open water bodies where wildlife is found.

Monitoring remediation and natural attenuation of Se in groundwater can be complicated by the number of measurements required. The Se concentration alone may not be enough to determine if Se is permanently removed, as it can decrease downgradient from a source due to dispersive dilution. Additionally, wells drilled outside of the main plume body, or screened above or below the plume, may yield falsely low Se concentrations. Reducing Se from its most mobile phase, selenate (Se(VI); SeO_4^{2-}), can lead to more permanent Se removal. Reduction to selenite (Se(IV); SeO_3, $HSeO_3^-$) produces a less mobile phase, as Se(IV) can quickly adsorb when the pH is 5 – 7 to iron minerals, clays, and calcium carbonate coatings (Neal et al. 1987; Goldberg and Glaubig 1988). At lower pH, when iron minerals and calcite dissolve, and clays begin to denature, Se can further auto-reduce, remaining immobile, due to the large stability fields of Se(0). Sulfate reducing conditions or microbial reduction can form elemental Se (Se(0)) and selenides (Se(-I), Se(-II)). Selenides can be metal, and highly insoluble (e.g., $FeSe_2$, FeSe), organic and bound to organic phases, or volatile ($H_2Se_{(g)}$, dimethyl selenide, dimethyl diselenide). Selenium speciation measurements help determine whether Se is being removed due to reduction, but because the reduced phases are more likely to be found in the solid phase, solid samples are required to make the most of speciation techniques. Redox measurements may be useful in determining whether sufficiently reducing conditions exist to reduce Se, however, the accuracy of Eh measurements can be limited by sample water chemistry (Lindberg and Runnells 1984). Measuring for specific, common, redox sensitive species can be more effective (e.g. Oxygen, nitrate, Fe, Mn, S, and methane), but requires the analysis of multiple species.

Alternatively, we could use Se stable isotopes to determine the processes occurring in the subsurface. Stable isotope measurements have been used for multiple other elements to distinguish processes such as leaching, precipitation, sorption, redox reactions, and tracing contaminant sources in groundwater and surface water (Wiederhold 2015; Teng et al. 2017). Selenium isotopes have already been applied to examine processes occurring in the environment, both in seleniferous soils (Schilling et al. 2015) and in a U-roll front deposit (Basu et al. 2016).

However, no attempt has as of yet been made to model possible mechanisms that could have caused changes in δ^{82}Se along the cross-section of an Se-bearing groundwater plume.

Before δ^{82}Se values are of any use in field measurements, laboratory or theoretical studies need to be conducted to determine the expected change in these values for a given process. This chapter discusses the history of Se isotopes, measurement method of Se isotopes used in this thesis, and required mathematical corrections.

1.1.1 A brief history of Se stable isotope measurement methods

Selenium stable isotopes were measured in the 1960s using a gas source mass spectrometer (GS-MS) with two collector slits to simultaneously measure ^{76}SeF$_6$ and ^{82}SeF$_6$ (Krouse and Thode 1962; Rees and Thode 1966). This research group also performed some early modeling of Se stable isotope fractionation factors (Krouse and Thode 1962; Rees and Thode 1966; Rashid and Krouse 1985). Additional measurements would be made with the advent of thermal ionization mass spectrometry (TIMS) (Wachsmann and Heumann 1992; Johnson et al. 1999), and multi-collector inductively-coupled mass spectrometry (MC-ICP-MS), eventually coupled with hydride generation (HG) to obtain higher intensities (Rouxel et al. 2000; Johnson 2004; Elwaer and Hintelmann 2007). These technologies required lower concentrations of Se for isotopic measurements (Need >1 μg for GS-MS; < 1 μg for TIMS; ~10 ng for HG-MC-ICP-MS; Johnson 2004), allowing for the measurement of environmental concentrations.

A double spike technique was applied to Se isotopes to correct for instrumental fractionation on the TIMS during the 1990s (Johnson et al. 1999). The spiked Se isotopes on the TIMS were ^{82}Se and ^{74}Se, and the reported ratio was $^{80/76}$Se (Johnson 2004). Because of Ar isobaric interferences, ^{80}Se cannot be measured without error on an MC-ICP-MS (Table 1), leading to $^{82/76}$Se being the typically reported ratio, and ^{77}Se and ^{74}Se used as the double spike (Clark and Johnson 2008). Se isotope measurements have also been conducted using HG-MC-ICP-MS without double spike, using only sample-standard bracketing for interference correction (Rouxel et al. 2002; Elwaer and Hintelmann 2007). The current common method of measuring Se isotopes involves HG-MC-ICP-MS with a double spike and the NIST SRM 3149 standard

(Shrimpton et al. 2018; Kipp et al. 2020; Schilling et al. 2020). Some researchers use a Te double spike, rather than a Se one (König et al. 2019). Others have used methane to boost signal intensities (Floor et al. 2011; Kurzawa et al. 2017).

Table 1.1: Selenium isotopes and some of the isobaric interferences

^{74}Se	^{76}Se	^{77}Se	^{78}Se	^{80}Se	^{82}Se
^{74}Ge,	^{76}Ge,	^{61}Ni^{16}O,	^{62}Ni^{16}O,	^{64}Ni^{16}O,	^{82}Kr,
^{56}Ni^{16}O,	^{58}Fe^{18}O,	^{59}Co^{18}O,	^{38}Ar^{40}Ca,	^{40}Ar^{40}Ca,	66An16O,
^{40}Ar^{34}S,	^{60}Ni^{16}O,	^{36}Ar^{41}K,	^{38}Ar^{40}Ar,	^{40}Ar^{40}K,	^{40}Ar^{42}Ca
^{36}Ar^{38}Ar,	^{40}Ar^{36}S,	^{40}K^{37}Cl,	^{41}K^{37}Cl,	^{40}Ar^{40}Ar,	^{36}Ar^{46}Ti,
^{37}Cl^{37}Cl,	^{36}Ar^{40}Ar,	^{76}SeH,	^{77}SeH,	^{32}S^{16}O^{16}O^{16}O,	^{34}S^{16}O^{16}O^{16}O,
^{39}K^{35}Cl,	^{39}K^{37}Cl,	^{76}GeH,	^{36}Ar^{40}ArHH,	^{48}Ca^{16}O^{16}O	^{81}BrH,
^{42}Ca^{16}O^{16}O,	^{40}Ca^{18}O^{18}O,	^{36}Ar^{40}ArH,	^{156}Dy^{++},	^{79}BrH,	^{40}Ar^{40}ArHH,
^{152}Sm^{++},	^{75}AsH^{+},	^{38}Ar^{38}ArH,	^{156}Gd^{++}	^{38}Ar^{40}ArHH,	^{164}Er^{++}, ^{164}Dy^{++}
^{152}Gd^{++}	^{154}Sm^{++},	^{155}Gd^{++}		^{158}Dy^{++},	
	^{154}Gd^{++}			^{158}Gd^{++}	

Sample purification has followed two main techniques. One technique involves using ion chromatography to separate out Se(VI) from other ions in solution. This separation can involve a single AG1-X8 resin column (Schilling et al. 2015). For more complicated matrices such as rock digests, or where there is a desire to measure multiple elements from the same sample a AG 50W-X8 resin can be used before the AG1-X8 to separate out Fe, Se, and Te (Yierpan et al. 2018). The second technique relies on thiol groups present in thiol cotton fiber (TCF) or thiol cellulose powder (TCP) (Elwaer and Hintelmann 2008) to bond to Se(IV), removing it from solution. The Se can then be re-oxidized to extract it from the TCF.

1.2 Stable isotope terms and definitions

Selenium stable isotope ratios are reported relative to SRM 3149 (NIST), so that values can be compared between laboratories (Wiederhold 2015). The difference between the sample and standard is reported in per mille (‰):

$$\delta^{82}Se(‰) = \left(\frac{^{82}/_{76}Se_{\text{Sample}}}{^{82}/_{76}Se_{\text{Standard}}} - 1 \right) \times 1000 \qquad \text{(Eq. 1.1)}$$

The δ^{82}Se values changes when one isotope is favored over another (heavier or lighter) through processes that partition the element between two separate reservoirs. Possibilities include an

adsorbed or precipitated phase and an aqueous phase, or organic and non-organic phases. Fractionation is described by the fractionation (α; Eq. 1.2):

$$\boldsymbol{\alpha_{X-Y}} = \frac{\boldsymbol{R_X}}{\boldsymbol{R_Y}} \tag{Eq. 1.2}$$

Where R_X is the isotope ratio of the element in one compound or pool, and R_Y is the isotope ratio of the element in a second, separate phase or pool. In this thesis, R_x is the reactant and R_y is the product. Because it can be difficult to visually distinguish the differences in α, the magnitude of the change in isotope rations can also be described by the fractionation factor (ε; Eq. 1.4). The difference between the δ values of two pools is approximately equal to ε, and will be constant for a system that undergoes equilibrium fractionation.

$$\boldsymbol{\varepsilon_{X-Y}} = (\boldsymbol{1} - \boldsymbol{\alpha_{X-Y}}) \times \boldsymbol{1000}‰ \approx \boldsymbol{\delta_X} - \boldsymbol{\delta_Y} = \Delta_{X-Y} \tag{Eq. 1.4}$$

Selenium generally undergoes kinetic fractionation (Johnson 2012), where reactant and product co-exist with little to no back reaction (Rayleigh-type fractionation). In equilibrium fractionation, there is a forward and backward reaction with heavier isotopes being preferred in one of the phases. Fractionation for Se has been found to be mass dependent (Johnson and Bullen 2004; von Strandmann et al. 2014).

1.3 Stable isotope fractionation during various processes

Laboratory reduction experiments have the largest fractionation factors (Table 1.2). Little fractionation occurs during adsorption of Se(VI), and minimal fractionation occurs during adsorption of Se(IV) (Table 1.2; Johnson 2012; Xu et al. 2020, 2021). The amount of fractionation that occurs during oxidation close to zero (Johnson et al. 1999); however, when the multiple oxidation products undergo separation through adsorption or reduction, an increase in $\delta^{82}Se$ is observed in Se(VI) (Wasserman et al. 2021). There is no isotopic exchange between the two most oxidized forms of Se (Se(IV) and Se(VI)) in aqueous solutions, without a redox reaction occurring (Tan et al. 2020).

Table 1.2: Fractionation factors determined through laboratory experiments. Some ε have been converted from $^{80/76}\varepsilon$ using the relationship $1.48\ ^{80/76}\varepsilon = ^{82/76}\varepsilon$ (Johnson 2012).

Reaction	Process	$^{82/76}\varepsilon$ (‰)	Reference
Se(VI) to Se(IV)	HCl at 25 °C	18	(Rees and Thode 1966)
	Green rust	11.1	(Johnson and Bullen 2003)
	Zero valent iron	3.0 – 9.2	(Shrimpton et al. 2015, 2018)
	Pure bacterial culture	6 – 7.2	(Herbel et al. 2000)
	Pure bacterial culture, nutrient limited	9.2 – 11.8	(Schilling et al. 2020)
	Microbial sediment slurry	3.9 – 4.7	(Ellis et al. 2003)
	Microbial sediment slurry, diffusion limited	1.8	(Clark and Johnson 2008)
Se(IV) to Se(0)	NH$_2$OH, ascorbic acid	15 – 19	(Krouse and Thode 1962; Rees and Thode 1966; Rashid and Krouse 1985)
	FeS$_2$	9.7	(Mitchell et al. 2013)
	Pure bacterial culture	9 – 13.7	(Herbel et al. 2000)
	Pure bacterial culture, nutrient limited	6.2 – 7.8	(Schilling et al. 2020)
	Microbial sediment slurry	8.4	(Ellis et al. 2003)
Se(0) oxidation	Incubated soil	< 0.5	(Johnson et al. 1999)
	Ferroselite, berzelianite, $\Delta_{Se(VI)-mineral}$, proposed mechanism is reduction/adsorption of Se(IV)$_{(aq)}$	1.5 – 14	(Wasserman et al. 2021)
Se(VI) adsorption	Goethite, hematite, 2-line ferrihydrite, manganese oxide, alumina oxide	< 0.08	(Mitchell et al. 2013; Xu et al. 2020)
	Montmorillonite, kaolinite	~0	(Xu et al. 2021)
Se(IV) adsorption	Goethite, hematite, 2-line ferrihydrite	0.7 – 0.9	(Mitchell et al. 2013; Xu et al. 2020)
	Manganese oxide	0.00 – 1.24	(Xu et al. 2020)
	Alumina oxide	< 0.08	(Xu et al. 2020)

	Montmorillonite, kaolinite	< 0.23	(Xu et al. 2021)
Se volatilization	Cyanobacteria	< 1.7	(Johnson et al. 1999)
	Soil microbes	< 0.9	(Johnson et al. 1999)
	Fungi (selenite to methylselenide)	~9	(Schilling et al. 2011b)
Se uptake	Wetland plants	< 1.5	(Herbel et al. 2002)
	Algae (*C. reinhardtii*)		(Hagiwara 2000)

Selenium isotopes have been applied at a seleniferous site to determine the origin of the Se in different reservoirs (Schilling et al. 2015). Fractionation factors were not modeled, but the magnitude and direction of known fractionating processes were used to determine that local Se contamination originated from parent bedrock or another source, and not the seleniferous soils. Changes in $\delta^{82}Se$ were used to calculate a fractionation factor at a uranium roll front deposit of $\varepsilon = 2.25 \pm 0.61$ ‰ (Basu et al. 2016). The authors determined that the sharp increase in $\delta^{82}Se$ is best explained by reductive processes.

1.4 Measurement methods used in this thesis

1.4.1 Aqueous concentration measurements

Samples for concentration analysis were filtered (0.45 µm or 0.2 µm, Supor membrane) and acidified to 2% HNO_3 (Omnitrace Ultra HNO_3, Millipore). Multiple elements (Table 1.3) were measured by an inductively coupled optical emission spectrometer (ICP-OES; iCAP 6000) using QCS-26 (inorganic ventures) at multiple different concentrations as a calibration standard. The same standard is run as an internal control at 10 and 2 ppm. The measurement method also uses an external standard (6020 CAL-1, inorganic ventures) run intermittently to verify the method. If the relative standard deviation (RSD) for a is above 5%, as determined by the internal standard, the samples are analyzed again.

Table 1.3: Detection limits (DL) and quantification limits (QL) of elements analyzed by ICP-OES

Element	DL (mg L^{-1})	QL (mg L^{-1})
Aluminum	0.2	0.6

Antimony	0.09	0.3
Arsenic	0.1	0.3
Boron	0.2	0.6
Cadmium	0.2	0.6
Calcium	0.2	0.6
Chromium	0.2	0.6
Cobalt	0.1	0.4
Copper	0.2	0.5
Iron	0.2	0.7
Lead	0.2	0.6
Lithium	0.1	0.4
Magnesium	0.2	0.6
Manganese	0.1	0.4
Nickel	0.1	0.4
Potassium	0.1	0.4
Selenium	0.1	0.4
Silica	0.07	0.2
Sodium	0.2	0.5
Strontium	0.03	0.1
Sulfur	0.2	0.7
Thallium	0.2	0.7
Titanium	0.2	0.6
Vanadium	0.2	0.2
Zinc	0.2	0.8

1.4.2 Selenium purification method

Selenium isotope samples in all studies were purified using thiol cotton fiber (TCF), made and tested to mostly the same specifications as previous work (Shrimpton et al. 2015). The TCF is made in-house using cotton balls (medical grade, Dukal Corp), 98% thioglycollic acid (Acros Organics), sulfuric acid (trace metal grade, Fisher), acetic acid (reagent grade, Fisher), acetic

anhydride (reagent grade, Fisher), and ultrapure water (MilliQ). First, 20g of cotton balls are weighed into a clean 500 mL teflon bottle (acid washed in 10% HNO_3, triple rinsed with ultrapure water before first use). Next, 125 mL thioglycollic acid, 70 mL acetic anhydride, 40 mL acetic acid, 0.5 mL sulfuric acid, and 5 mL ultrapure water are slowly added in order. Mixing these solutions will create heat, so it is important to add reagents slowly and swirls cotton balls between steps to avoid burning the cotton. The mixture is capped and shaken until it appears homogeneous, then placed in a 60 °C water bath for 24 hours. The bottle is then removed, shaken, and returned it to the water bath for an additional 24 hours. The product can then be vacuum filtered in small batches, using a glass or ceramic filter, qualitative filter paper (Whatman, ashless), and a vacuum flask with a liquid trap placed before the vacuum pump. The powder that collects on the filter paper is rinsed with ultrapure water until it is bright white, and less sticky. Stirring the powder during vacuum filtration with a clean pipette tip can increase the rate of filtration. The powder is then scraped off the filter paper and allowed to air dry at room temperature for at least two days. The TCF is stored in a brown plastic bottle away from heat sources, prolonging its shelf life to one year (Yu et al. 2001).

Each new batch of TCF is tested for Se recovery. The average recoverability of Se from the TCF is $96 \pm 13\%$ (1 σ), while the median recoverability is 99%. The worst recovery was seen in one year old TCF, which had a more variable recoverability ($90 \pm 17\%$, minimum of 73%). The TCF recipe was slightly altered in 2018, with a decreased sulfuric acid volume (now 0.5 mL, was formerly 0.7 mL). The newer TCF has average Se recovery of $99 \pm 2\%$.

Selenium isotope samples must be reduced to Se(IV) prior to purification using TCF. First, sufficient sample volume to obtain 0.6 µg of Se is pipetted into a centrifuge vial, followed by 0.6 µg of a 50:50 [77]Se:[74]Se spike mixture. Sufficient ultrapure concentrated HCl (Omnitrace, distilled again in house) is added to bring the final concentration to 6 M HCl. The samples are left to reduce overnight. Samples are diluted to 2 M HCl using ultrapure water the following morning, prior to being purified using TCF.

A vacuum manifold solid phase extraction (SPE) set up is used. The 1 mL SPE columns are fritted before loading 0.1 g of TCF, wetting with ultrapure water, and allowing to sit for 30 min.

The water is then drained, without allowing the TCF to dry, and the TCF is gently compressed with a clean frit insertion tool. The TCF is then rinsed with 1 mL of ultrapure water, 1 mL of 6 M HCl, and 1 mL of 2 M HCl. The TCF is not allowed to dry out between each rinse solution. The sample is then loaded onto the columns, followed by 2 mL of ultrapure water, 2 mL of 6 M HCl, and 2 mL of 2 M HCl. Finally, air is sucked through the columns until they are dry. There is no need to collect the eluent, except for quality control purposes, as all Se(IV) is bound to the TCF.

To extract the Se from the TCF, it must be oxidized. The resin is first loosened from the SPE columns by inserting a clean, blunt syringe needle into the output of the column and pushing up on the frit. The TCF can then be gently tapped into a labelled 15 mL centrifuge tube. Next, 50 μL of concentrated HNO_3 (Omnitrace ultra) are added, the sample is loosely capped, and heated in a 70–80 °C water bath for 20 min. Samples are then removed from the water bath and allowed to cool before adding 2.5 mL of ultrapure water and mixing using a vortex mixer with the caps tightly sealed. The 15 mL tubes are centrifuged at 500 RPM for 5 min. The sample is then gently decanted into a clean, labelled 15 mL centrifuge tube. Each TCF pellet undergoes the same HNO_3 extraction process a second time to ensure all Se has been removed, and the supernatant is decanted into the same centrifuge tube as used for the first extraction. Samples are filtered (0.2 μm) into a new 50 mL tube before adding 5 mL of concentrated HCl (Final concentration: 6 M HCl), to ensure any decanted TCF is filtered out of solution before the Se is reduced back to Se(IV). Samples are left to sit overnight before diluting them the next day (2 M HCl and 40 μg L^{-1} Se). Samples, standard, and blanks used in Se isotope ratio measurements are all purified using this method. Any method differences are noted in individual chapters.

1.4.3 Selenium isotope ratio measurement

Selenium isotope ratios were measured on a Neptune multi-collector inductively-coupled plasma mass spectrometer (MC-ICP-MS), using a hydride generator to increase signal intensities (LI-2, CETAC). The samples, standards, and blanks were in 2 M HCl (Omnitrace HCl, Millipore, distilled again in laboratory). The rinse solution was 3 M HCl (Omnitrace HCl, Millipore, distilled again in laboratory). The concentration of analyzed samples was 80 μg L^{-1} in chapters 5

and 6, and 40 µg L^{-1} in chapters 3 and 4, due to improvements in efficiency made to the measurement method; original rinse times (CH 5, 6) were one hour including measurement. Decreasing the sample concentration by half and increasing the sample flow rate from a pump speed of 7 to 11 rpm decreased rinse time to only 21 minutes including measurement time, greatly improving the time efficiency of sample analysis while maintaining the same signal intensity. Halving sample concentrations also led to lower matrix concentrations of other elements from the TCF, and made measuring Se isotopes less labor intensive with regards to sample purification.

   Sequences involved a purified, spiked standard (NIST SRM 3149) run at the beginning of analysis and again after every fourth sample. Unpurified 2 M HCl dummy blanks were placed before each TCF purified 2 M HCl blank, to ensure the probe did not contaminate the blank solution. The rinse used a 50 mL vial of 3 M HCl, instead of relying on the wash station, which was used for two minutes before the 3 M HCl rinse to clean the autosampler probe. An example sequence of four samples is given below (Table 1.4):

Table 1.4: Sample sequence for Se isotopes on Neptune MC-ICP-MS

Name	Uptake time (s)	Number of cycles
Dummy Blank 1	300	10
TCF Blank 1	180	100
Standard 1	180	150
Rinse 1	1080	100
Dummy Blank 2	300	10
TCF Blank 2	180	100
Sample 1	180	150
Rinse 2	1080	100
Dummy Blank 3	300	10
TCF Blank 3	180	100
Sample 2	180	150
Rinse 3	1080	100

Dummy Blank 4	300	10
TCF Blank 4	180	100
Sample 3	180	150
Rinse 4	1080	100
Dummy Blank 5	300	10
TCF Blank 5	180	100
Sample 4	180	150
Rinse 5	1080	100
Dummy Blank 6	300	10
TCF Blank 6	180	100
Standard 2	180	150
Rinse 6	1080	100

The original sequence method used in chapters 5 and 6 used 300 cycles for every measurement (samples, standards, and rinse), and did not include dummy blanks. The signal was found to be sufficiently stable that decreasing the cycles did not impact measurement precision. Decreasing measurement time and rinse time decreased time between sample and standard measurements, and allowed for more accurate blank subtractions. If there is a long gap in time (e.g. months) before running samples from the same experiment, a sample that was run in a previous session is re-run to ensure comparability. Samples are measured in duplicate, or in triplicate if error from duplicate samples is outside the external measurement error.

1.4.4 Data processing

Data are exported from the Neptune software with values outside 2σ on measured intensities as blank cells. They are processed using a double spike inversion program written by the author using Python. This program performs the blank subtraction, and mathematically calculates non-blank subtractable interferences. All signals are initially only blank subtracted, and an initial looped iteration is undergone to determine a more accurate best guess for instrumental fractionation and natural fractionation using the same double spike inversion math found in

Siebert et al. (2001). Next, the raw (uncorrected) sample signals are corrected mathematically for any Ge, As, Kr, Ar_2, SeH, and Ar_2H interferences and the new calculated instrumental and natural fractionations for that sample (Figure 1.1). A second iteration loop is performed until the calculated sample argon signal intensity converges to < 0.000000001 difference between loops. The second iteration further refined the instrumental and natural fractionation factors by estimating the real-time gas interferences including hydrides, instead of relying only on blanks. This loop begins by calculating the amount of ^{80}Se that should be in solution based on the amount of ^{78}Se, as an initial guess. It uses this guess and the calculated Kr from the blank to determine $^{40}Ar_2$. The estimated $^{40}Ar_2$ can be used to calculate the $^{40}Ar^{36}Ar$, $^{40}Ar^{38}Ar$, and $^{40}Ar_2H_2$ interferences. The hydride contribution to the signal intensity is estimated from $^{82}SeH/^{82}Se$, which is calculated by taking the 83 sample signal minus its blank, divided by the 82 sample signal minus the calculated ^{82}Kr interference and the calculated $^{40}Ar_2H_2$ interference (Figure 1.1). All other math is mass conversions from one isotope to another, corrected using the instrumental fractionation factor.

74 $$^{74}Ge = (^{73}Ge_m/^{74}Ge_m)^{Fins} \times 73_b \times ^{74}Ge_n/^{73}Ge_n$$ $$^{74}Se = 74_S - ^{74}Ge - 74_b$$	76 $$^{76}Ge = (^{73}Ge_m/^{76}Ge_m)^{Fins} \times 73_b \times ^{74}Ge_n/^{76}Ge_n$$ $$^{40}Ar^{36}Ar = ^{40}Ar_{2est} \times 76_b/(80_b - ^{80}Kr)$$ $$^{76}Se = 76_S - ^{76}Ge - ^{40}Ar^{36}Ar$$
77 $$H_{ratio} = 83_S - 83_b/82_S - ^{82}Kr - ^{40}Ar_2H_2$$ $$^{76}SeH = ^{76}Se \times H_{ratio} \times (^{76}Se_m/^{76}SeH_m)^{Fins}$$ $$^{77}Se = 77_S - 77_b - ^{76}SeH$$	78 $$^{77}SeH = ^{77}Se \times H_{ratio} \times (^{77}Se_m/^{77}SeH_m)^{Fins}$$ $$^{40}Ar^{38}Ar = ^{40}Ar_{2est} \times (78_b - ^{78}Kr)/(80_b - ^{80}Kr)$$ $$^{78}Se = 78_S - ^{40}Ar^{38}Ar - ^{77}SeH$$
80 $$^{80}Se = ^{78}Se \times (^{78}Ge_m/^{80}Ge_m)^{Fins} \times ^{80}Se_n/^{78}Se_n$$ $$^{80}Kr = (^{83}Kr_m/^{80}Kr_m)^{Fins} \times 83_b \times ^{80}Kr_n/^{83}Kr_n$$ $$^{40}Ar_{2est} = 80_S - ^{80}Se - ^{80}Kr$$	82 $$^{82}Kr = (^{83}Kr_m/^{82}Kr_m)^{Fins} \times 83_b \times ^{82}Kr_n/^{83}Kr_n$$ $$^{40}Ar_2H_2 = ^{40}Ar_{2est} \times [(82_b - ^{82}Kr)/(80_b - ^{80}Kr)]$$ $$^{82}Se = 82_S - ^{82}Kr - ^{40}Ar_2H_2$$

Figure 1.1: Interference correction calculations for second iteration loop of the double spike inversion program. Subscript S is for sample signal, b is for blank signal, m is for atomic mass, and n is natural abundance. Fins is the instrumental fractionation. Equations are given in order of isotopic mass, not in order of execution within the program.

External error is calculated as twice the standard deviation of the $\delta^{82}Se$ of SRM 3149 (NIST), with the average ratio used to calculate the $\delta^{82}Se$ taken over the course of one year. The external error is around 0.40 ‰. Precision on replicates is usually less than external error (e.g., 75% of samples in the microbial reduction experiment had a lower error, with an average error of 0.2 ‰). When replicate error is higher than the external error, the sample is purified and measured again to ensure there were no complications during spiking or purification.

1.5 Research Objectives

The primary objective of this thesis is to match Se isotope fractionation factors to removal mechanisms, thus allowing Se isotope ratio measurements to be used as tools for evaluating the effectiveness of remediation in the environment. The aims of this research are:

- Use *ab initio* calculations to estimate the degree of stable Se isotope fractionation for a transformation between two molecules

- Test whether a Na_2S solution added to a Se(IV) solution can reliably precipitate a reduced product (SeS_2, Se_nS_{8-n}, or Se(0))

- Determine the isotopic fractionation associated with the reduction of Se(IV) by Na_2S, and whether the extent of fractionation varies depending on the final product, and whether the fractionation can be differentiated from biotic reduction by sulfur reducing bacteria

- Test the effectiveness of a sulfate reducing natural microbial consortium to reduce Se(VI) or Se(IV) to an immobile product, and determine the resulting isotopic composition over time

- Determine the amount of Se fractionation due to reduction by zero valent iron (ZVI) in a column experiment, as well as the removal mechanism

- Link processes to Se isotope measurements from groundwater samples taken along the length of a historic plume partially in fractured rock by modeling the isotope data using fractionation factors and available geochemical data

1.6 Thesis Organization

This thesis includes seven chapters, involving five distinct experiments using Se isotopes or synchrotron-based methods to delineate Se removal processes. Each chapter is presented as a

research paper. Chapter five has been published. The second chapter involves calculating fractionation factors using *ab initio* methods. Several molecules containing Se were chosen, and modelled using Hartree-Fock (HF) and density functional theory (DFT) methods. The vibrational energies were then taken from these models, and used to compute β values, and finally fractionation factors. The third chapter involves Se stable isotope fractionation during the abiotic reduction of Se(IV) by $H_2S_{(g)}$. A $Na_2S_{(aq)}$ solution was added in increasing concentrations to a solution with a constant Se concentration, which reduced Se and precipitated Se in the form of $Se_{8-n}S_n$ or Se(0) and S(0) compound. The color changed depending on the precipitate formed. This precipitate was examined using PXRD at the synchrotron. Aqueous S speciation and Se isotopes were also measured. The fourth chapter involves the fractionation of Se(VI) and Se(IV) by natural microbial consortium. Batch vials were loaded with lucerne hay, sand, and ZVI, then inoculated with a naturally occurring SRB consortium. Samples were collected for cations, Se isotopes, and SEM imaging. The fifth chapter examines the isotope and real-time synchrotron measurements of Se during treatment within a zero valent iron column. Selenium was introduced into a column with an X-ray transparent window to allow for XANES measurements during the experiment. The concentration of Se was increased stepwise during the experiment to obtain varying fractions of Se removal to calculate a fractionation factor. This chapter has been previously published in Environmental Science and Technologies (Shrimpton et al. 2018). The sixth chapter investigated the use of Se isotopes as a tool in determining the processes occurring in a 65-year-old Se groundwater plume. Wells along a cross section of the site were sampled for cation and Se isotope analysis, and the models were fit to the resulting data using fractionation factors found in the literature. Modelling results were supported using redox and speciation data collected by others for assessing the field site. The seventh chapter provides a summary of the scientific contributions and conclusions.

Chapter 2: Calculating Fractionation of Selenium Stable Isotopes from Molecular Models using Gaussian 09

2.1 Abstract

Selenium isotope fractionation is a tool for determining processes occurring in the environment. Gaussian 09 was used to model several selenium-bearing molecules using a density functional theory (DFT) method. The obtained vibrational frequencies were then used to model the equilibrium isotopic fractionation that would result from one molecule transforming into another. Reduction of SeO_4^{2-} to SeO_3^{2-} has a fractionation factor of 13.4 ‰, which is the same magnitude as laboratory experiments for reduction by green rust, hydrochloric acid, and zero valent iron. Protonation of SeO_3^{2-} to $HSeO_3^-$ is 0.8 ‰. Bonding with a larger divalent ion (Ca^{2+}) increased the fractionation to 2 ‰ for both SeO_4^{2-} and SeO_3^{2-}. Modeling selenium isotopic fractionation provides baseline information on the magnitude of fractionation expected for a particular transformation in systems that lack laboratory experiments.

2.2 Introduction

Given the expensive nature of sampling regimes for groundwater or for collecting deep soil samples, selenium isotope measurements could determine whether naturally attenuated selenium from contaminated sites have the potential to become bioavailable at lower cost (Schilling et al. 2015). The distribution of selenium and many other elements in nature is heterogeneous, so extensive sampling networks are commonly required to understand the concentration distribution, and fate of selenium in the environment (Bailey 2017). In the case of shallow groundwater, contaminant concentration distributions may change seasonally (Williams et al. 2013). Decreased concentrations downgradient can also be caused by the dilution of contaminated water by diffusion and dispersion in the aquifer, rather than reduction or adsorption.

Selenium has five common oxidation states: Se(VI) (SeO_4^{-2}), Se(IV) (SeO_3^{-2}), Se(0), Se(-I), and Se(-II). The first two oxidation states form soluble oxyanions, making them bioavailable and the most likely to result in ecosystem poisoning. However, Se(IV), or selenite, has a greater

tendency to adsorb in a system than Se(VI), or selenate (Bailey 2017). Elemental Se (Se(0)) is insoluble, and the selenides tend to form low solubility compounds. The reduction of selenium to lower oxidation states can effectively remove selenium from solution, making it less mobile, and likely less bioavailable (Winkel et al. 2012; Shrimpton et al. 2015).

Isotopic fractionation is caused by the preferential participation of a molecule containing heavier or lighter masses during some process, be it diffusion, a redox reaction, adsorption from the liquid to a solid phase, or volatilization (Wiederhold 2015). If the process results in the separation of phases, or the two resulting molecules can be analytically separated, then fractionation is measurable. Processes that result in the breaking of bonds generally produce larger degrees of fractionation than physical processes (*e.g.*, diffusion), because there is a greater difference in bond energies in the presence of light or heavy atoms.

Because fractionation of selenium isotopes is the result of differences in the molecular structure, bond strengths, or energies caused by lighter or heavier selenium atoms, it is possible to calculate fractionation factors from vibrational energies (Bigeleisen and Mayer 1947; Urey 1947; Krouse and Thode 1962). Due to the difficulty of measuring vibrational energies for isotopically pure solutions, as well as obtaining solutions containing only one isotope of selenium of a specific species, it is desirable to determine the molecular vibrational frequencies using models (Schauble et al. 2001; Schauble 2007; Black et al. 2011).

Density functional theory (DFT) is a method to solve for a molecule's geometry and calculate the vibrational frequencies. The DFT method is computationally slower than Hartree Fock (HF), but can produce more accurate models, and hence more accurate estimations of vibrational frequencies (Schauble et al. 2004). Different basis sets can be used, with the relative accuracy of each dependent on the size of the molecules and atoms involved (Scott and Radom 1996).

It may be possible to compare experimental data with theoretical fractionation calculations to determine whether the assumed reaction mechanism is accurate. Previous studies have been performed using measured vibrational frequencies corrected for different masses (Krouse and Thode 1962; Rees and Thode 1966), but limited work was performed, and the results are inconsistent with modern selenium stable isotope measurements (Johnson 2012). One *ab initio*

study focused on selenium isotope fractionation, although it emphasized organic compounds, and used a slightly different computational method than this study (Li and Liu 2011).

The processes that control the removal of selenium from groundwater can be complicated, and may involve more than one step (Johnson 2004; Bailey 2017). Knowledge of the extent of fractionation associated with each of these steps could aid in determining whether values measured from experimental data are on the appropriate order of magnitude for the reaction considered, or if an inappropriate reaction mechanism has been assumed for the experiment. The foremost requirements are the construction of reasonable molecular models and applying the correct equations for calculating fractionation.

Molecular models for selenium species of interest (SeO_4^{-2}, $CaSeO_4$, SeO_3^{-2}, $HSeO_3^-$, and $CaSeO_3$) were constructed to estimate the equilibrium fractionation factors of selenium isotopes associated with each process and to compare the calculated fractionations with experimental data. Systems were limited to those for which the assumptions for the applied equations are valid, which include the reduction of selenate to selenite in solution, the protonation of selenite, and the addition of calcium to solution. The relevancy of using models to determine the reaction mechanism was then investigated by comparing the results to those from laboratory experiments.

2.3 Methods

Selenium isotope ratios are noted in delta notation (Eq. 2.1). Ratios are compared to a standard (NIST SRM 3139) so that values are comparable between different laboratories. Delta values are reported in permill (‰) as the changes in ratios between the sample and the standard are generally quite small.

$$\delta^{82/76}Se = \left(\frac{{}^{82}Se\big/{}^{76}Se_{\text{sample}}}{{}^{82}Se\big/{}^{76}Se_{\text{standard}}} - 1 \right) \times 1000‰$$

(2.1)

To determine the amount of fractionation occurring from experimental data, the fractionation factor (α) is calculated. The fractionation factor is defined for selenium isotopes in this work as the isotope ratio of the reactant over the isotope ratio of the product (Eq. 2.2). This definition is

18

reversed compared to other systems, but it is defined this way so that when discussing the isotope value in solution, the fractionation in epsilon notation (ε, Eq. 2.3) is positive. The α value is commonly close to one, so ε is typically reported instead. Fractionation (ε) can also be approximated from the isotope separation (Δ) of the measured delta values of the product and the reactant in the experiment (Eq. 2.4). However, this approximation is only valid in systems where the fractionation factor (α) is small (Hayes 2004). The degree of fractionation that occurs in selenium isotope systems is large relative to other elements of similar atomic numbers, so this approximation is often invalid (Johnson 2012).

$$\alpha = \frac{\dfrac{^{82}Se}{^{76}Se}\text{reactant}}{\dfrac{^{82}Se}{^{76}Se}\text{product}}$$

(2.2)

$$\varepsilon = (\alpha - 1) \times 1000\text{‰}$$

(2.3)

$$\varepsilon \approx \delta_{\text{reactant}} - \delta_{\text{product}}$$

(2.4)

A second method of obtaining α, and hence ε, is from curve fitting experimental data. This technique is useful in systems where it is difficult to accurately measure the isotope ratio of either the product or the reactant, but relies on the experimental system obeying the rules for Rayleigh distillation (Eq. 2.5); the system must be closed, and the reaction must be irreversible for the application of this technique to be a valid assumption (Hayes 2004). A linear regression can be performed on the natural log of the delta values, normalized to the initial delta, and the natural log of the fraction of selenium remaining in the reacting phase. The slope of this line of best fit will be close to ε, if the earlier assumptions for the Rayleigh equation are valid.

The fractionation (ε) can be determined from experimental data for a closed system with irreversible reactions and instantaneously forming products if the initial delta ratio and sufficient

sample delta ratios can be measured for an assortment of fractions of selenium remaining in the reacting phase (F). The negative sign is added to compensate for Eq. 2.2 being inverted.

$$ln \left| \frac{1+\frac{82}{76}Se_{initial}}{1+\frac{82}{76}Se_{sample}} \right| = -\varepsilon \; ln[F] \qquad (2.5)$$

The theoretical fractionation of an element can be calculated using vibrational frequencies (Urey, 1947). Simplifying the original equations by requiring that the molecule have only one atom of the element undergoing isotopic substitution, be non-linear, and undergo mass dependent fractionation, yields the following set of equations (Bigeilson and Mayer, 1947; Schauble *et al.*, 2007):

$$U = \frac{v_i \hbar}{kT} \qquad (2.6)$$

The U value for the heavy and light isotope substituted molecule is calculated for each vibrational frequency (v_i) by multiplying by Planck's constant and dividing by the Boltzmann constant times the temperature in Kelvin. These U values can then be used to calculate β.

$$\beta = \prod \left[\frac{U_{heavy}}{U_{light}} e^{\frac{\left(U_{light}-U_{heavy}\right)}{2}} \frac{\left(1-e^{-U_{light}}\right)}{\left(1-e^{-U_{heavy}}\right)} \right] \qquad (2.7)$$

The β value for the reactant and product molecule is calculated by taking the product of the U for the heavy isotope substituted molecule and the U of the light isotope substituted molecule for every vibrational frequency. The β values are then substituted into equation 2.2 to determine the fractionation factor for a given reaction.

To solve these equations and estimate a theoretical fractionation factor, it is necessary to obtain vibrational frequencies for each molecule. It would be most ideal to measure the vibrational frequencies of an isotopically pure system, though measurements of non-ideal systems can be corrected to be for one isotope (Krouse and Thode 1962; Rees and Thode 1966). However, there is potentially an easier method that takes advantage of modern technology. Molecules of interest can be modeled with the different isotopes substituted into their structures

to more accurately reflect bond lengths and vibrational frequencies for each state (Schauble et al. 2001).

In this study, β values were calculated for SeO_4^{-2}, $CaSeO_4$, SeO_3^{-2}, $HSeO_3^-$, and $CaSeO_3$, using data generated from Gaussian 09 (Frisch et al. 2009). These β values were then used to compute theoretical equilibrium fractionation factors between each molecule. The Gaussian 09 program (Frisch et al. 2009) was used to model multiple selenium containing molecules using the two selenium masses most commonly reported for fractionation studies, ^{82}Se and ^{76}Se. Two different methods were used to obtain optimized molecular geometry to calculate the vibrational frequencies. The HF method with the 6-31G basis set was used to obtain an initial approximation of the structure of each molecule. The molecular structure was then refined using the density functional theory (DFT) method with unrestricted B3LYP and the cc-pVTZ basis set. Only the DFT results are reported here. The modeling of multiple molecules was prioritized over locating the ideal basis set for these molecules, due to the time involved for each calculation. However, the results obtained are sufficient when compared to experimental error of selenium isotope measurements for an initial assessment of this method. Fractionations that have been calculated from models constructed using Gaussian 09 will then be compared to theoretical fractionations calculated by others and experimental data.

2.4 Results

The geometry of the molecules SeO_4^{-2}, $CaSeO_4$, SeO_3^{-2}, $HSeO_3^-$, and $CaSeO_3$ were all initially optimized using the HF model (Figures 2.1 – 2.5). These geometries were then further optimized using the DFT method. The vibrational frequencies for these molecules were obtained from the DFT optimized models for each isotope of interest (Tables 2.1 – 2.5).
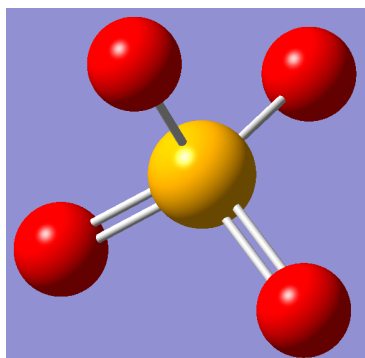
Figure 2.1: Model for the selenate (SeO_4^{-2}) molecule.
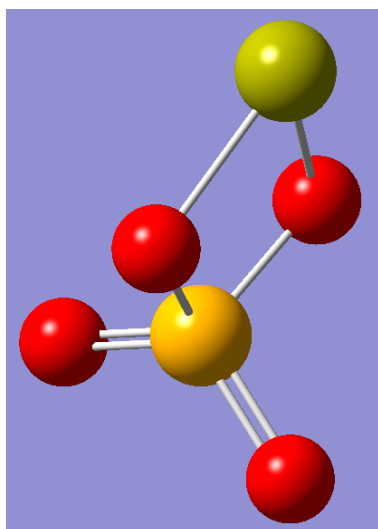
Figure 2.2: Model for the calcium selenate ($CaSeO_4$) molecule.
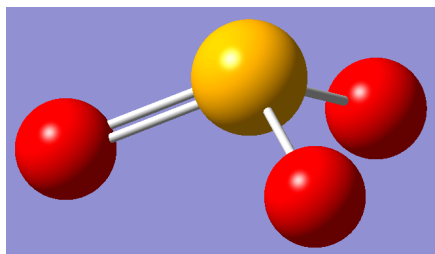
Figure 2.3: Model for the selenite (SeO_3^{-2}) molecule.
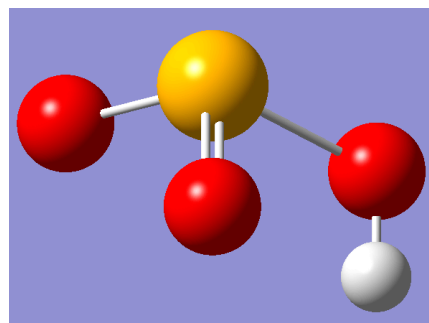
Figure 2.4: Model for the hydrogen selenite ($HSeO_3^-$) molecule.
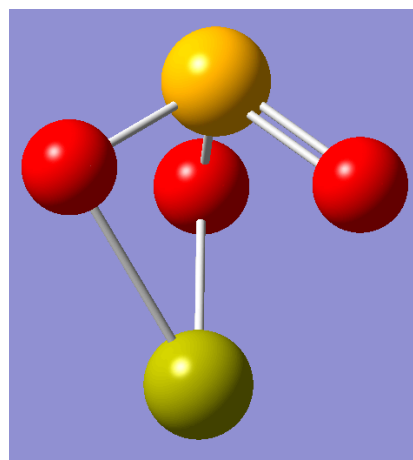
Figure 2.5: Model for the calcium selenite ($CaSeO_3$) molecule.

Table 2.1: Vibrational frequency results for the selenate molecule (SeO_4^{-2}). Selenium atoms with masses of 82 and 76 were modeled.

	Frequency	
Vibration	82 DFT	76 DFT
1	324.01	324.01
2	324.01	324.01
3	415.4	418.71
4	415.4	418.71
5	415.4	418.71
6	797.53	797.53
7	842.72	850.43
8	842.72	850.43
9	842.72	850.43

Table 2.2: Vibrational frequency results for the calcium selenate molecule ($CaSeO_4$). Selenium atoms with masses of 82 and 76 were modeled.

	Frequency	
Vibration	82 DFT	76 DFT
1	76.02	76.16
2	274.95	277.48
3	279.79	280.14
4	284.83	284.83
5	389.45	393.96
6	397.76	400.39
7	484.64	484.95
8	613.6	613.7
9	656.07	661.18

10	710.55	713.4
11	936.49	940.93
12	997.51	1006.88

Table 2.3: Vibrational frequency results for the selenite molecule (SeO_3^{-2}). Selenium atoms with masses of 82 and 76 were modeled.

	Frequency	
Vibration	82 DFT	76 DFT
1	332.17	333.33
2	332.8	333.96
3	405.94	410.01
4	759.18	765.64
5	759.46	765.92
6	774.2	777.64

Table 2.4: Vibrational frequency results for the hydrogen selenite molecule ($HSeO_3^-$). Selenium atoms with masses of 82 and 76 were modeled.

	Frequency	
Vibration	82 DFT	76 DFT
1	217.08	217.42
2	285.83	286.77
3	331.91	332.96
4	388.16	390.68
5	492.61	497.25
6	869.36	873.75
7	902.15	908.73
8	1015.25	1016.42

9	3742.8	3742.8

Table 2.5: Vibrational frequency results for the calcium selenite molecule (CaSeO$_3$). Selenium atoms with masses of 82 and 76 were modeled.

	Frequency	
Vibration	82 DFT	76 DFT
1	229.69	229.71
2	231.77	231.78
3	382.74	384.23
4	383.5	384.99
5	401.84	405.93
6	536	539.1
7	716.76	721.14
8	717.34	721.73
9	778.43	781.67

The vibrational frequencies were then used to calculate beta (β) values for every molecular model using equations 2.6 and 2.7 (Table 2.6).

Table 2.6: Beta (β) values calculated from vibrational frequency results for each modeled molecule.

Molecule	DFT β
SeO$_4^{-2}$	1.03867
CaSeO$_4$	1.03652
SeO$_3^{-2}$	1.02489
HSeO$_3^-$	1.02407
CaSeO$_3$	1.02267

The β values were used to calculate epsilon values (ε) using equation 2.2 and 2.3 (Table 2.7). For this study, ε will be referred to as the theoretical fractionation for a particular reaction.

Table 2.7: Epsilon values in ‰ calculated from DFT optimized model vibrational frequencies. The reactant molecule is the top row, and the produced molecule is in the left row for the fractionation calculation.

Molecule	SeO_4^{-2}	$CaSeO_4$	SeO_3^{-2}	$HSeO_3^-$	$CaSeO_3$
SeO_4^{-2}	0	-2.07	-13.3	-14.1	-15.4
$CaSeO_4$	2.07	0	-11.2	-12.0	-13.4
SeO_3^{-2}	13.4	11.3	0	-0.80	-2.16
$HSeO_3^-$	14.3	12.2	0.80	0	-1.37
$CaSeO_3$	15.6	13.5	2.17	1.37	0

2.5 Discussion

All calculated isotope fractionations yield positive values when moving from a higher oxidation state selenate molecule to a lower oxidation state, and when adding an additional atom to the molecule (Tables 2.7). The reduction of selenium, and the breaking of the double bond associated with the extra oxygen atom, has always been reported as a positive fractionation in the isotope literature because the reactant is enriched in the heavier isotopes (Johnson 2012). These values are in reasonably close agreement with the values calculated using a different basis set by others (Li and Liu 2011); there is an average standard deviation of 0.21 ‰ of their results compared to this study.

The reduction of selenate (SeO_4^{2-}) to selenite (SeO_3^{2-}) has a theoretical fractionation of 13.4‰ for the DFT model. Literature values for this reduction process vary from as high as 18‰ due to reduction by HCl, to as low as 1.7‰ due to reduction by bacterial cultures (Johnson 2012). As the fractionation values for bacterial cultures are heavily dependent on the species of bacteria and the abundance and growth of those bacteria, it is reasonable to assume biotic fractionation is more controlled by a kinetic process unaccounted for by the equilibrium DFT modeling approach applied in this study. Fractionation during bacterially mediated reduction of selenate to selenite

ranges from 11.8–1.7‰ (Johnson 2012; Schilling et al. 2020). Accounting for changes to the fractionation factor caused by fresh, growing cultures compared to established cultures decreases that range from 11.8–9.2‰ for natural, unaugmented systems (Schilling et al. 2020).

Abiotic fractionation of SeO_4^{2-} reducing to SeO_3^{2-} is typically higher, from 18–9.6‰ (Johnson 2012; Shrimpton et al. 2018), though values as low as 3.0‰ have been reported (Shrimpton et al. 2015). The theoretical fractionation of 13.4‰ from the DFT model is similar to the higher range of fractionation, and is close to the range of $11 - 18$ ‰ cited early on as the degree of fractionation associated with abiotic reduction (Johnson 2004). It is possible that the high fractionation measured for HCl-based reduction (18 ‰) included reduction to even lower oxidation states (Rees and Thode 1966), although the authors argue reduction from selenite to elemental selenium should produce no fractionation. However, during HCl reduction selenium can go 'missing' due to adsorption, volatilization, or precipitation (Bye and Lund 1988), which should cause a greater degree of fractionation according to more recent studies (Johnson 2012). The fractionation of selenium due to reduction of selenate to selenite by HCl was also measured before the advent of multi-collector inductively coupled plasma mass spectrometry, resulting in lower precision The unusually low value of 3.0‰ for the reduction of selenate by zero valent iron (Shrimpton et al. 2015) is likely due to a combination of kinetic effects that were not accounted for, with rapid sorption and further reduction on the solid phase likely decreasing the total amount of fractionation observed in solution.

Theoretical modeling results indicate a much more modest fractionation is attributed to associations between selenite or selenate with a calcium ion than for reduction. An additional batch experiment for the reduction of selenate to selenite by zero valent iron included calcium carbonate saturated water, and obtained a higher fractionation of 4.3‰ (Shrimpton et al. 2015). Calcium is known to increase the degree to which selenate and selenite adsorb nearer neutral pH values (Neal et al. 1987; Goldberg and Glaubig 1988). Selenate and selenite molecules were modeled coupled to a calcium atom, to assess the effect of association with Ca^{2+} ions on fractionation. Although the theoretical fractionation from the reduction of calcium selenate to calcium selenite remained similar to the theoretical fractionation from the reduction of selenate

to selenite (Table 2.7), the formation of calcium selenate from selenate had a theoretical fractionation of 2.07‰, a much lower fractionation than the theoretical equilibrium fractionation for reduction of selenate to selenite (13.4‰).

The formation of hydrogen selenite ($HSeO_3^-$) from selenite has a theoretical fractionation of 0.8‰ with the DFT model. Experimentally determined literature values for the sorption of selenite span the small range of 0 ‰ for sorption onto alumina oxides (Xu et al. 2020), , to 0.93‰ for sorption to ferrihydrite (Mitchell et al. 2013). Similar fractionations are associated with selenite adsorption to hematite (0.7–0.9‰) and Mn oxide minerals (1.24‰ at pH 5, -0.08‰ at pH 8) (Xu et al. 2020). The fractionation for the adsorption of selenite and selenate onto montmorillonite and kaolinite is close to zero (Xu et al. 2021). Hydrogen selenite has been found to form during the adsorption process to certain iron minerals (Zhang and Sparks 1990). Additionally, the pH range at which selenite is reported to adsorb to alluvial soils (Neal et al. 1987) is similar to the stability range of the $HSeO_3^-$ species (pH < 7; Johnson, 2004). The adsorption of selenite onto metal oxide minerals is accompanied by a small change in its structure, and likely involves the substitution of an H atom (Su and Suarez 2000).

The DFT calculations do not support the previously held idea that there is no measurable fractionation during the oxidation of selenium (Johnson 2004). Newer experiments have demonstrated that fractionation is expected during oxidation, although it is presumed to result from the formation of both selenite and selenate, followed by the separation of these two oxidation states along a flow path due to processes such as adsorption, rather than any actual isotopic change during oxidation (Wasserman et al. 2021). A boundary effect is likely involved in preventing oxidation from directly resulting in fractionation in nature. Oxidation may be better modeled using kinetic effects to resolve this discrepancy.

2.6 Conclusions

Modeling selenium isotope fractionation using Gaussian 09 can provide a baseline for investigating the degree of fractionation that could be expected from a given system. The theoretical calculations of selenium isotope fractionation match values from Li and Liu (2011),

with average standard deviations of 0.21 ‰. However, the fractionation for the reduction of selenate to selenite is higher than measured in most laboratory experiments. The protonation of selenite yields a fractionation factor similar to adsorption, another process that can make small changes to the structure of selenium molecules. Although adding a divalent cation to a selenium molecule has not been directly measured in laboratory studies, the lower fractionation factor than during reduction could give additional insight to lower fractionations observed in systems with more complicated chemistry. Involving kinetics will likely improve results (Rees and Thode 1966), allowing them to more closely match measured fractionation factors.

Chapter 3: Selenium isotope fractionation during the reduction of Se(IV) by sodium sulfide

3.1 Abstract

Selenium is both an important nutrient and toxic contaminant. Reduction by sulfur reducing bacteria (SRB) can remove Se from groundwater. Selenium reduction by SRB results in Se isotope fractionation, but distinguishing whether Se reduction, and the associated Se isotope fractionation are due to direct Se respiration or abiotic processes remains challenging. This study examined abiotic Se(IV) reduction by $H_2S_{(g)}$ to determine the associated Se isotope fractionation, and compared the results with recent studies of Se(IV) reduction in systems containing SRB. Abiotic reduction of Se by $H_2S_{(g)}$ was investigated using two experimental approaches. First, a solution containing Na_2S was added in increasing concentrations to reduce and precipitate Se from solution. The second experiment examined the effect of contact time between the precipitate and aqueous Se. Powder X-ray diffraction results yielded three distinct spectra for each of the three colors of precipitate that formed, which corresponded to Se_nS_{8-n} or Se(0) and S(0). The $\delta^{82}Se$ values of the residual dissolved Se increased as the Se concentration decreased and with increased contact time between solution and precipitate. The Rayleigh fractionation was calculated to be 7.9 to 10.9‰. When contact time is short (< 6 h), differentiating abiotic from biotic reduction is not possible. A longer contact time between the precipitate and solution may provide a larger fractionation unique to abiotic reduction, as biotic fractionation factors in natural, unaugmented systems should be less than 8.4‰.
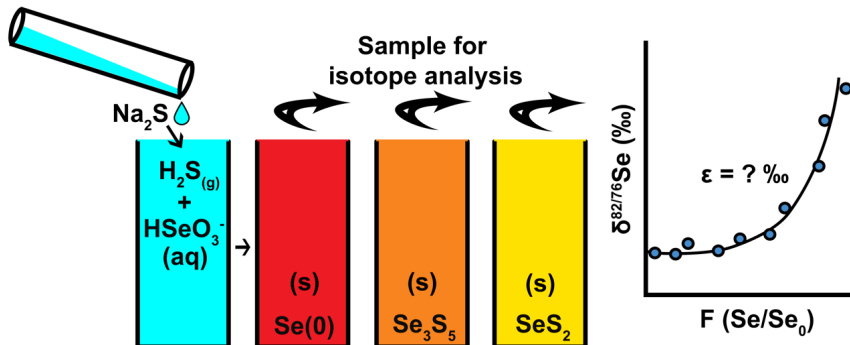
3.2 Introduction

Dissolved Se can be removed from groundwater by natural attenuation (Basu et al. 2016) or *in situ* treatment systems (Tang et al. 2015). Decreasing Se concentrations in aquifers and treatment systems can be caused by dispersive dilution along the flow path, adsorption of Se onto the aquifer material (Goldberg and Glaubig 1988; Xu et al. 2020), reduction of Se to a less mobile oxidation state (Tang et al. 2015), or an improperly located well screen and seasonal variations in the groundwater flow path (Mills 2016). Reduction and precipitation of reduced Se phases provide the greatest potential for long-term Se removal from groundwater, whereas other processes may only delay Se from reaching a potential receptor or result in no removal of Se. Thus, measurements of Se concentrations, in the absence of a mechanistic analysis, may not be sufficient to determine the effectiveness of a Se removal strategy. Determination of Se isotope ratios can provide insight into Se removal mechanisms.

The removal of Se from solution by sulfur reducing bacteria (SRB) plays an important role in both the natural environment and passive water-treatment systems. However, determining whether Se(IV) reduction and removal are due to reaction with $H_2S_{(g)}$ generated by SRB or to direct Se respiration is challenging (Tang et al. 2015; Deen et al. 2018). At pH < 7, $H_2S_{(g)}$ can abiotically reduce Se(IV) to products including $Se(0)_{(s)}$ (red or gray) and sulfur-selenium ring compounds with the general formula Se_nS_{8-n}, commonly most stable as $Se_3S_{5(s)}$ (orange) (Geoffroy and Demopoulos 2011; Tang et al. 2015; Jung et al. 2016). Se_nS_{8-n} compounds are insoluble (Geoffroy and Demopoulos 2011).

Isotope fractionation during the reduction of Se in systems involving SRB has been investigated (Herbel et al. 2000; Schilling et al. 2020); however, determining whether the reduction was due to the biotic respiration of Se or abiotic reduction of Se(IV) by $H_2S_{(g)}$ remains unclear. An experiment in which Se(IV) was reduced by FeS and FeS_2, interpreted with the assumption that removal was due to sulfide in solution producing either Se(0) or $FeSe_{(s)}$, yielded a fractionation of $^{82/76}\varepsilon = 9.7‰$ (Mitchell et al. 2013). The current study examined the fractionation of Se isotopes during the abiotic reduction of Se(IV) by S(-II) at a pH of 6.5 to determine whether $\delta^{82}Se$ values can be used to differentiate abiotic reduction from respiratory

processes; such information can aid in the design or optimization of remediation systems at Se-contaminated sites. The objective was to define both the removal mechanism and fractionation factors associated with differing experimental conditions.

3.3 Materials and Methods

3.3.1 Experimental Design

Variable concentration experiment. Three sacrificial replicate batch experiments (A, B, and C) were conducted using different initial Na_2S concentrations and similar pH and Se(IV) concentrations. Sodium sulfide (Na_2S) stock solutions (Batch A: 12 mmol L^{-1} Na_2S; Batch B: 7 mmol L^{-1} Na_2S; Batch C: 8 mmol L^{-1} Na_2S) prepared using solid Na_2S (Na_2S anhydrous, Alfa Aesar, $Na_2S \bullet 9H_2O$, Sigma-Aldrich), stabilized with NaOH in ultrapure water (MilliQ), as a sulfide source. The Na_2S solution was made fresh for every batch experiment in a fume hood before being transported into an anaerobic chamber.

A Se(IV) stock solution was prepared by dissolving anhydrous Na_2SeO_3 (Alfa Aesar) in Ar-purged ultrapure water (26 mmol L^{-1} batch A, 25 mmol L^{-1} batch B and C). One milliliter of Se(IV) stock solution was dispensed into each 50 mL test tube and diluted with ultrapure water - 3.3). Each vial was pre-acidified with HCl prior to adding the Na_2S solution, to result in a final pH of 6.5 after combining the Se(IV) and Na_2S solutions. Pre-acidification favors the precipitation of Se_3S_5 rather than elemental Se(0) (Geoffroy and Demopoulos 2011). The precipitate generated was fine grained and sticky. The pH was measured using pH strips to avoid fouling a pH probe. After transferring the vials to an anaerobic chamber, sufficient Na_2S solution was added to each test tube using a graduated cylinder to bring the final volume up to 50 mL (Table 3.1-3.3)

Table 3.1: Volumes and final concentrations of each solution added in batch A at the beginning of the variable concentration experiment.

Sample	Na_2S (mL)	Na_2SeO_3 (mL)	Ultrapure Water (mL)	[Se] (mmol L^{-1})	[S] (μmol L^{-1})
0A	0.0	1	49.0	0.52	0.00

1A	1.4	1	47.6	0.52	17.21
2A	2.8	1	46.2	0.52	34.31
3A	4.2	1	44.8	0.52	51.62
4A	5.6	1	43.4	0.52	68.83
5A	7.0	1	42.0	0.52	86.04
6A	8.4	1	40.6	0.52	103.24
7A	9.8	1	39.2	0.52	120.45
8A	11.2	1	37.8	0.52	137.66
9A	12.6	1	36.4	0.52	154.87
10A	14.0	1	35.0	0.52	172.07

Table 3.2: Volumes and final concentrations of each solution added in batch B at the beginning of the variable concentration experiment.

Sample	Na_2S (mL)	Na_2SeO_3 (mL)	Ultrapure Water (mL)	[Se] (mmol L^{-1})	[S] (μmol L^{-1})
0B	0	1	49	0.50	0.00
1B	1	1	48	0.50	6.92
2B	2	1	47	0.50	13.83
3B	3	1	46	0.50	20.75
4B	4	1	45	0.50	27.66
5B	5	1	44	0.50	34.58
6B	6	1	43	0.50	41.50
7B	7	1	42	0.50	48.41
8B	8	1	41	0.50	55.32
9B	9	1	40	0.50	62.24
10B	10	1	39	0.50	69.16

Table 3.3: Volumes and final concentrations of each solution added in batch C at the beginning of the variable concentration experiment.

Sample	Na_2S (mL)	Na_2SeO_3 (mL)	Ultrapure Water (mL)	[Se] (mmol L^{-1})	[S] (μmol L^{-1})

1C	1	1	48	0.50	8.23
2C	2	1	47	0.50	16.46
4C	4	1	45	0.50	32.92
5C	5	1	44	0.50	41.14
6C	6	1	43	0.50	49.37
8C	8	1	41	0.50	65.83
10C	10	1	39	0.50	82.29

After 2-3 h, samples were passed through 0.45 µm syringe filters to preserve the precipitate. The syringe filters for samples 4B, 5B, 6B, and 5C leaked, and these samples were re-filtered with disposable filters after 10 to 22 h. Filter membranes were air-dried under anoxic conditions in the anaerobic chamber prior to storage of the precipitate for powder X-ray diffraction (PXRD) analysis. Aqueous sampling for batch experiment A was limited to collection of samples for cation and isotope analysis, whereas batch experiments B and C also included the determination of aqueous $S_2O_3^{2-}$ and SO_4^{2-} concentrations. Samples for Se isotope ratio determinations were filtered (0.2 µm) but not acidified. Samples for cation analysis were filtered and acidified HNO_3 (to 2%), and samples for S speciation were filtered with no acidification. All samples were stored in a cold room (4 °C) prior to analysis.

Temporal batch experiment. An additional sacrificial batch experiment, designed to evaluate the extent of isotope exchange between the aqueous Se and solid reaction product, utilized constant Na_2S and Se(IV) concentrations (2.60 ± 0.01 mmol L^{-1} and 2.08 mmol L^{-1}, respectively) and higher aqueous volumes (200 mL total in 250 mL amber bottles). The Se:S ratio was chosen to result in approximately 70% of Se removal from solution, in order to obtain larger differences in δ^{82}Se values for different fractionation factors. This experiment was conducted in triplicate. Argon-purged Se(IV) solution was added to each reaction vessel and pre-acidified with HCl outside of the anaerobic chamber before being combined with a freshly made basic Na_2S solution inside the anaerobic chamber. Sampling was conducted after 3 h, 6 h, 20 h, 48 h, 1 week, and 2 weeks. Gravity filtration to separate the solids from the supernatant solution took approximately 10 min to complete using a filter holder (0.45 µm filter paper) and receiver (polysulfone, Thermo

34

Scientific Nalgene). Samples were collected to determine the concentrations of cations, aqueous S speciation, and Se isotopes ratios, using the same protocols as described above for the variable concentration experiment.

3.3.2 Chemical Analysis

Cation concentrations were determined by inductively coupled plasma optical emission spectrometry (ICP-OES; Thermo iCAP). Sulfur speciation determinations were made by ion chromatography (IC; Dionex DX600) using an IonPac AS9-HC column (4 × 250 mm). The IC eluent was 9 mmol $NaCO_3$ with a flow rate of 1.0 mL min^{-1}. The speciation technique applied to these samples was limited to two forms of S (SO_4^{2-}, $S_2O_3^{2-}$).

3.3.3 Synchrotron X-ray Diffraction

Solid samples from the variable concentration batch experiments were stored in plastic Nalgene bottles in an anaerobic chamber. Precipitates of differing colors (dark red, red, and orange) were analyzed separately by PXRD at the Canadian Light Source (CLS). Because the solid was firmly attached to the filter paper in a shellac-like glaze, pieces of the filter paper were cut and inserted into Kapton® capillary tubes immediately prior to analysis. The ends of each tube were sealed with Locktite 454™ epoxy. Synchrotron-based PXRD was performed at the Canadian Macromolecular Crystallography Facility (CMCF) CMF_BM beamline. Beamline specifications are described in full elsewhere (Fodje et al. 2014). Samples were exposed to 18 keV ($\lambda = 0.6888$ Å) of radiation for 10 to 20 s. A Rayonix MX300HE area detector was used to capture the diffraction images. Data were processed using GSASII (Toby and Von Dreele 2013). The data processing procedure involved background subtraction using a blank Kapton® capillary tube loaded with clean filter paper, calibration to a standard (LaB_6), and integration. Due to beamtime limitations, samples from the temporal batch experiment could not be analyzed using this technique.

3.3.4 Isotope Methods

The method used for purifying and measuring Se isotope ratios can be found in detail elsewhere (Shrimpton et al. 2015). In brief, thiol cotton fiber (TCF) extraction resin was pre-

made in the laboratory, weighed into 1 mL solid-phase extraction (SPE) columns, and cleaned using ultrapure water and decreasing concentrations of HCl. The sample was mixed with a double spike of ^{74}Se and ^{77}Se at a 1:1 mass ratio before reducing overnight in concentrated HCl. Samples were diluted to 1 M HCl a few hours prior to purification. Samples were loaded onto the cleaned columns, and impurities removed by rinsing with 2 mL each of ultrapure water, 6 M HCl, and 1 M HCl. The Se was detached from the TCF by transferring the TCF loaded with sample into a test tube, adding 50 µL of concentrated HNO_3, heating the test tube in a water bath for 20 min at ~80 °C, then solubilizing the oxidized Se in ultrapure water, centrifuging, and decanting the supernatant liquid. The TCF oxidation and decanting steps were performed twice to remove as much Se as possible. Extractions were filtered (0.45 µg) before a final reduction step to prevent loss of Se to residual TCF in the decanted supernatant. Selenium isotope ratios were measured using a hydride generator coupled to a multi-collector inductively coupled mass spectrometer (MC-ICP-MS; Thermo-Finnigan Neptune). A $NaBH_4$ and NaOH solution was mixed with the 2N HCl of the sample to generate the hydride. The external error (2 σ) with respect to Se isotope ratio measurements was ± 0.4‰.

3.4 Results and Discussion

3.4.1 Selenium Concentrations

Variable concentration experiment. Increasing the concentration of Na_2S in solution resulted in linear removal of Se(IV) (Figure 3.1). Removal occurred via precipitation of a solid, which began immediately upon the addition of the Na_2S solution, except when the initial pH was above 7. Although the targeted final pH was around 6.5, the final pH ranged by 0.5 ± 0.2 pH units. Precipitation was complete 2-3 h after initiating the reaction; however, previous studies suggest the reaction proceeds to completion within 10 min (Geoffroy and Demopoulos 2011; Pettine et al. 2012). The discrepancy may be due to a surplus of Se in the current experiment, rather than a surplus of S used in previous experiments.
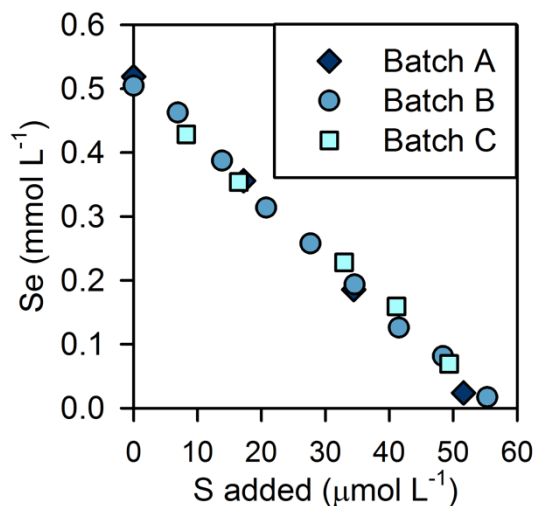
Figure 3.1: Concentration of Se(IV) remaining in solution after addition of S in the variable concentration experiment. Data points shown represent only those samples with sufficient Se for isotopic analysis. Each batch is an individual experiment conducted at different times.

Temporal batch experiment. When the precipitate remained in contact with the solution for an extended period (> 6 h), the Se concentration remained stable (Figure 3.2). After 1 week, the Se concentrations began to increase. This change could be due to oxidation arising from the ingress of oxygen into the anaerobic chamber. Catalyst plates, used to remove oxygen from the chamber atmosphere, were removed from the anaerobic chamber during the experiment to prevent fouling of the Pd catalyst.
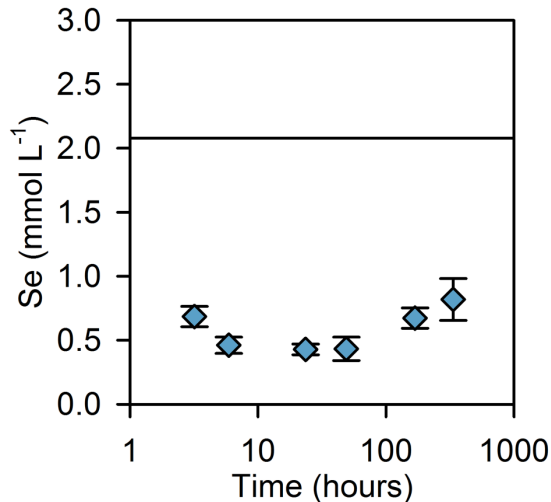
Figure 3.2: Concentration of Se in solution over time during the temporal batch experiment. The black horizontal line represents the initial concentration.

3.4.2 Sulfur Speciation Results

Variable concentration experiment. Only samples with analyzable Se isotopes were measured for aqueous S speciation. The aqueous sulfur species analysis indicated increasing SO_4^{2-} concentrations with increasing Na_2S addition (2.8 to 3.7 µmol L^{-1}; $0.2 \pm 0.1\%$ of total S added). Thiosulfate ($S_2O_3^{2-}$) concentrations (9.1 to 42 µmol L^{-1}; $1.4 \pm 0.9\%$ of total S added) that were higher in samples with greater Na_2S addition (Figure 3.3). Combined, these two sulfur species account for $< 3\%$ of the mass of S added. The presence of oxidized S species can result in the oxidation of Se(0) at pH > 7 (Goff et al. 2019). The pH was not measured during sample collection. If the pH increased after the precipitation reaction, it is possible that oxidized S species could oxidize Se(0), leading to the increased aqueous Se concentrations at one and two weeks.
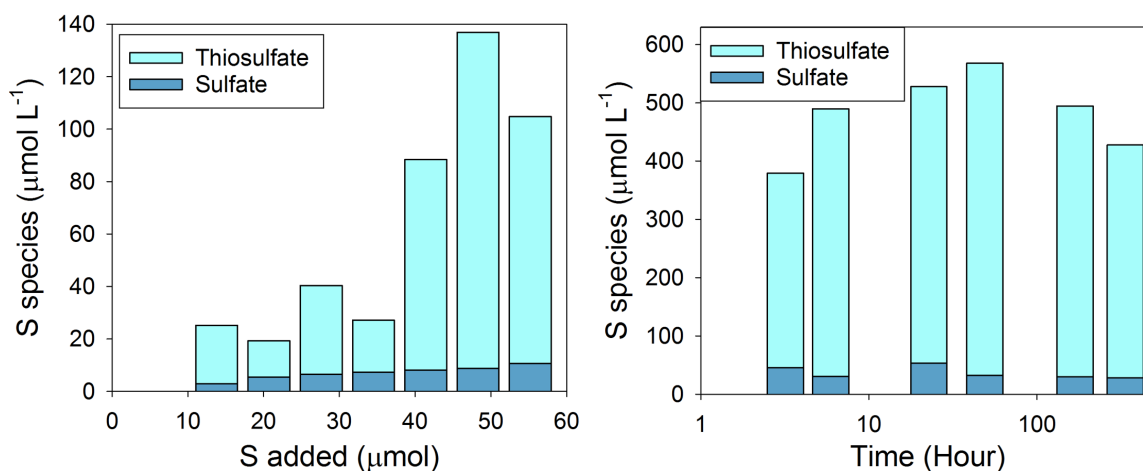
Figure 3.3: Aqueous sulfur speciation in variable concentration batch experiment B (left) and in the temporal batch experiment (right).

Temporal batch experiment. The concentrations of $S_2O_3^{2-}$ in the batch experiment solution varied from 333 to 535 µmol L^{-1} (17 ± 3% of total S added). It increased from 3 h and peaked after 2 d before decreasing again (Figure 3.3). Greater variability in the SO_4^{2-} concentration (32 to 53 µmol L^{-1}; 1.4 ± 0.4% of total S added) was evident in this experiment than in the variable concentration experiment, likely due to the higher initial Na_2S and Se(IV) concentrations, larger batch volumes, and longer time available for shifts in S speciation. Because all S speciation measurements were conducted at the end of the experiment, some oxidation of the initial samples may have occurred.

3.4.3 XRD Analysis

Variable concentration experiments. The precipitates changed in color as the reaction products aged. Immediately following the experiment, the precipitate colors ranged from lemon yellow, to orange, to bright red. After six months, orange precipitates had turned darker orange or red, dark orange precipitates had turned red, and precipitates that were already red or yellow did not change in color.

The PXRD analysis results show an uneven baseline, which may be due to the presence of the filter paper within the sample holder (Figure 3.5). The ring patterns show the presence of an amorphous phase in all samples, with discernable peaks in some samples. Sample 3A (Table 3.1)

39

did not have any identifiable peaks after background subtraction and is likely an amorphous compound. Se removal in this sample was greater than 95%. The lemon-yellow precipitate that formed in the 3A batch experiment may be elemental S, which can be amorphous. The precipitates from Sample 7B (with only 16% Se remaining in solution) and 5A (which showed complete Se removal) were both orange and exhibited qualitatively similar PXRD ring patterns; differences in the 1D XRD patterns may be due to the presence of filter paper in the samples. Visual comparison of the number and location of peaks in the 7B and 5A samples to previously reported $Se_{1.09}S_{6.91}$ and $Se_{3.04}S_{4.96}$ compounds (Geoffroy and Demopoulos 2011) suggests the compounds are similar. Sample 10B was dark red, had a different diffraction pattern, and is qualitatively similar to a mixture of Se(0) and S(0) observed by others in a similar experiment (Geoffroy and Demopoulos 2011). Complete Se removal was also observed for Sample 10B.
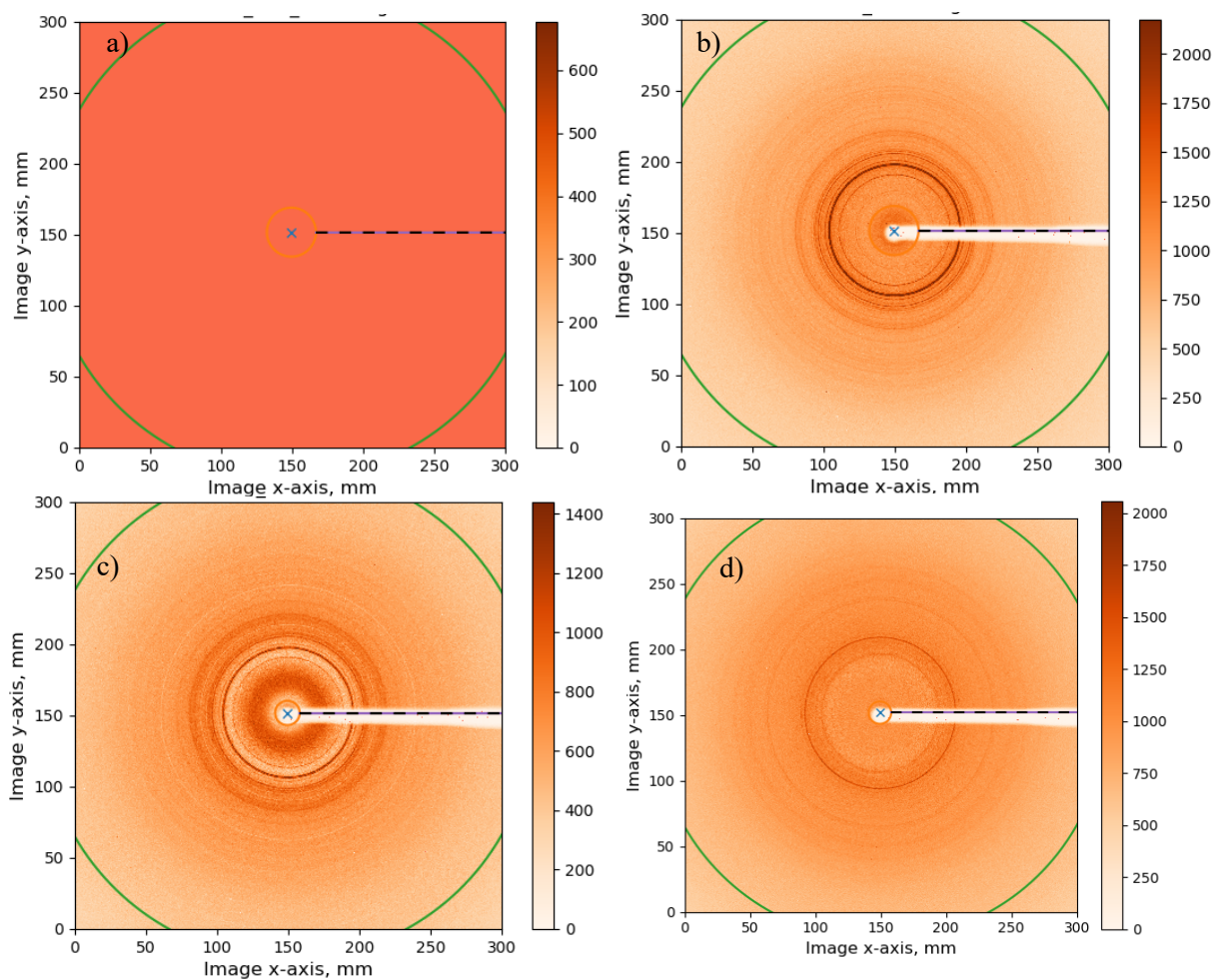
Figure 3.4: 2D X-ray diffraction patterns for solids collected from the variable concentration experiment: a) 3A (near-complete removal of Se from solution); b) 5A (complete removal of Se from solution); c) 7B (84% of Se removed from solution); d) 10B (complete removal of Se from solution).
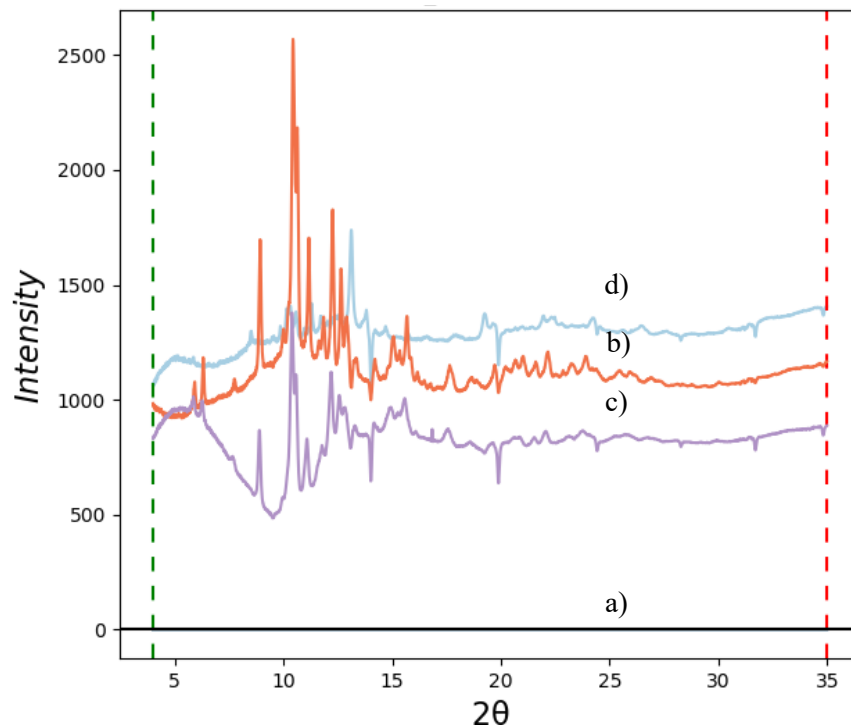
Figure 3.5: 1D XRD patterns extracted from 2D synchrotron PXRD measurements: a) 3A (black); b) 5A (orange); c) 7B (purple); d) 10B (blue).

3.4.4 Selenium Isotope Results

Variable concentration experiments. δ^{82}Se values measured in solution increased as the amount of Se in solution decreased (Figure 3.6) If a single removal mechanism is assumed, the change in δ^{82}Se values can be described using the Rayleigh model with a fractionation factor of ε = 9.4‰.
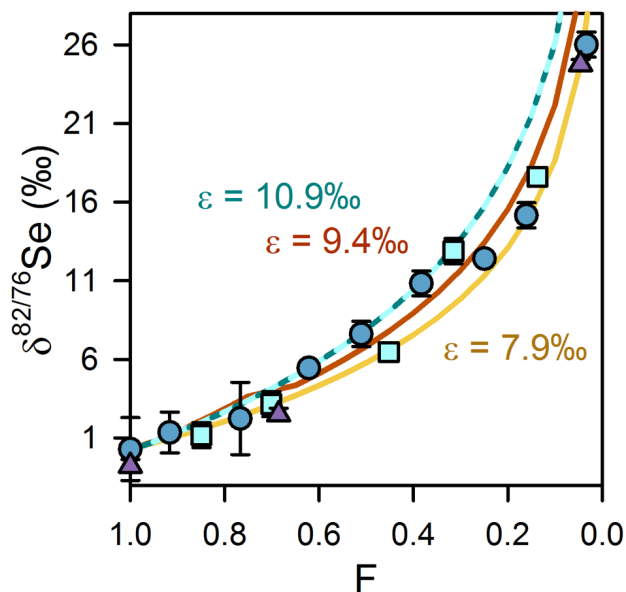
Figure 3.6: Aqueous isotope results from variable concentration batch experiments: A (triangles), B (circles), and C (squares). The three Rayleigh type curves are different fits to encompass outlying data.

However, samples with either the majority of Se remaining (F > 0.5) or depleted (F < 0.2) seem better fit by a fractionation factor of 7.9‰, whereas most samples with F values between 0.5 and 0.2 are better fit with a fractionation factor of 10.9‰ (4B, 5B, 6B, and 5C). Unfortunately, no solid phase was preserved from the samples that most clearly fit the fractionation factor of 10.9‰ due to leakage from the syringe filters. The precipitate was orange at the time of filtration, which suggests it was selenium sulfide. These samples remained in contact with the solid phase for longer (10 to 22 h) due to the leaks in the syringe filters. The variation in fractionation factors may be due to isotopic exchange between the aqueous Se and the solid phase, trending toward equilibrium fractionation.

A maximum fractionation factor of 7.8 ± 0.8‰, previously observed during the reduction of Se(IV) by SRB (Schilling et al. 2020), falls within the error of the lower proposed fractionation factor observed in the variable concentration experiment. The reduction mechanism proposed in the SRB experimental study was extracellular electron transfer, in which bacterial growth is limited by resource availability, as would also be expected in natural systems (Schilling et al. 2020). When Se(IV) was added to a sediment slurry using organic-rich wetland material with a

natural consortium of microbes, the resulting fractionation factor was 8.4‰ (Ellis et al. 2003). The slurry study is also close to a natural system in which there is no flow, although because the batch reactors were placed on orbital shakers the reactions would not be diffusion-limited, as may occur in natural systems (Ellis et al. 2003). The fractionation from the slurry system falls within the lower range of fractionation (7.9 to 9.4‰) of the present experiment.

Pure bacterial reduction of Se(IV) in experiments that did not mimic natural systems (i.e., microbes were not resource limited) had much higher fractionation factors, ranging from 9 to 12.6‰ (Herbel et al. 2000). The upper fractionation factor of 10.9‰ noted in the present study falls within this range, but these conditions would not be expected to occur naturally unless microbes are injected into the subsurface and then provided with an electron donor as part of remediation efforts. It is unknown whether an established, indigenous microbial community fed nutrients would also see higher fractionation without prior testing, but provided there is room for growth, higher Se isotope fractionation is likely; studies with pure microbial cultures fed a surplus of nutrients and in the process of expanding caused Se isotope fractionation as high as 13.7‰ during the reduction of Se(IV) (Herbel et al. 2000). A fractionation of 9.7‰, attributed to the reduction of Se(IV) by FeS_2, was observed by others (Mitchell et al. 2013). Reduction by S and precipitation of Se(0) and FeSe minerals was proposed as the removal mechanism (Mitchell et al. 2013). The FeS_2 study is the only other study focused on Se(IV) isotope fractionation associated with abiotic Se(IV) reduction, and reports values within the range of the upper fractionation curve from the variable concentration experiment (10.9‰).

Differentiating the removal mechanism based on the degree of fractionation may be possible depending on the cause of the multiple apparent fractionation factors during the variable concentration experiment. One possible cause is the precipitant formed. The structure of the precipitate is affected by the Se:S ratio, which was adjusted in these experiments to calculate ε, and the pH, which was similar in all vessels. However, two of the differently colored precipitates with PXRD spectra available (yellow and orange; no Se remained in solution for the sample with red precipitate) can be fit by the lowest fractionation factor (7.9‰), suggesting different precipitates may not result in different fractionation. A different fractionation factor may result

from modifying the contact time between the solid and solution, because contact time was longer for the four samples that had the highest fractionation.

Temporal batch experiment. The δ^{82}Se values of the aqueous Se increased from −4.4‰ at 3 h to stabilize at 9.9 ± 0.9‰ after 6 h (Figure 3.7). The lowest δ^{82}Se value, at 3 h, also corresponds to a higher aqueous Se concentration (0.68 ± 0.08 mmol L^{-1}) and less Se removal (Figure 3.2). Precipitation of the solid phase occurred rapidly in this experiment (within seconds and continuing for 3 h) under far from isotopic equilibrium conditions. The changes in δ^{82}Se values may indicate isotopic exchange between the aqueous Se and the precipitate, trending toward equilibrium fractionation. The δ^{82}Se value, however, increased with time in contact with solution, reaching a maximum value between 3 and 6 h. Plotting these δ^{82}Se values versus fraction of Se remaining in solution (F) does not produce a single Rayleigh type curve due to insufficient variability in concentrations (0.19 < F < 0.42). In the variable concentration experiment, some of the solution and solid samples were in contact for longer than 4 h. Isotopic exchange between the initial precipitation and the solution over this period may have resulted in the higher δ^{82}Se values reported, as a reversible reaction between the precipitate and solution could allow for fractionation to approach equilibrium. Similar shifts in δ^{82}Se isotope ratios are observed in the temporal experiment.
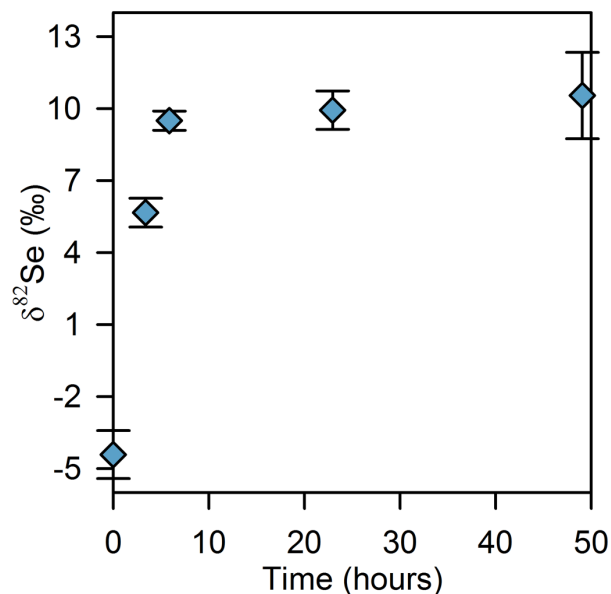
Figure 3.7: Aqueous isotope results from a set Se:Na$_2$S ratio in the temporal batch experiment. Error bars represent standard deviation between replicates, which was higher than measurement error.

After 48 h in the temporal experiment, the δ^{82}Se values decreased slightly and the precipitates changed color from bright orange to pink and finally to hickory brown, which is likely indicative of oxidation reactions. The presence of oxidized sulfur species at higher pH, as well as the potential ingress of oxygen, could both result in the oxidation of these later samples.

3.5 Conclusions

Overall, the findings of these experiments suggest fractionation in an abiotic system cannot be distinguished from biotic reduction by SRB (7.8‰) (Schilling et al. 2020) if the contact time between the Se(IV) in solution and the precipitate is brief (< 4 h). Under prolonged contact time between the Se(IV) solution and the precipitate, the fractionation factor increased to 9.4 – 10.9‰, which is distinguishable from the fractionation associated with biotic processes. This comparison does not include fractionation in systems with rapid bacterial growth from an establishing culture, which can have a much higher fractionation factor (Herbel et al. 2000; Schilling et al. 2020). Other abiotic processes, such as Se(IV) reduction by iron-bearing minerals (Johnson and Bullen 2003; Mitchell et al. 2013), can also have high fractionation factors (e.g.,

9.7‰ for reduction by Fe_2S (Mitchell et al. 2013)), making it difficult to distinguish between abiotic reduction processes in nature.

Chapter 4: Isotope fractionation of selenite by natural microbial consortium

4.1 Abstract

Selenium contamination can result from anthropogenic activities, such as mining. Selenium can be removed from water via microbial reduction, either naturally in groundwater flow systems, or in treatment reactors. A batch experiment was conducted to reduce Se(IV) using a natural microbial consortium of sulfur reducing bacteria (SRB). Batch vessels included organic mulch (lucerne hay) and sodium lactate as initial electron donors. Zero valent iron (ZVI) was added to provide a metal ion source. Selenium was rapidly and completely removed from solution. SEM images indicate a healthy microbial population, although it was not possible to identify any solid precipitates. Selenium isotope measurements indicate multiple processes occurred which are difficult to differentiate without further information on speciation. Potential processes include reduction of Se(IV) to Se(0), the formation of organic Se compounds, some of which can be volatile, Se binding to organic matter, and generation $H_2Se_{(g)}$. These results suggest that although SRB can remove Se(IV) from solution, it is important to examine the final reaction products to assess stability and bioavailability.

4.2 Introduction

Selenium (Se) is an element of growing interest, because the release of Se into the environment from anthropogenic activities, such as coal mining, can result in the collapse of local fish populations (Lemly 2002), as well as decreased reproductive success in birds and mountain sheep (Wayland et al. 2006; Kneteman 2016). Multiple factors can impact whether Se is released from mine waste to groundwater, which may subsequently discharge to surface water and affect local fauna. One of these factors is the activity of the subsurface microbial community, which can alter the mobility of Se. Microbial reduction of selenite [Se(IV)] can form Se(0), which is essentially insoluble, or $H_2Se_{(g)}$, which can react with many metals to form sparingly soluble metal selenides (Nancharaiah and Lens 2015). Microbes can thus enhance natural attenuation of Se.

It can be difficult to determine whether microbial reduction is occurring in the subsurface without extensive sampling. Measurements of aqueous concentrations in samples can show a decline in concentration, but without definitive information about why the concentration is changing, and speciation measurements of Se can be misleading because more reduced forms of Se can preferentially adsorb to aquifer material, making it challenging to complete mass-balance calculations without measurements on a solid sample.

Stable isotope ratio measurements provide an additional tool to augment inferences based on concentration, speciation, Eh, and pH measurements. Selenium stable isotope ratios are unaffected by dispersive dilution, change only slightly during adsorption ($\varepsilon < 1.0$ ‰), and are more strongly fractionated by reduction ($\varepsilon = 2–11$ ‰) (Johnson 2012; Xu et al. 2020, 2021). Se isotopes have been applied in the field in soil pore-water studies (Schilling et al. 2015), and as indications of redox zones in uranium roll front deposits (Basu et al. 2016). However, these studies were limited by the availability of known fractionation factors. To use Se isotope ratios as a quantitative tool, knowledge of the degree of isotope fractionation associated with potential processes of interest is required. Studying measurements from simple systems will assist in employing Se isotope ratio measurements in more complicated systems, or in systems currently lacking known fractionation factors.

Reduction can occur through multiple pathways, including direct respiration of selenite (SeO_3^{2-}), reduction to selenide (HSe^-), or the indirect formation of Se(0) nanoparticles (Stolz et al. 2006; Wells and Stolz 2020). However, most pathways are not specific to Se metabolism (Wells and Stolz 2020). Microbial respiration pathways that reduce Se(IV) to Se(0) or Se(-II) have been identified (Fernández-Martínez and Charlet 2009), and some microbes will also further reduce Se(0) to Se(-II) (Wells and Stolz 2020).

Microbial reduction of Se, either by pure cultures (Herbel et al. 2000; Schilling et al. 2020), from sediment samples (Ellis et al. 2003), or assumed from Se extracted from soil (Schilling et al. 2011a, 2015) provide fractionation factors or estimates of the expected degree or direction of isotopic fractionation. However, these studies either do not replicate natural systems (Herbel et al. 2000), do not determine the reaction products formed (Ellis et al. 2003), use only pure

cultures (Schilling et al. 2020), or do not isolate the immobilization mechanism (Schilling et al. 2015). Isotope fractionation during the reduction of Se in systems involving sulfate reducers has been investigated (Herbel et al. 2000), but it remains unclear whether reduction was due to biotic respiration, because abiotic reduction of Se(IV) by $H_2S_{(g)}$ or S(-II) may also occur (Tang et al. 2015). Examining the solid-phase reactants and products, and microbial communities, together with measuring the degree of fractionation, may provide an improved understanding of Se isotopic data from natural systems. In the present study, the reduction of Se(IV) to Se (0) or Se(II) was examined, and differences in Se isotope ratios observed.

4.3 Methods

4.3.1 Experimental setup

Two batch experiments were conducted to determine the degree of fractionation caused by a natural microbial consortium. The sulfur reducing microbial consortium was extracted from brewer's sludge. An input concentration of 6 mg L^{-1} Se(IV) and Se(VI) was selected for each experiment, because total Se concentrations below 8 mg L^{-1} were not observed to result in a change in the fractionation factor during microbial reduction in previous experiments (Ellis et al. 2003). Unfortunately, the experiment using Se(VI) did not undergo reduction during the experimental time frame, and results will not be discussed here. Three pairs of controls were also run: one set containing no Se, one no solids, and one no SRB. These controls were sampled at the beginning and end of the experiment, and contained a 50/50 mixture of Se(VI) and Se(IV).

Lucerne hay (Rocky Point Mulching, Australia) was dry sieved at < 1.75 mm (-0.75 ϕ) to remove large pieces of straw. Pre-sieved 0.210 – 0.297 mm (50-70 mesh) sand (white quartz, Sigma Aldrich) was acid washed using 1.2 M HCl to remove fines and iron impurities. The sand was then rinsed with double distilled water 5 times. Because the pH of the rinse water had not returned to neutral following rinsing, a small quantity of sodium bicarbonate ($NaHCO_3$) was used to adjust the pH to 7. The sand was then rinsed two more times with double distilled water to remove any remaining $NaHCO_3$. Next, 250.2 g sand was transferred to the beaker containing 28.0 g mulch. Excess water was carefully decanted, and the wet mixture was stirred until

homogeneous. The resulting mixture was weighed to determine the water content. Batch vessels were loaded with the final wet mixture, which contained approximately equal volumes of sand (8.9 g) and lucerne hay (1 g), along with 4 g of water.

Zero valent iron (ZVI) powder (100 mesh, $\leq$ 149 µm) was carefully acid washed three times using 1.2 M HCl, then washed twice using 0.12 M HCl. A magnet was used to aid in decanting (Figure 4.1). Approximately 0.1 g of ZVI was then added to each vessel. The filled vessels were promptly transferred to an anaerobic chamber prior to adding the input solution.
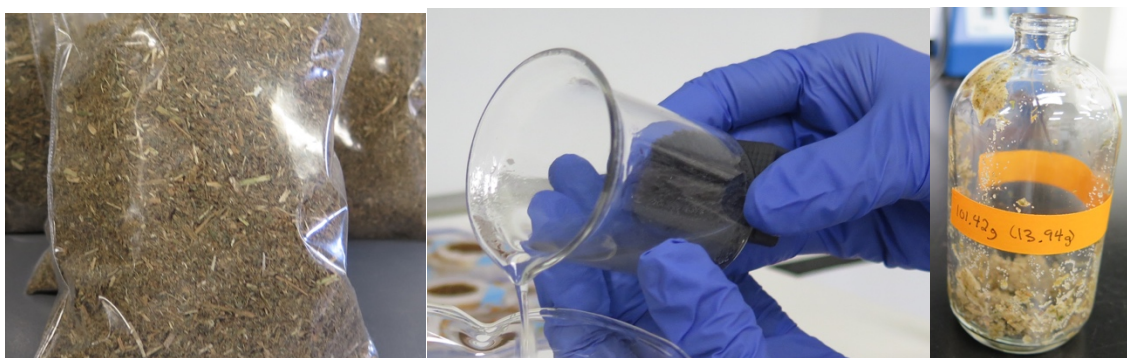
Figure 4.1: Left, dry sieved lucerne hay. Middle, magnet used to acid wash ZVI. Right, reaction vessel containing sand and lucerne hay.

A solution containing 50 mg L^{-1} SO$_4^{2-}$ (as MgSO$_4$) and 1% lactate was bubbled with nitrogen gas for two hours to remove oxygen. The solution was stored in the anaerobic chamber overnight. Within 30 minutes of the addition of the solid material to the reaction vessels, 89 mL of the stock solution was transferred into each vessel using sterile Serri pipettes. All of the reaction vessels were inoculated with 10 mL of the SRB consortium, except for two controls. The vessels were sealed using butyl rubber crimp tops, removed from the anaerobic chamber, and placed on a shaker table at 70 RPM, to ensure sufficient mixing of components. The mixture was left to mature for five days before starting the experiment. After six days, vessels were spiked with 1 mL of concentrated Se(IV) using a sterile syringe and a 0.2 µm filter.

4.3.2 Sampling

Sacrificial sampling was conducted in order to prevent mass loss for isotopic measurements, and the ingress of oxygen into sample vials, which were stored outside of an anaerobic chamber. Vessels were sampled at specified intervals (5 min, 20 min, 30 min, 3.5 hr, 7 hr, 18 hr, 29 hr, 48 hr, 73 hr, 95 hr, and 172 hr). Every second sampling time included a replicate. Controls, which included vessels with no SRB, no solids, and no Se, were sampled at the beginning and end of the experiment.

Liquid samples, collected for determination of cation concentrations, Se isotopes ratios, and pH, were withdrawn through the butyl rubber cap using sterile needles and syringes, then filtered using sterile 0.2 μm Supor membranes, or sterile 0.22 μm Durapore membranes (depending on the availability of filters). Neither filter type is known to interfere with Se. The pH was estimated using pH indicator strips.

An unknown, likely organic precipitate (such as humic acid) formed upon acidification of cation samples with HNO_3. Selenium concentrations were initially below detection in most of the acidified samples. A portion of the unacidified isotope samples were subsequently used for cation analysis; 9 mL of the unacidified, filtered isotope sample was combined with 1 mL of fresh 30% H_2O_2 and allowed to react for one week to ensure the destruction of the organic component. The sample color changed from a dark brown or red to pale yellow during this time, and several samples formed a bright red precipitate. Samples were then acidified with 2 drops of HNO_3. The addition of HNO_3 rapidly dissolved the red precipitate, leaving a clear pale yellow, or colorless solution. Samples were then filtered using 0.2 μm filters and analyzed promptly by inductively-coupled-plasma optical emission spectroscopy (ICP-OES).

All equipment used for solid sampling was washed and sterilized using ethyl alcohol prior to and between collection of samples. A combined solid and liquid sample was collected for scanning election microscope (SEM) examination by scooping the solid material into a glass vial, adding colloid-containing liquid, fixing the microbial activity using glutaraldahyde (final concentration of 2.5% v/v), and crimp sealing the mini-sample.

4.3.3 SEM Analysis

The glutaradahyde fixed samples were dried prior to SEM analysis. For each sample, the supernatant was carefully removed by pipette, covered with 20% ethanol, and then the solid sample was microwaved at 150 W for 40 seconds. The procedure was then repeated with 40%, 60%, 80% ethanol, followed by three rinses of 100% ethanol to ensure an approximately 100% ethanol matrix. Samples were then transferred to microporous capsules under ethanol, to prevent drying under atmospheric conditions. The samples were then dried under a CO_2 atmosphere to prevent cell collapse for imaging.

4.3.4 Lucerne Hay Analysis

The lucerne hay was digested to determine its composition. The digestion was carried out in duplicate. Following Banuelos and Pflaum (1990), 0.5 g of lucerne hay was weighed into a Teflon digestion vial, followed by 3 ml of concentrated HNO_3 and 100 µl of 0.5 M ammonium cerium (IV) nitrate. After mixing and allowing the vials to sit overnight, they were heated on a hot plate in an aluminum block to 110 ˚C for 3 hours, with glass funnels placed on top to act as vapor traps. Then 8 ml of 30% H_2O_2 was added in 2 mL increments every 15 minutes. After heating an additional 45 min, 1 ml of 23 M formic acid was added in two 0.5 ml increments at 15-minute intervals. The hot plate temperature was increased to 125 ˚C, and heating continued until no more fumes were emitted. The final digestion was then filtered (0.2 µm) into 15 mL vials. Cation concentrations were obtained by subsampling 0.5 mL of the digestion fluids, and diluting to a final volume and HNO_3 concentration of 6 mL and 2% respectively. Concentration was then analyzed by ICP-OES.

4.3.5 Isotope Analysis

The complete sample preparation and purification method can be found elsewhere (Shrimpton et al. 2018). Briefly, samples were spiked 1:1 with a 1:1 ratio of ^{77}Se:^{74}Se prior to reducing overnight in 6 M HCl. Samples were then diluted to 1 M before purification using thiol cotton fiber (TCF) made in house (Shrimpton et al. 2015). The Se was extracted off the resin using a minimum quantity of HNO_3. The solution was then filtered with a 0.45 µm syringe filter to

removed remnant TCF before being reduced overnight in 6 M HCl. Isotope samples were measured on a Neptune MC-ICP-MS (Thermo Finnigan) using hydride generation. A standard (NIST SRM 3149) was run at the beginning and after every fourth sample to support the double spike technique with sample-standard bracketing. The data were then run through an in-house interference correction program that also performs blank subtraction and fractionation correction using the double spike method (Siebert et al. 2001; Shrimpton et al. 2015).

Fractionation factors for this study were calculated using a linear approximation to the Rayleigh model: $\ln(\delta_A + 1000 / \delta_0 + 1000) = -\varepsilon_{A-B} \ln(F_A)$. The negative sign yields positive fractionation factors when the $\delta^{82}Se$ increases for the analyzed Se pool during a reaction.

4.4 Results and Discussion

4.4.1 Visual Observations

Sample vessels were left for six days prior to spiking with Se to allow the microbial consortium to break down the lucerne hay. During this time, the color in reaction vessels containing SRB culture changed from black to grey or greenish-grey (Figure 4.2).
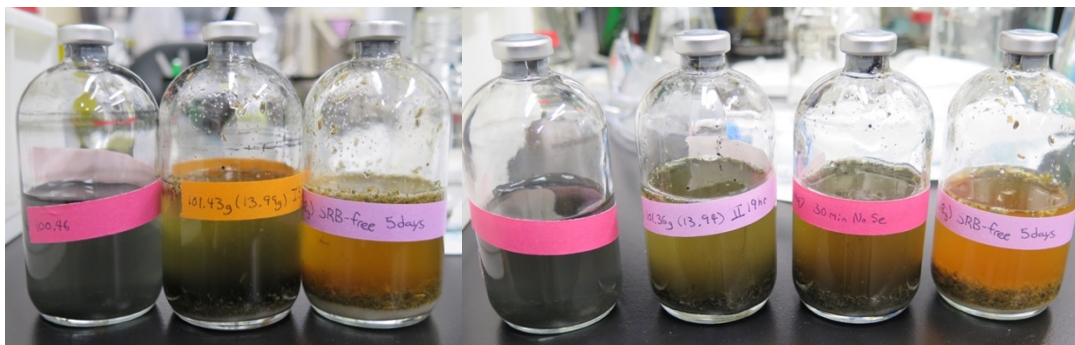
Figure 4.2: Reaction vessels prior to spiking input with Se(IV). Left: the day they were made; right: the day they were spiked, prior to spiking. The vial on the left is a control containing no solids, while the vial on the right had no SRB culture added.

The color of the solution darkened when Se was added, and remained dark for all spiked vessels throughout the experiment (Figure 4.3). The control containing no SRB culture gradually darkened throughout the experiment, but did not turn black. The control vessel with no Se

remained grey, rather than turning black. The control containing no solids remained largely unchanged in appearance throughout the experiment. A black precipitate accumulated in the sand in all vessels except for the vessel that was SRB-free.

Figure 4.3: Sample vessels and controls 4 days after spiking with Se(IV). Note dark appearance of sand in all vessels except where there is no solid or no SRB.

The acidified cation samples all produced a fine, light brown precipitate after one day, even when treated with UV radiation immediately after filtration to ensure sample sterility. A precipitate also accumulated in the Se-free controls. The only samples with minimal precipitate were the no solid controls. There was a greater abundance of precipitate in samples from longer time points. It is probable that humic acids, derived from the decomposing organic matter, became insoluble when the pH decreased, resulting in the accumulation of the precipitates (Gustafsson and Johnssont 1994). Although Se(IV) can adsorb to humic substances, the reaction requires several hours to take place (Stevenson 1994). However, because samples were not analyzed immediately after acidification, any Se(IV) in solution could have been affected by adsorption prior to removal of the humic substances, resulting in low Se concentrations in acidified samples untreated with H_2O_2.

After undergoing treatment with H_2O_2, all brown precipitate was dissolved. A red precipitate that formed during the H_2O_2 treatment rapidly dissolved upon addition of HNO_3. The red precipitate is likely amorphous Se(0) or Se(-II), based on color and solubility in HNO_3 (Martens

and Suarez 1997). Most samples with red precipitates were from early time points of the experiment.

4.4.2 Geochemistry
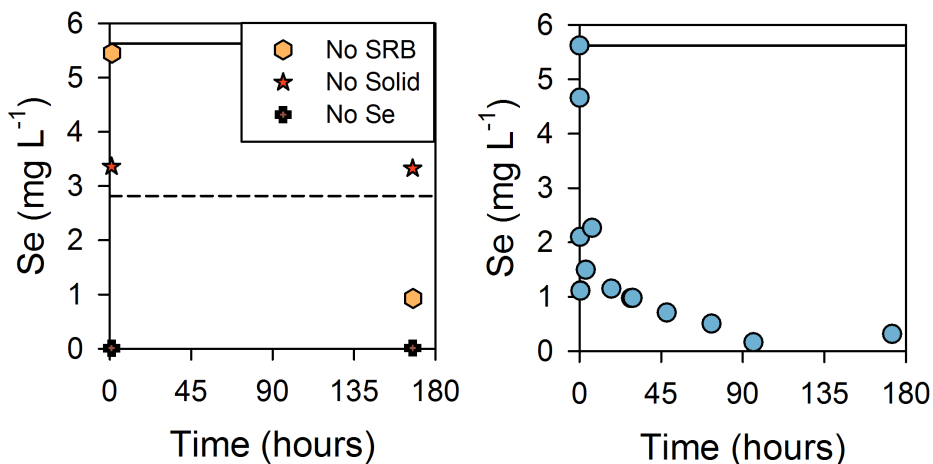
Figure 4.4: Left: Se concentration in controls at the beginning and end of the experiment. Controls containing Se were spiked with a 1:1 Se(VI):Se(IV) mixture. Solid line is the total Se added, dashed line is the contribution from Se(VI). Right: Aqueous Se concentration in Se(IV) experiment over time. The solid line is the concentration of Se(IV) added.

The Se concentrations in the controls were variable (Figure 4.4). At the beginning of the experiment, the no SRB controls showed Se concentration slightly lower (5.45 mg L^{-1}) than the total Se added (5.63 mg L^{-1}). The Se concentration decreased to 0.93 mg L^{-1} by the end of the experiment (Figure 4.4), suggesting that SRB were present in the solid inoculum used in the experiment, or that the ZVI removed the Se. When the SRB were present in the absence of solid material, the total Se concentration immediately decreased to slightly higher than the estimated initial Se(IV) concentration, and did not change throughout the rest of the experiment (~3.2 mg L^{-1}). Selenium concentrations remained below the quantifiable limit in the control with no Se added (< 12 µg L^{-1}). The digestion of lucerne hay confirmed the organic matter contained no extractable Se.

In the system containing both SRB and solid material, Se(IV) concentrations decreased rapidly, followed by a more gradual decrease over time (Figure 4.4). The different removal rates

are likely due to at least two separate processes: initial adsorption to the organic matter, followed by more gradual reduction and further removal. During biological Se reduction, nano-colloidal Se(0) may be formed, which would remain in suspension and could possibly pass through a 0.2 μm filter (Nancharaiah and Lens 2015). When $H_2Se_{(g)}$ is formed, it will react with any metal ions in solution to form metal selenide minerals (Nancharaiah and Lens 2015). It is less likely that volatile $H_2Se_{(g)}$ was released during the experiment, unless there are no longer any metal ions present in solution. However, volatile organic Se species, if present, will not necessarily react with aqueous metal ions, and may have escaped the sample bottles during analysis.

Most cation concentrations sharply increased briefly at the beginning of the experiment, followed by a decrease and then a gradual increase over time (Figure 4.5). The spike in S, Fe, Ca, and Mg concentrations coincides with the initial rapid removal of Se from solution. These concentrations decreased once Se removal became more gradual. Concentrations did not decrease below the input, but were typically lower than the elemental concentrations found in the no Se control sampled at the beginning of the experiment (dashed line, Figure 4.5). Only S concentrations decreased to input levels after the initial concentration spike. Sulfur, Fe, Ca, and Mg concentrations all increase in solution once aqueous Se removal has proceeded to near completion (after four days). There was always Fe available in solution to bind volatile $H_2Se_{(g)}$.
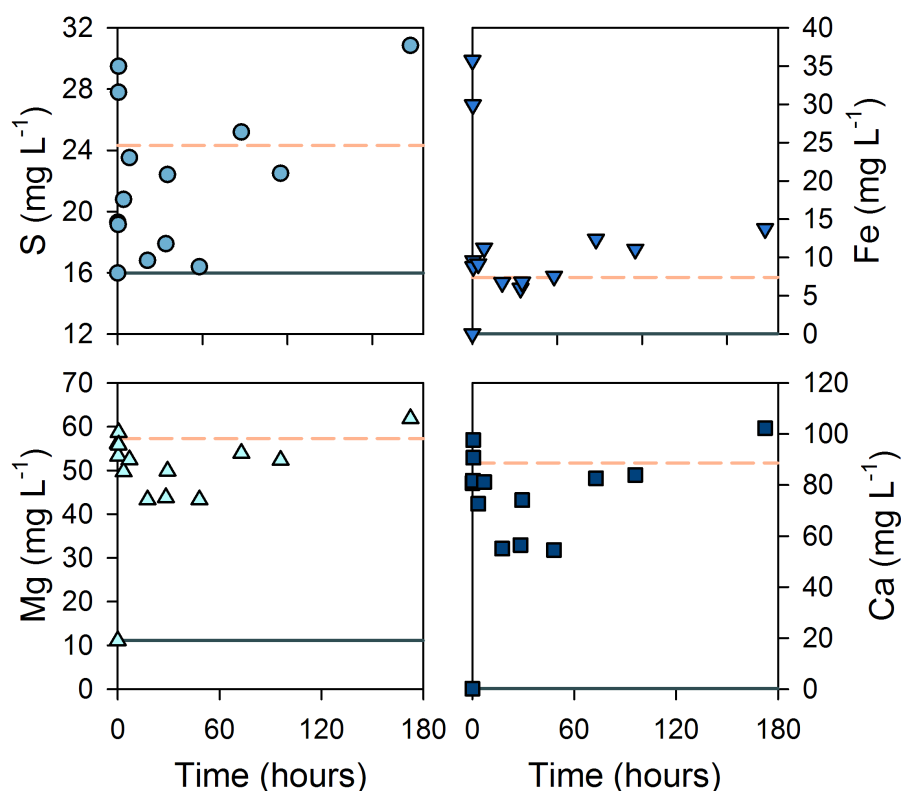
Figure 4.5: Aqueous concentrations of other elements in solution over time. Solid lines indicate concentrations present in the stock solution, dashed lines are concentrations leached into solution from the solid material prior to the addition of Se.

4.4.3 SEM Images

SEM images from batch vessels and controls show bacteria associated mostly with the organic component, or in the crevices of sand particles (Figure 4.6). Little variability can be distinguished between the images over time. Lucerne hay straw remains visually uncolonized by microbes within the six-day incubation period (two hours after adding Se). There is still visible plant vascular tissue four days after the addition of Se. Solid precipitates cannot be differentiated from the thick colonies of microbes.
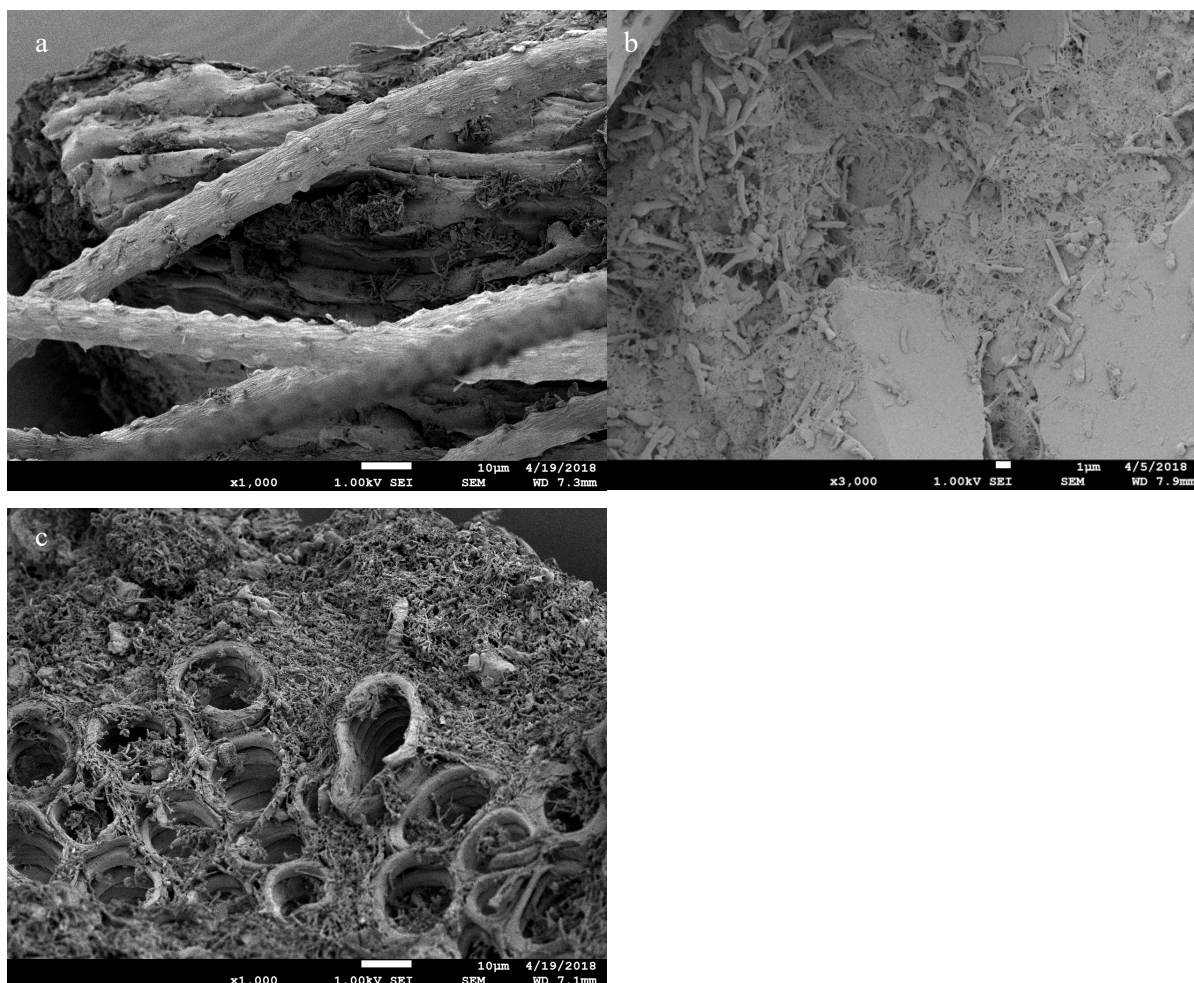
Figure 4.6: SEM images of: a) straw with few microbes (from 2 hr into experiment), b) crevice of a sand grain (from 30 min into no Se control), c) vascular tissue (from 4 d into experiment)

The lack of visible organic degradation suggests the microbes have access to a more labile source of electrons, such as the ZVI. It is still possible that the organic matter is undergoing chemical degradation, despite vascular tissue still being visible. The existence of microbes in sand crevices suggests that there may also be nutrients available for growth in these locations, or that microbes were scraped off exposed surfaces when the batch vessels were stirred (probably the latter).

4.4.4 Isotope Analysis

As Se(IV) is removed from solution, the aqueous δ^{82}Se values initially increase before decreasing (Figure 4.7). This initial increase fits a Rayleigh type fractionation of 19‰. However, it is inappropriate to attempt to fit a Raleigh curve using only two points; the initial fractionation could be as low as 10‰ and still be within measurement error. A negative fractionation factor would need to be invoked for the subsequent decrease in δ^{82}Se values (Figure 4.7). Negative fractionation factors (as defined here) have not been reported for Se isotopes in the literature for reductive processes (though plants are known to take up lighter Se, resulting in lower δ^{82}Se values within the plant tissues (Clark and Johnson 2010; Schilling et al. 2015)). Either a currently unstudied process is resulting in the isotope fractionation, or more than one process is occurring, and it is not the most oxidized phase that is being measured in solution.
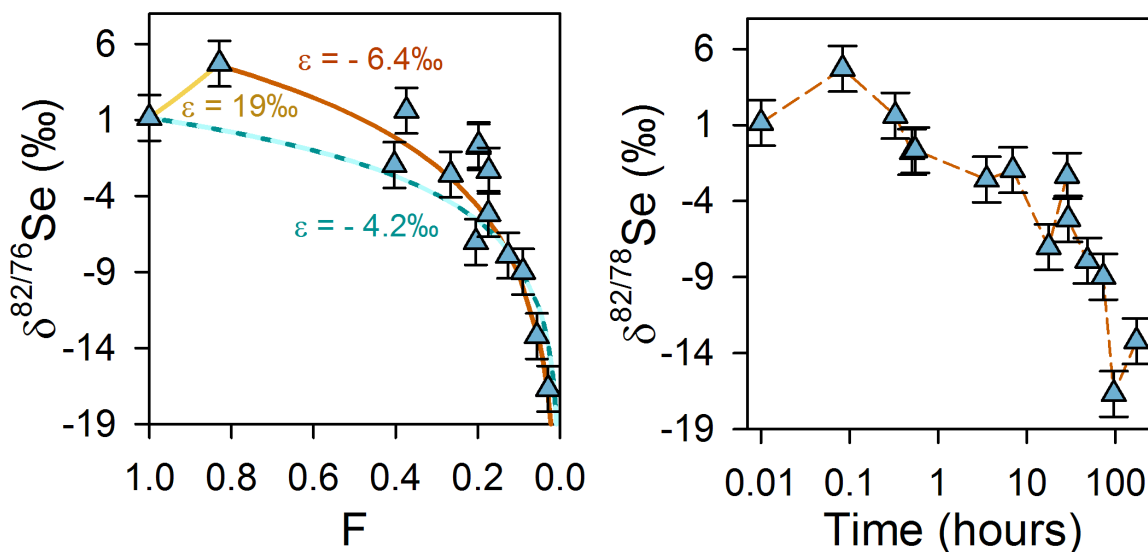
Figure 4.7: Left: Isotope ratio measurements relative to fraction of Se remaining in solution. Overall fractionation shown by the dashed line. The two-step process is represented by solid lines. Right: Isotope ratio measurements over time.

It is more revealing to examine how δ^{82}Se changes over time, because there are three periods (initially, after 10 hours, after 100 hours) where the δ^{82}Se increases instead of decreasing (Figure 4.7). Although the final two increases may be due to natural variability in the samples, these

increases could also be due multi-step processes: initial reduction of Se(IV) to insoluble Se(0), followed by the formation of various Se-organic compounds/complexes, or sulfur complexes which may be volatile or soluble (Young et al. 2010; Winkel et al. 2015; Goff et al. 2019). As each product is formed, respectively lighter Se would be released into solution, followed by an eventual increase in the δ^{82}Se value as this new product also reacts and becomes depleted in solution. The small increase in the Se concentration that match increases in δ^{82}Se at 7 h and 172 hours (Figure 4.4, 4.7) support this hypothesis. If it is possible to separate (or even quantify) the various products, an appropriate fractionation factor could be calculated, and would likely be positive as defined by this study ($\alpha = R_{reactant} / R_{product}$).

4.5 Conclusions

Selenite is rapidly removed from solution, the Se concentration decreasing by 5 mg L^{-1} within the first hour of the experiment. The presence of and adsorption to humic acid in the system may have increased the removal rate, resulting in no measurable Se in solution after four hours. The isotope data suggests either a negative fractionation factor, or (more probably), the release of soluble or volatile reduced species into solution over time. Conducting speciation analysis and separation of species prior to isotope analysis may be vital in measuring appropriate fractionation factors, as well as determining the true mechanism at work.

Chapter 5: Real-time XANES measurement of Se reduction by zero-valent iron in a flow-through cell, and accompanying Se isotope measurements

5.1 Abstract

An anoxic flow-through cell experiment was conducted to examine mechanisms controlling the real-time reduction of selenate (Se(VI)) by zero-valent iron (ZVI), which is commonly used in permeable reactive barriers to treat dissolved contaminants including Se(VI). Changes in selenium (Se) isotope composition were examined by increasing the influent Se concentration over time, thus changing the proportion of Se removed from solution. At the conclusion of the experiment, an anoxic Se-free solution was pumped through the cell to assess the stability of the reaction products. At all stages, X-ray absorption data were obtained from the solid phase and Se isotope data from the aqueous phase. Reduced Se in the form of adsorbed Se(IV), Fe_2SeO_4, Se(0), and iron selenides accumulated on the ZVI over time. A linear regression function was fit to the $\delta^{82/76}Se$ values of the effluent, yielding an isotopic separation of 9.6‰. A Rayleigh curve was fit to the isotope data from the effluent samples collected during the rinse stage with an effective fractionation of 2.4‰. The results from this experiment can be used to elucidate the effect of multiple concurrent mechanisms on Se isotope behavior.
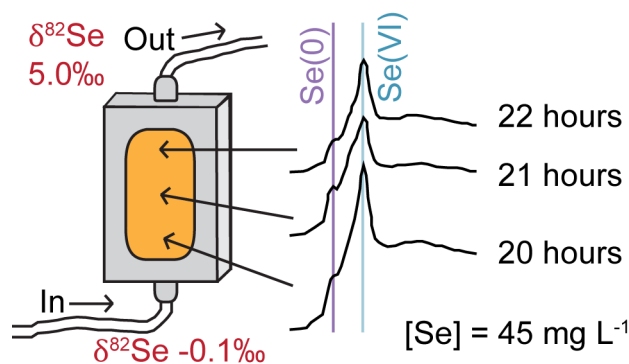
5.2 Introduction

Selenium (Se) is an important nutrient for humans; however, it is toxic at an intake above 400 µg/day (Levander and Burk 2006). Consequences of larger doses in humans include an increased risk of diabetes (Winkel et al. 2012), cancer, hair and nail loss, anxiety and depression, and liver damage (Plant et al. 2003). High levels of Se in the environment can cause teratogenic effects and mortality in livestock and other fauna (Plant et al. 2003; Van Dyke et al. 2013). As a result, the Canadian water quality guideline for protection of aquatic life is 1 µg L^{-1}, and the US EPA's aquatic life criterion for lentic systems is 1.5 µg L^{-1} (Beauvais 2016; Canadian Council of Ministers of the Environment 2016).

Sources of Se contamination include runoff from agriculture, mining, smelting, and natural sources, such as the weathering of Se-rich shale (Lemly 2004; Wen and Carignan 2011; Winkel et al. 2012). Selenium bioaccumulates and bioconcentrates in wetlands (Young et al. 2010; Van Dyke et al. 2013), and Se contamination of groundwater poses a risk to the environment as it has the potential to enter sensitive systems such as wetlands, or other surface water bodies.

Selenium occurs in five oxidation states. Under oxidizing conditions, selenate (Se(VI)) is the most mobile, while selenite (Se(IV)) tends to sorb more strongly, making it less mobile (Winkel et al. 2012; Goldberg 2013). Elemental Se and selenides, Se(-I) and Se(-II), occur under reducing conditions. As Se redox kinetics are kinetically slow, multiple oxidation states can coexist (Zhang and Moore 1996; Johnson and Bullen 2004; Goldberg et al. 2006). Elemental Se and metal selenides have very low solubility. Reduction and precipitation of dissolved seleno-oxyanions provides an efficient method of removing Se from solution (Lenz and Lens 2009).

Previous studies have examined the efficacy of Se removal from aqueous solutions by multiple materials. This includes batch adsorption studies in soils (Neal et al. 1987; Goldberg and Glaubig 1988) as well as a variety of reduction studies using microbes, fungi, and various Fe minerals (Johnson et al. 1999; Herbel et al. 2000; Ellis et al. 2003; Schilling et al. 2011b; Mitchell et al. 2013). Adsorption and reduction of Se by Fe in the form of sheets or foil (Qiu et al. 2000), granular filings (Amrhein et al. 1998; Gibson et al. 2012; Liang et al. 2013; Shrimpton et al. 2015), and nano-particles (Mondal et al. 2004; Loyo et al. 2008) have been found to be

reasonably effective for Se removal in batch reactions. Flow-through column experiments have examined Se behavior (Morrison et al. 2002; Sasaki et al. 2008; Misoka 2012), but the solid phase was sampled only after the experiments were complete.

Selenium has six stable isotopes: ^{74}Se, ^{76}Se, ^{77}Se, ^{78}Se, ^{80}Se, and ^{82}Se. All isotopic values in this paper are expressed in terms of $^{82/76}Se$. These isotopes exhibit fractionation due to reduction as well as adsorption, while undergoing little fractionation due to oxidation or uptake by phytoplankton or animals (Clark and Johnson 2010; Johnson 2012). It is thus possible to use Se isotopes to determine whether reduction reactions are occurring in a system. For instance, Se isotopes will fractionate due to reducing and removal processes in uranium-bearing sediment (Basu et al. 2016), and in soils, the isotopic difference between discrete pools of Se have helped elucidate redox cycling (Schilling et al. 2011a, 2015).

Selenium isotope analysis has not been conducted during previous column experiments; however, experiments have been performed to examine transport via diffusion in microbial reduction systems, consisting of sediment cores and sediment samples underlying a Se-rich water column (Clark and Johnson 2008). Diffusion through reducing sediment was found to remove Se(VI) from solution, but caused little isotope fractionation, generally in the range of 0.61 ± 0.07‰ to 0.20 ± 0.05‰ for $\delta^{82/76}Se$. In comparison, batch sediment slurry microbial experiments show much more fractionation (Ellis et al. 2003), as high as 4.7‰ for the reduction of Se(VI) to Se(IV) and 8.4‰ for the reduction of Se(IV) to Se(0) (Johnson 2012). Abiotic reduction in batch systems can cause greater fractionation, with as much as 11.1‰ caused by reduction of Se(VI) to Se(IV) by green rust (Johnson 2012) and 4.3‰ by zero-valent iron (ZVI) in the presence of $CaCO_3$ (Shrimpton et al. 2015).

The objective of this study was to assess Se isotope fractionation during treatment of dissolved Se(VI) by ZVI under saturated flow conditions. A flow-through cell (FTC) experiment was conducted using a small cell fitted with a Kapton window to allow simultaneous X-ray absorption spectroscopy (XAS) measurements and aqueous effluent collection (Jamieson-Hanes et al. 2014). The experimental design provides the opportunity to record the oxidation states and the relative abundances of Se present within the cell throughout the experiment. Aqueous

effluent samples were subsequently analyzed to obtain geochemical and Se stable isotope data. The results from this experiment were used to determine the mechanisms resulting in removal of Se from solution, and the extent of isotope fractionation associated with these processes. These results were used to evaluate the potential application of Se isotope measurements to indicate the extent of remediation processes.

5.3 Materials and Methods

5.3.1 Experimental Design

The FTC experiment was conducted at the GSE-CARS beamline 13-BM-D at the Advanced Photon Source (APS; Argonne, Il, USA) to facilitate simultaneous XAS measurements. The design of the FTC was similar to previous experiments (Jamieson-Hanes et al. 2014, 2017). A block of HDPE measuring 14.0 x 17.8 x 6.4 cm had a 3.8 × 7.6 × 1.3 cm (37.5 mL internal volume) section cut out and filled with 100g of ZVI packed to form a porous medium. The long, narrow ZVI particles were previously sieved to select a diameter range of 0.25-1mm (18-60 mesh). An 80μm thick Kapton™ film is secured over this window using an HDPE cover and a rubber O-ring to prevent gas and water leaks. Small holes (2 mm in diameter) were drilled into the top and bottom of the cell to allow for the installation of an influent port and an effluent port.

The input solution was composed of varying concentrations of Se(VI) using a sodium selenate (Na_2SeO_4) stock solution of known concentration and calcium carbonate ($CaCO_3$) (See Supporting Information). To observe potential changes in Se isotope composition for a constant mechanism, the fraction of total Se remaining in solution (F) must vary, or the $\delta^{82/76}Se$ values will not change. In this experiment, the initial input concentration of Se(VI) was 15 mg L^{-1}. The input concentration was increased by 15 mg L^{-1} in 8-h increments to a final concentration of 90 mg L^{-1}, resulting in a progressive increase in F. The solution was saturated with $CaCO_3$ to more closely approximate natural groundwater. Saturation with respect to $CaCO_3$ was achieved by bubbling $CaCO_3$-containing solutions with CO_2, then filtering out the excess solid. Excess CO_2 and O_2 were then removed by purging with Ar gas. An $Ar_{(g)}$-filled mylar balloon was used to maintain an $O_{2(g)}$-free headspace above the Se input solution. A $CaCO_3$-saturated solution that

contained no Se was pumped through the cell at the end of the experiment to obtain XAS measurements of the solid phase in the absence of aqueous Se and estimate the retention of Se by ZVI.

Effluent from the cell passed through micro-electrodes that continuously recorded the pH and Eh during the experiment. Aqueous samples were collected in 11.2 ± 0.6 mL aliquots using a fraction collector. Every sixteenth sample was sacrificed for an external pH check. A selection of samples were acidified with concentrated HNO_3 (Ultrapure, EMD Millipore) for cation analysis, while others were acidified with concentrated HCl (trace metal grade, Fisher Scientific) for isotope analysis; all acidified samples were filtered (0.2μm, Supor® polyethersulfone, Pall Aerodisc Syringe Filters) and evenly distributed over the course of the experiment. All other samples were unfiltered and stored unacidified. There was insufficient volume and concentration to measure aqueous Se speciation. Concentrations were analyzed by ICP-OES and HR-ICP-MS (Thermo Fisher Scientific iCAP and Element 2).

5.3.2 XAS Methods

Measurements were conducted to obtain X-ray absorption near edge structure (XANES) spectra. Measurements were compared to standards including Se(0), Na_2SeO_3, Se(IV) on ferrihydrite, Na_2SeO_4, and Se(VI) on ferrihydrite. Additional standards were obtained from the actinide reference database for spectroscopy (AcReDaS) (Rossberg et al. 2014), including achávalite (FeSe) (Charlet et al. 2007), tetragonal iron selenide (FeSe) (Scheinost and Charlet 2008), ferroselite ($FeSe_2$) (Scheinost et al. 2008), and ferric selenite ($Fe_2(SeO_3)_4$) (Missana et al. 2009). ATHENA software was used to process the XAS data (Ravel and Newville 2005).

XANES spectra were collected at three locations in the FTC: near the input, at the center of the cell, and near the effluent end of the cell window. Each location was scanned three times before moving to the next, returning to the input end after each cycle. The three scans were sufficiently similar so that beam induced damage was determined to be minimal during the experiment.

5.3.3 Isotope Methods

Isotope analysis was performed on all aqueous Se species. A double spike method was used to correct for any fractionation caused during sample preparation and analysis (Zhu et al. 2008). Spiking ^{74}Se and ^{77}Se provides reportable ratios of $^{82/76}$Se and $^{82/78}$Se. Of these, $^{82/76}$Se is typically reported; the $^{82/78}$Se ratio is then used to test for errors in measurement (Zhu et al. 2014). Samples were spiked with a 1:1 mixture of ^{74}Se:^{77}Se at a 1:1 spike to sample ratio, prior to reduction in a 8 M HCl matrix and purification using thiol cotton fiber (TCF) (Elwaer and Hintelmann 2008; Shrimpton et al. 2015). Samples were filtered to remove any residual TCF before the final reduction step, and allowed to sit overnight prior to analysis (Shrimpton et al. 2015). Failure to filter samples prior to reduction can lead to decreased intensities and stability issues during analysis (Stüeken et al. 2013), making filtration worthwhile despite the small loss of sample mass. Samples were analyzed on a Neptune multi-collector inductively coupled plasma mass spectrometer (Thermo Scientific) coupled with a hydride generator for signal enhancement (HG-MC-ICP-MS). The reducing solution consisted of 0.4% NaBH$_4$ and 0.2% NaOH. Purification blanks were analyzed between each sample, and a spiked standard (NIST SRM 3149) was run after every fourth sample. Error bars were calculated using twice the standard deviation (2σ) of replicate measurements of the NIST SRM 3149 $\delta^{82/76}$Se value over multiple days.

Isotope ratios are reported in the delta notation relative to the NIST SRM3149:

$$\delta^{82/76}Se\ (‰) = \left[\frac{(^{82}Se/^{76}Se)_{sample}}{(^{82}Se/^{76}Se)_{standard}} - 1\right] \times 1000 \tag{5.1}$$

In order to report a positive fractionation (ε), the fractionation factor (α) is defined as:

$$\alpha_{A-B} = \frac{Ratio_A}{Ratio_B} \tag{5.2}$$

where A is the initial reactant in solution and B is the product in solution. The fractionation is defined by the following equation:

$$\varepsilon_{A-B} = (\alpha_{A-B} - 1) \times 1000‰ \tag{5.3}$$

When the concentration of Se changes in the effluent solution without altering the effluent concentrations, the following approximation to the Rayleigh model can be used:

$$ln\left(\frac{\delta_A + 1000}{\delta_{initial} + 1000}\right) = -\varepsilon_{A-B} \ln(F_A) \tag{5.4}$$

where δ values are in ‰. Linear regression will yield unitless ε as the negative of the slope.

When the system is composed of multiple input concentrations, but the removal mechanism is constant, the amount of isotopic fractionation is better described by the isotopic separation (Δ) (Kaplan 1975):

$$\Delta = \delta_{F=0} - \delta_{F=1} \tag{5.5}$$

which describes the difference in $\delta^{82/76}Se$ between the aqueous reactant and the $\delta^{82}Se$ of all products on the solid (F = 1), which can be approximated by the $\delta^{82}Se$ value in solution when aqueous Se is depleted (when F = 0).

5.4 Results and Discussion

5.4.1 Geochemical Analysis

Input and effluent concentrations are plotted for comparison because the input solution was changed during the experiment (Figures 5.1 and 5.2). The effluent concentration of Se stabilized within 2 h of changing the input concentration (Figure 5.1). The Se removal rate increased by approximately 7.7 mg per 8-h time period for the first 32 h of the experiment, starting at 0.53 mg h^{-1} during the 15 mg L^{-1} input concentration stage, and rising to 1.5 mg h^{-1} during the 60 mg L^{-1} input concentration stage (see Supporting Information). For the remainder of the experiment until the rinse step, the removal rate remained near an average of 1.4 mg h^{-1}. The mass of Se removed increased with each increase in input Se concentration, and therefore the range in F values (C/C$_o$) was less than anticipated (Figure 5.1). Note that the percent removal decreased as the input concentration increased; despite the increasing removal rate, the percent mass removed was almost constant from 16 to 32 h (Figure 5.1).
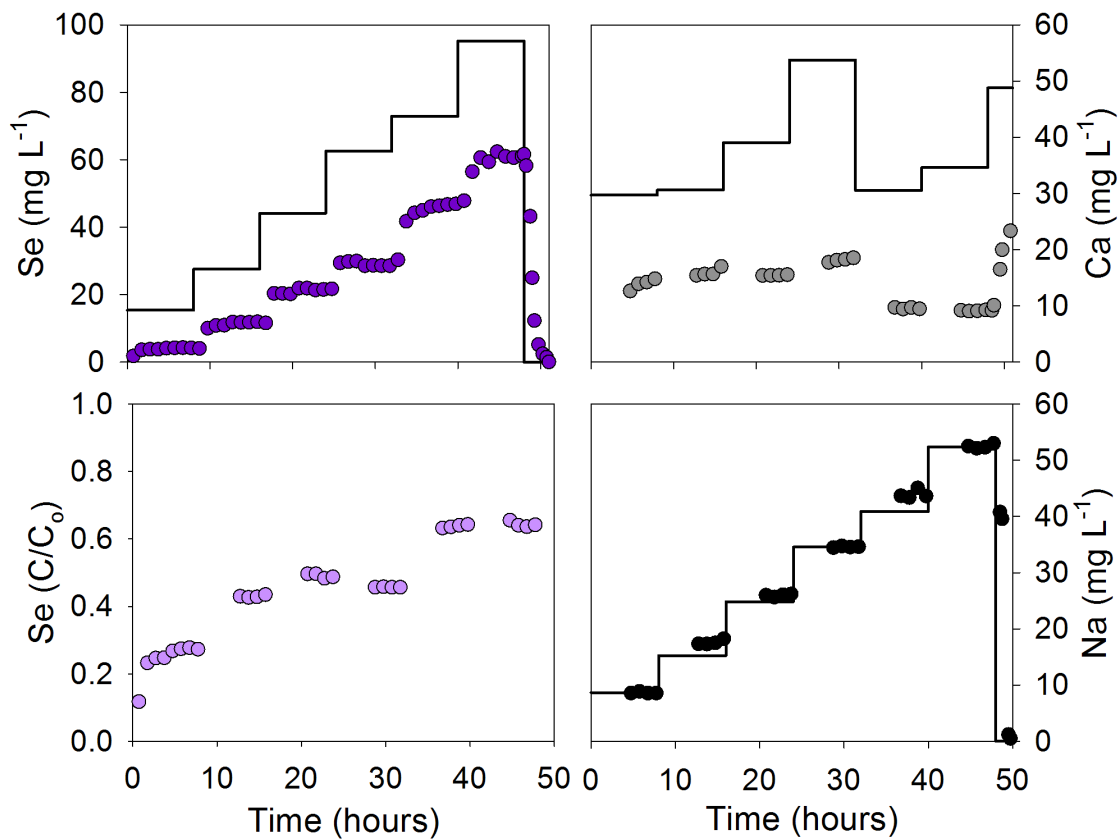
Figure 5.1: Concentrations of Se, Ca, and Na in the input solution (represented by solid black lines), together with effluent concentrations (points), plotted versus time. The input Se and Na concentrations were reduced to zero during the rinse step (started after 48 h).

Selenium concentrations in the effluent during the rinse step gradually decreased as the supply of available Se diminished (Figure 5.1). This rate was slower than could be explained by conservative transport with mechanical dispersion alone, as reflected by the more rapid removal of Na (Figure 5.1).
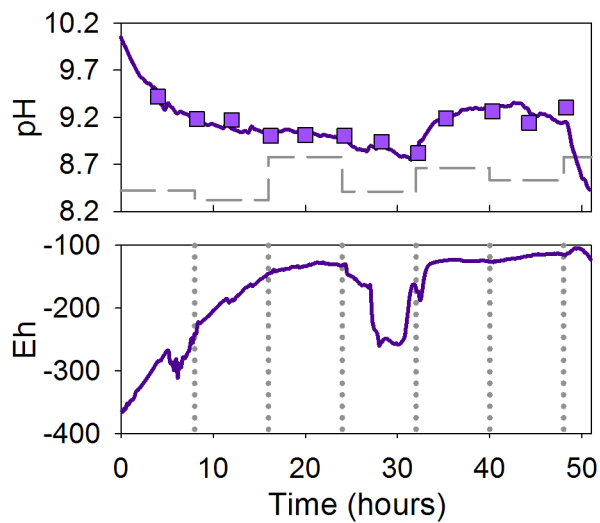
Figure 5.2: pH and Eh micro-electrode measurements of the effluent (solid lines), together with external pH checks conducted periodically on effluent samples (squares) plotted versus time. The grey dashed line represents the pH of the input solution. Vertical dotted lines mark the times when the input solution was changed.

External pH checks were in good agreement with values recorded by the micro-electrode (Figure 5.2). The pH was greater in the effluent than the input solution. Variations in the pH of the input solution did not appear to affect the pH of the effluent. Effluent pH decreased over time, with the exception of a sharp increase and plateau after 32 h. The increase occurred at the same time as a sudden drop in Ca input concentration (Figures 5.1, 5.2). The pH dropped sharply during the rinse step when Se was absent from the solution despite a higher input pH. Eh initially increased, gradually plateaued around 20 h, and exhibited a brief, sharp dip at 27 h (Figure 5.2). Reducing conditions were maintained throughout the experiment. The dip in Eh occurred at the same time as a peak in Ca concentration, a lower input pH, and a lower than expected Se input concentration, which may be related to a longer CO_2 bubbling step for this input solution. Eh remained relatively constant following the change to the Se-free (rinse) input solution.

5.4.2 XAS Results

Spectra were collected continuously, except when measurements were interrupted to allow collection of aqueous samples to prevent excessive evaporation. Because the spectra from the

input, middle, and effluent locations of the FTC could not be collected simultaneously, combined spectra collected at one position were broken into scanning cycles, called 'time steps' for ease of comparison. Each time step was approximately 160 min long. A beamline interruption near the end of the experiment resulted in the loss of three scans at the effluent end of the cell for time step 13.

The peak shape at the input end of the cell was initially most similar to Se(VI) (Figure 5.3), with a small shoulder of more reduced species (Figure 5.3). This shoulder was less pronounced in the middle and effluent end of the cell (Figure 5.3). As the experiment progressed, the shoulder on the left broadened toward the energy level of Se(-I) (Figure 5.3). The general peak shape at the input and center locations did not change much after 13 h had elapsed, whereas the peak shape at the effluent end of the cell remained relatively unchanged after the initial 16 h.

During the rinse step, the prominent Se(VI) peak disappeared, and the scan more closely resembled a combination of reduced Se species, including Se(IV), Se(0), and Se(-I) (Figure 5.3). Spectra similar to the rinse step have been observed when analyzing granular ZVI following batch experiments (Loyo et al. 2008; Shrimpton et al. 2015). Similar products are likely produced under both flow and static conditions, with the differences in spectra during the main FTC experiment derived from the Se(VI) remaining in solution.
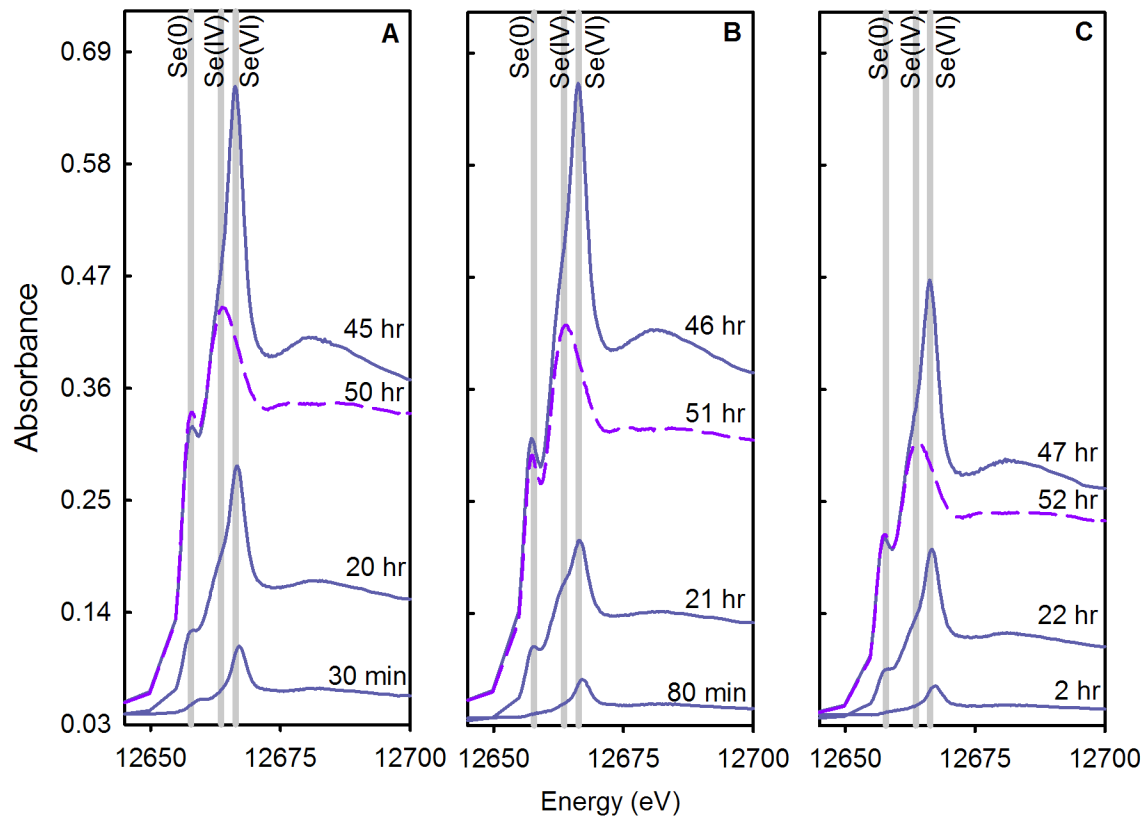
Figure 5.3: Absorbance spectra for the input (A), middle (B), and effluent end (C) of the cell face. The final time point (dashed line) is from the rinsing of the cell with $CaCO_3$-saturated water.

Because the storage ring current remained constant throughout the experiment, the absolute absorbance of the spectra can be used as a proxy for the mass of Se present at each location in the cell. Selenium accumulated mainly at the input end of the cell, but increased at all monitored locations over time (Figure 5.3). The amount of Se in the middle of the cell gradually approached the level observed at the input end, becoming approximately equal prior to the rinse step. Due to the progressive accumulation of Se along the flow path, flow was likely linear rather than well mixed. During the rinse step, the total Se present decreased due to the removal of Se from the input solution. There was a 30 min interruption to the beam shortly after the rinse phase began, so that the initial decrease in Se absorbance and the species present are unknown. However, the total X-ray absorbance decreased by only ~10% during the 3 hour rinse phase, indicating most of the Se was retained on the solid phase, and that the majority of the effluent would be loosely-

72

bound Se and Se(VI) that could not be reduced by the iron during its residence time. More Se remained at the input end than in the middle of the cell during this period, which may be an artifact of the collection of spectra at the input location first.

Linear combination fitting was performed to estimate the proportion of Se in different oxidation states present on the ZVI (Figure 5.4). The standards included were based on the maximum goodness of fit of the reduced chi-squared value. The tetragonal FeSe standard was excluded as it produced a worse fit in all cases. The standards included in the final fit were achávalite (hexagonal FeSe), ferroselite ($FeSe_2$), gray elemental Se, ferric selenite ($Fe_2(SeO_3)_3$), Se(IV) adsorbed onto ferrihydrite (Se(IV) on Fh), sodium selenite pentahydrate ($Na2SeO3 \cdot 5H_2O$), sodium selenate decahydrate ($Na_2SeO_4 \cdot 10H_2O$), and Se(VI) adsorbed onto ferrihydrite (Se(VI) on Fh). Adsorbed protonated Se has a visibly different peak when compared to $NaSeO_4$, and $Fe_2(SeO_3)_3$ has a visibly shifted peak from both Na_2SeO_3 and SeO_3^{2-} adsorbed onto ferrihydrite (See supporting information), so these two SeO^{2-}-containing species could be differentiated. For spectra collected at the beginning of the experiment, the best fit was usually found to contain all standards except achávalite. Toward the end of the experiment, Se(VI) was found to be more exclusively in an adsorbed state.
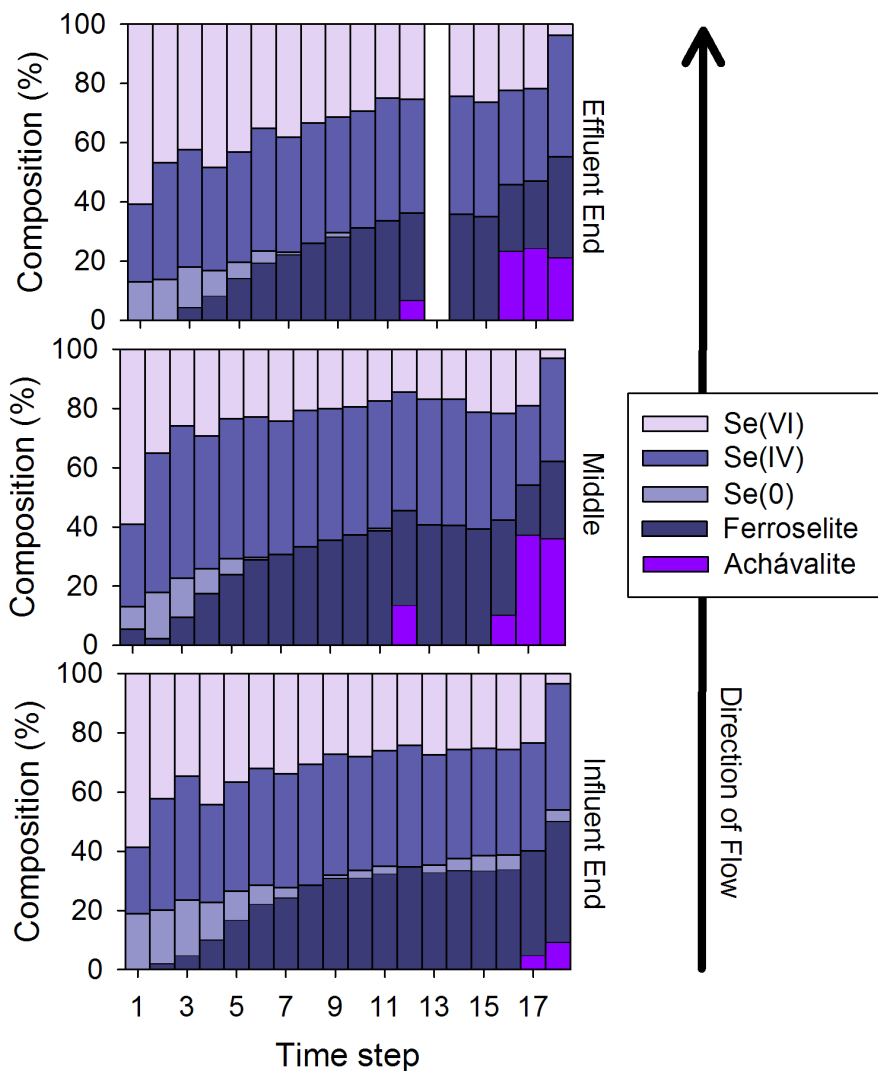
Figure 5.4: Linear combination fitting results from the influent, middle, and effluent end of the cell. Each time step was 160 min. Step 18 represents the rinse phase.

The oxidation states present were similar at all three cell locations (Figure 5.4); the composition was initially ~60% Se(VI), decreasing to ~20% over the experiment despite the introduction of increasingly higher concentrations of aqueous Se(VI). The Se(VI) was most similar to $Na_2SeO_4 \cdot 10H_2O$ at early times, but more strongly resembled Se(VI) on Fh by the fifth time step (14 h). The amount of Se(IV) in adsorbed form was relatively small compared to the amount of $Fe_2(SeO_3)_3$. However, removing the adsorbed Se(IV) from the fitting parameters

74

decreased the goodness of fit. The proportion of $Fe_2(SeO_3)_3$ steadily increased to ~40% until the eighth time step (22 h), at which time it decreased to ~35% until the end of the experiment. The proportion of $Fe_2(SeO_3)_3$ increased during the rinse step. Importantly, an adsorbed form of Se(IV) was likely present in this system, as selenite is known to adsorb onto Ca before being further reduced in Ca-Fe systems (Chakraborty et al. 2010).

Despite the multiple increases in aqueous Se(VI) concentrations in the input, the proportion of Se(VI) present remained constant after 16 h had elapsed, except at the effluent end of the cell. The relative proportions of most species present became constant after 32 h had elapsed, with the exception of the first appearance of achávalite in the system at this time. The abundance of Se(VI) declined during the rinse step, suggesting the signal was either from aqueous Se(VI) or Se(VI) loosely bound to the solid phase.

The percentage of Se(0) decreased as the experiment progressed (Figure 5.4). Elemental Se is expected to be the subsequent reduction product after Se(IV)(Kang et al. 2013). Se(0) was likely constantly produced throughout the experiment, but contributions by other products far exceeded the mass of Se(0) over the course of the experiment and thus it was not as abundant at later time steps.

At the end of the experiment, the greatest proportion of achávalite was found in the middle of the cell (Figure 5.4). This accumulation may have occurred because the reduced Se front had reached this area at the end of the experiment, and because sufficiently strong reducing conditions did not develop closer to the input end of the FTC. At the beginning of the experiment, $FeSe_2$ was only present in the middle of the cell and is perhaps another indication that the most strongly reducing conditions existed at this location.

5.4.3 Isotope Results

A variety of F values were obtained by altering the concentration of the input solution, resulting in smaller fractions remaining in the effluent solution with higher $\delta^{82/76}Se$ values earlier in the experiment. Although Se(VI) was not separated from Se(IV) prior to isotopic analysis of the aqueous samples, it is probable that Se(VI) was the dominant species in solution during the

75

first stage of the experiment, as Se(IV) sorption in $CaCO_3$ iron systems is rapid (Chakraborty et al. 2010; Shrimpton et al. 2015). Plotted as a fraction of the input concentration (F) versus $\delta^{82/76}Se$, the aqueous Se isotope data are best fit by a straight line (y = -9.64x + 9.70, R^2 = 0.983; Figure 5.5), yielding an isotopic separation of approximately 9.6‰. Experiments with fractionation of the same magnitude include 11.1‰ for reduction by green rust (Johnson 2012) and 9.6‰ for removal of Se(IV) by FeS_2 (Mitchell et al. 2013). A Rayleigh model was not used because some of the assumptions are violated (e.g., closed system, single-step reaction), and it yields a poor fit (ε = 6.3‰, R^2 = 0.827).
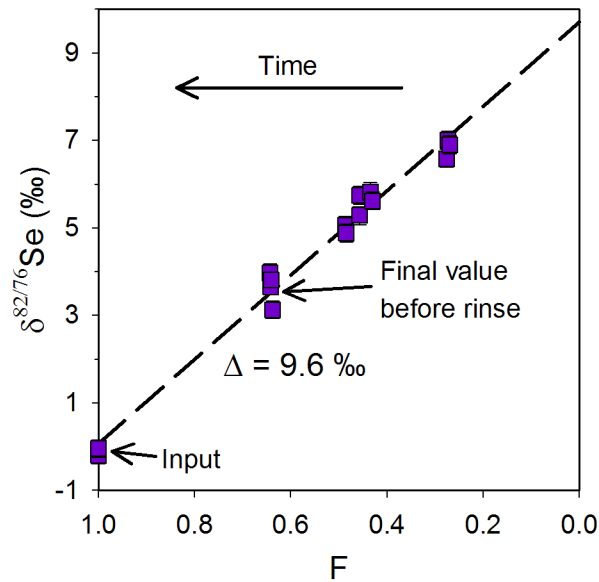
Figure 5.5: Stable isotope results for aqueous Se from the effluent, relative to NIST SRM3149, as a function of F.

Following the initial increase in removal rate, the capacity for removing Se(VI) for a given flow rate changed little over time. Increasing the mass of dissolved Se(VI) in the input solution increased the F value because the ZVI reduced a smaller proportion of the total Se(VI) initially present. Because the ZVI only removes a certain mass of Se, a 'mixing line' is produced between the $\delta^{82/76}Se$ value for the input and the theoretical $\delta^{82/76}Se$ value for 100% reduction; mixing lines are linear, so the $\delta^{82/76}Se$ values have a largely linear trend.

During the rinse step, the $\delta^{82/76}$Se value increased exponentially as the Se concentration gradually decreased in solution (Figure 5.1, 5.6). The loosely bound Se and adsorbed Se displaced from surface sites were likely flushed out of the cell by the Se-free solution during the rinse stage.
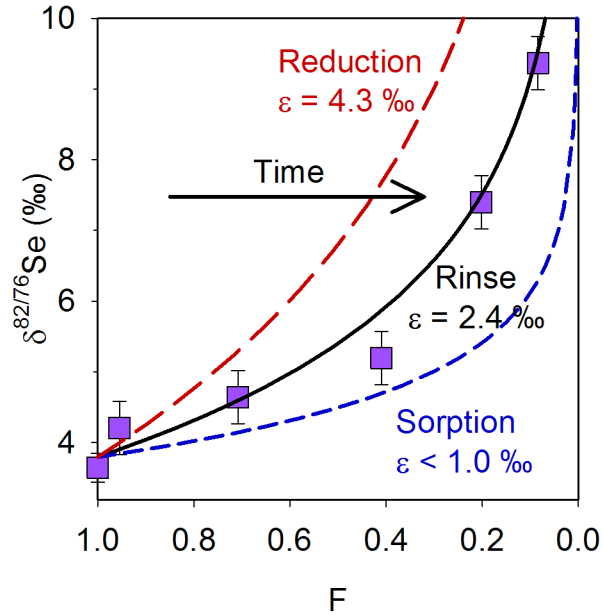
Figure 5.6: Selenium $\delta^{82/76}$Se isotope values from the rinse step. Fraction of total Se remaining in solution (F) was calculated based on the maximum concentration of the effluent before starting the Se-free rinse.

A lower value for $\delta^{82/76}$Se in the effluent compared to the input solution would indicate the re-mobilization of previously reduced, isotopically lighter Se (Johnson 2012). In contrast, if Se(VI) was being retarded and reduced in its exit from the FTC, isotopic ratios should exhibit fractionation with increasingly positive $\delta^{82/76}$Se values. Both Se(VI) and Se(IV) may be present in the effluent during the rinse, which could also result in a lower effective fractionation, or the amount of fractionation actually measured in the system. As the effective fractionation of 2.4‰ is between that of Se adsorbing to iron hydroxide minerals (1.00‰) and that of reduction by ZVI in a $CaCO_3$ saturated system (4.3‰) (Mitchell et al. 2013; Shrimpton et al. 2015) (Figure 5.6), both processes are likely occurring at this stage of the experiment. It is possible that the slope of the curve of best fit is being repressed due to a small amount of dilution of incoming Se-free

water as the remaining Se is retarded on its exit from the FTC. Dilution would result in an actual fractionation factor higher than 2.4 ‰, but the degree of dilution or potential of reduced mass being removed from the solid is difficult to calculate for this system.

5.5 Implications

Selenium isotope ratios, in combination with analysis of the solid phase characterization, can be used to determine processes occurring in the field where Se is being treated using ZVI. Additionally, ZVI will retain most previously fixed Se during short-term changes in aqueous geochemistry. Even systems measured in a controlled laboratory setting may be complex, and the isotopic fractionation controlled by more than one mechanism. While an effective fractionation can be determined from such data using models, it is important to note they do not describe a single mechanism, but rather a combination of mechanisms. Fractionation factors calculated from field data are likely also influenced by multiple mechanisms, and complimentary techniques could be used to help identify reaction mechanisms. For instance, the fractionation of 2.4 ‰ from the rinse step is similar to the fractionation of Se during reduction in groundwater with high concentrations of $CaCO_3$ ($\varepsilon = 2.3$ ‰) (Basu et al. 2016). Future studies including the effect of organic matter and other elements that may affect Se removal in the environment should be conducted to better elucidate which mechanisms could have a significant impact on Se isotope ratio measurements from field samples.

5.6 Supporting information (see appendix A)

Contains additional information on ZVI characteristics, methods for correcting isotopic interferences, the flow rate, removal rate calculations, spectra of the Se standards, and normalized spectra over time for the influent, middle, and effluent end of the flow-through cell.

Chapter 6: Selenium isotope fractionation in groundwater: a field study of a 65-year-old selenium plume

6.1 Abstract

Unintentional release of Se from the former Kennecott Utah Copper refinery site over a 45-year period resulted in the development of a plume of Se-bearing groundwater migrating from the source area toward a wetland complex adjacent to the Great Salt Lake. Selenium isotope data were combined with geochemical data and mixing models to interpret the mechanisms affecting Se transport at the site. Changes in Se isotope ratios along the length of the plume were observed, with $\delta^{82}Se$ = -26‰ upgradient of the source area, 1.3 – 2.3‰ within the source, and as high as 8.7‰ at the tip of the plume. Comparisons between the degree of Se isotope fractionation derived from previous laboratory studies and the trends in isotope ratios at the field site were used to infer processes controlling Se transport. These inferences are consistent with redox measurements. Most changes to $\delta^{82}Se$ values (1.3 – 3.4‰) and dissolved Se concentrations over the length of the plume can be explained by a combination of adsorption and dispersive dilution. Lower than expected $\delta^{82}Se$ values along the edge of the plume, in deep wells, and above the plume are attributed to dispersive mixing of plume water with low concentrations of Se remobilized from the solid phase. Sharp increases in $\delta^{82}Se$ values, which correspond with declines in dissolved Se concentrations under the wetland complex, are indicative of reductive processes in this area.

6.2 Introduction

Selenium is a micronutrient that is chronically toxic when ingested at high concentrations (> 400 µg per day) (Schilling et al. 2014). As a consequence of Se bioaccumulation, concentrations within former regulation limits have the potential to be fatal to various aquatic fauna and waterfowl (Hamilton 2004; Lemly 2004; Van Dyke et al. 2013). Fish are sensitive to Se exposure, which can cause liver and gill damage (Gobi et al. 2018), as well as reproductive failure or deformation of the young (Lemly 2002). Aquatic bird species can also experience reproductive failure and teratogenic effects (Hamilton 2004). Reptiles and amphibians can also

79

accumulate Se in their ovaries, although they are reported to be less sensitive than fish to Se contamination (Young et al. 2010; Van Dyke et al. 2013).

Selenium is normally rare in the natural environment, with aqueous concentrations generally in the ng L^{-1} range. Natural systems typically have Se concentrations below the water quality guidelines, *e.g.*, the Canadian water quality guideline for protection of aquatic life (1 µg L^{-1}, CCME, 2016), or the US EPA aquatic life criterions (3.1 µg L^{-1} for lotic systems, 1.5 µg L^{-1}, for lentic systems, Beauvais, 2016). However, Se can be released at higher concentrations through a variety of anthropogenic activities including mining, smelting, refining, agriculture, coal-combustion, and the excavation of Se-rich shales (Lenz and Lens 2009; Winkel et al. 2012; Morrison et al. 2012). Selenium is most commonly present in the environment as Se(VI), which forms the highly mobile oxyanion, selenate (SeO$_4^{2-}$). Reduction to Se(IV) (selenite, SeO$_3^{2-}$ and hydrogen selenite, HSeO$_3^{-}$), elemental Se (Se^0), or selenide (Se^{2-}) can decrease Se mobility or solubility and remove it from solution (Zhang and Sparks 1990; Fernández-Martínez and Charlet 2009; Pettine et al. 2015). High concentrations of organic carbon and anoxic conditions are both conducive to Se(VI) reduction and removal of dissolved Se (Fernández-Martínez and Charlet 2009). Selenite can also adsorb to many compounds found in soil or sediment. The extent of adsorption is dependent on the pH, with adsorption increasing significantly below pH 7 up to a pH of 5 for clay- and iron-bearing soils; the presence of calcite can increase this range as high as 9 (Neal et al. 1987; Goldberg and Glaubig 1988; Cowan et al. 1990; Goh and Lim 2004). Adsorption of Se(IV) to Fe, Al, and Mn minerals is also greater at lower pH (Xu et al. 2020). Bacteria and fungi can reduce Se, providing an additional pathway for natural sequestration (Schilling et al. 2011b; Nancharaiah and Lens 2015).

6.3 Selenium Isotope Fractionation

Selenium occurs as six stable isotopes: 74, 76, 77, 78, 80, and 82. Measurements of Se stable isotope ratios can be used to infer the mechanisms controlling Se concentrations in field systems (Schilling et al. 2015; Basu et al. 2016). During reduction of Se(VI) to any lower oxidation state, the heavier isotopes of Se preferentially remain in the more oxidized form, due to differences in bond energies (Wiederhold 2015). Reduction experiments in laboratory have resulted in a large

amount of fractionation ($\varepsilon > 3.0$ ‰; Johnson 2012; Shrimpton et al. 2015; Schilling et al. 2020). Fractionation of selenium has not been observed in association with diffusion or dilution of the aqueous phase (Johnson and Bullen 2004). Adsorption causes fractionation, but to a lesser extent than reduction ($\varepsilon < 1.0$ ‰; Johnson 2012; Xu et al. 2020). There is minimal fractionation due to adsorption onto clay minerals (Xu et al. 2021). Therefore, pore water containing heavier Se isotopic ratios relative to a source may be indicative of reduction. Oxidation of Se-bearing minerals can also cause heavier aqueous Se isotopic ratios relative to the mineral when coupled with Se(IV) adsorption, but the Se concentration in solution will also increase (Wasserman et al. 2021). The methylation of Se can produce a volatile product, resulting in aqueous isotopically lighter signatures (Schilling et al. 2011b).

Previous studies have examined Se isotope fractionation in wetland environments, or groundwater affected by selenium present in shales. Changes in stable Se isotope ratios were correlated to biochemical processes occurring in the subsurface in the soils at a seleniferous site in India (Schilling et al. 2015). Selenium isotope ratios have also been used to infer redox conditions in groundwater around a uranium roll front (Basu et al. 2016). Given the potential application of Se isotope measurements to assess Se impact on ecosystems, it is important to further constrain how Se isotope measurements can serve as a tool for interpreting reaction pathways in the subsurface.

Prolonged release of dissolved Se and the development of a well-defined plume of Se-bearing groundwater at the former Kennecott Utah Copper Refinery field site provides a unique opportunity to evaluate the potential of Se isotope ratios as a remediation or monitoring tool. This study focuses on whether Se isotopes can be used to identify reaction processes, and assess whether reduction and subsequent immobilization are occurring, or if changes in Se concentrations are due to dilution or other processes.

6.4 Site Description

The study area is located at the base of the northern slope of the Oquirrh Mountains, Utah, about 3.2 km south of the Great Salt lake (GSL), and 800 m south of the Garfield Wetlands, a

sensitive wetland system (Kennecott Utah Copper 2013). Previous activities at the site included refining of Cu, Ag, and Au concentrates, and disposal of both mill tailings and slag (US EPA 2002). The principal sources of dissolved Se at the site were the former electrolyte purification (EP) pond associated with the refinery, and the former Precious Metals (PM) building (Figure 6.1) (Kennecott Utah Copper 2013).
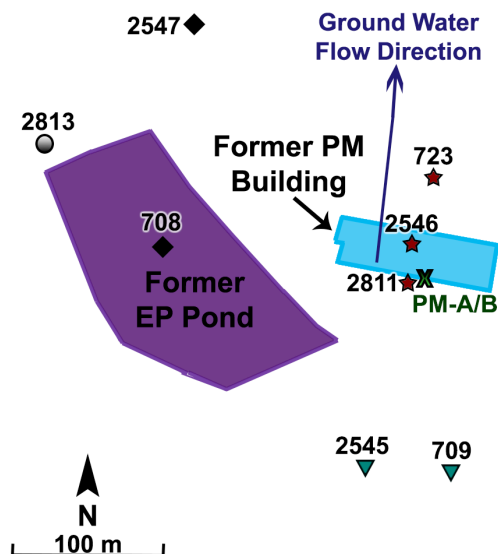
Figure 6.1: Map view of source zone region and monitoring well identifications. Diamonds are EP source wells, stars are PM source wells, triangles are wells screened outside or at the edge of the main plume body, and circles are wells screened within the main plume body.

Operations in PM building continued from 1950 to 1995, prior to demolition in 1996 (Kennecott Utah Copper 2013). During this period, large quantities of Se were unintentionally released to the subsurface, primarily via leaks in a Se-recovery circuit at the PM building. Leakage from the EP pond contributed to the Se in the subsurface during its operational lifespan from 1950 until 1974. Approximately 400 times more Se was released under the former PM building than from the former EP pond, most of which came from changes to the refinery made in 1986 (Golder 2018). During decommissioning and associated remedial efforts, substantial quantities of contaminated sediment were excavated and removed from both of these source zones, and low permeability caps were installed to inhibit the vertical infiltration of rainwater

and prevent re-mobilization of Se remaining in the vadose zone. Although Se concentrations have decreased significantly from the pre-remediation levels (Kennecott Utah Copper 2013), the rate of decline in groundwater was lower than anticipated compared to modeling conducted during the original remediation feasibility study (Kennecott Utah Copper 2013). Geochemical and hydrogeological investigations indicate that the vadose zone and deep sediment at the former PM building and at the former EP pond continue to be sources of ongoing release of Se to the groundwater flow system due to lateral groundwater recharge through these regions (Kennecott Utah Copper 2013).

Although the permeability of the reclamation caps was demonstrated to be within design parameters, subsequent modeling and physical examination of the caps suggested the potential for infiltration (Golder 2018). Prior to remediation efforts, flow into the subsurface was assumed to be vertical. Post remediation, vertical infiltration occurs outside the capped region, accompanied by lateral flow under the cap in response to seasonal precipitation patterns. The Se contaminant plume migrates from the vicinity of the EP pond and PM building north- and downward, through lacustrine material, gravel, and fractured bedrock, which consists of calcium carbonate coated quartzite and limestone, before discharging immediately south of the wetland area (Figure 6.2, 6.3). The Se plume does not extend as far as the GSL due to local hydrogeological conditions, which includes lateral groundwater density (brackish water wedge pushing the plume up as it approaches the wetland), active remediation, and natural attenuation. Due to the natural downward gradient at the source zone, combined with the high density of the processes water, and recharge from storm water runoff, the contaminant plume extends at least 165 m (547 ft) into the aquifer. In addition, the plume was pulled north and deeper by a high intensity of pumping at the Garfield wells (located in the Garfield Wetlands area), which largely came to a halt in the 1990s. Groundwater then flowed to the North-Northwest in the vicinity of the wetland area (Figure 6.2). The construction of a new tailings impoundment and deposition of tailings to the east of the plume may have directed the flow further to the west due to its presence as a hydrogeological barrier, not through contribution of groundwater seepage.
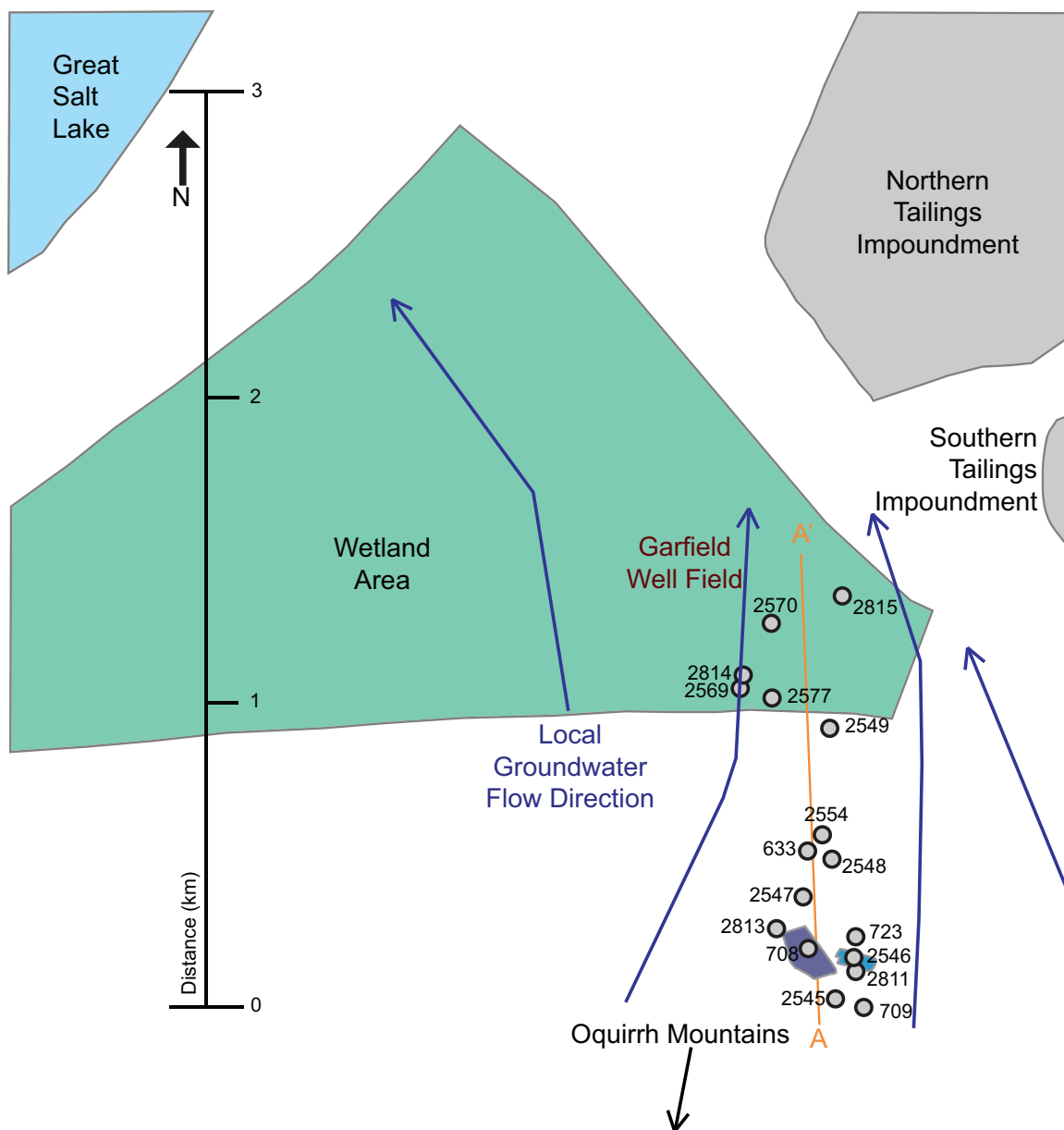
Figure 6.2: Map view of field site and monitoring well identifications. The wetlands area lies within the green shaded region. Blue groundwater flow direction arrows are drawn from 2013 density corrected potentiometric lines. Cross section A-A' is shown in figure 6.3.

The source zones in the vadose zone are characterized by different aqueous and solid Se concentrations, as well as different solid phases. Solid Se concentrations of greater than 5,000 mg kg^{-1} are observed 3.0–6.1 m below the former PM building (Golder 2018). The maximum

measured Se concentration in the sediment (14.98 g kg^{-1}) was observed between 4.6 and 9.1 m (15 and 30 ft) below ground surface. At this location, the highest historical dissolved Se pore water concentration (1936 mg L^{-1}) was measured in a sample taken from 4.6 m (15 ft) below ground surface in 2012 (Kennecott Utah Copper 2013). The dissolved Se is almost entirely present as Se(VI), with less than 1% Se(IV). Measured concentrations in the vadose zone at these locations have fluctuated over time, but are, on average, decreasing (Golder 2018). Nearby groundwater wells had much lower aqueous concentrations of 9.77 mg L^{-1} and 3.21 mg L^{-1} in wells 2546A and 2811A, respectively. Selenium in the solid phase is found as both crystalline and amorphous Se(0), associated with Fe oxide minerals, Fe silicate minerals, and Se metal or metal oxide compounds (e.g,, Se-Ag, Se-Te, and Pb-Se-Te-Cu oxide complexes; Golder, 2018).
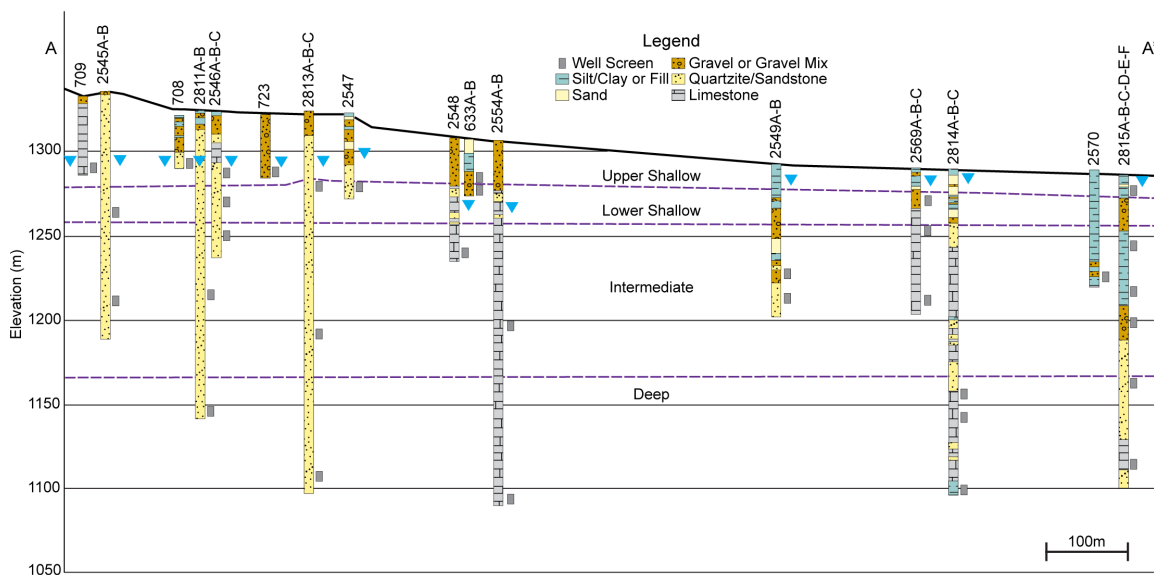
Figure 6.3: Relative position of and lithology at the wells along the flow path, as well as screen depth. Dashed lines separate the aquifer zones. Blue triangles indicate 2012 water levels at the depth of the shallowest well screen. Position of cross-section is indicated in Figure 6.2.

Lower Se concentrations were measured in the soil at the former EP pond site, with contaminated soil of concentrations greater than 1,000 mg kg^{-1} observed at 3.0–10.7 m (Golder 2018). A maximum concentration of 2.8 mg kg^{-1} was observed 6.7 m to 13.7 m (22 to 45 ft) below ground surface in the solid phase. The maximum dissolved Se concentration (1.99 mg L^{-1})

associated with the former EP pond site was observed in a vadose zone sample collected from a deep solid-water suction lysimeter 9.3 m (30.5 ft) below ground surface. The groundwater Se concentration at this location is 3.6 mg L^{-1}, collected in 2013 from well 708. Colloidal Se compounds (including Se(0)), and smaller quantities of adsorbed Se associated with Fe oxide minerals, phosphate, or barium sulfate, are the principal forms of Se below the former EP pond area.

Table 6.1: Redox classification for wells in the source region, the intermediate (refinery) region, or the wetlands region. Wells with no 2016 redox measurements are not listed.

Well	Redox Conditions	Aquifer Zone
2545A	oxic	lower shallow
708	Fe-reducing	upper shallow
2811A	Fe-reducing	intermediate
2811B (no isotopes)	sulfidic	deep
2546A	Fe-reducing	upper shallow
2546B	oxic	lower shallow
723	oxic	upper shallow
2813A/B	Fe-reducing	lower shallow/ intermediate
633A/B	Fe-reducing	shallow (upper/lower)
2549A/B	oxic	intermediate
2554A	Fe-reducing	intermediate
2554B	Fe-reducing	deep
2548	Fe-reducing	intermediate
2577 (Kessler Spring)	Fe-reducing	shallow
2569A	oxic	lower shallow
2569B	Fe-reducing	intermediate
2814A/B	'oxic' (possible error)	deep
2815E	Fe-reducing -> sulfidic	deep
2810F	Fe-reducing -> sulfidic	deep

The redox zones in the region were delineated comprehensively in 2016 (Golder 2018), 3 years after isotope sample collection. Zones were classified based on the presence or absence of various components, such as oxygen (oxic), Fe(II) and/or ammonia (Fe-reducing), and dissolved

H$_2$S (sulfidic), rather than by using oxidation-reduction potential (ORP) measurements, which were often less accurate. A list of wells with redox zones and screen depths has been compiled from Golder (2018) (Table 6.1). In summary, the shallow groundwater source zone is oxic, becoming sulfidic at greater depths. Beyond the source area, wells are generally oxic or Fe-reducing, whereas wells in the wetland region tend to be either Fe-reducing or sulfidic. Reduction of Se(VI) to Se(IV) can occur under Fe-reducing conditions provided dissolved NO$_3^-$ concentrations are limited (Lenz and Lens 2009), leading to the retardation of Se transport via adsorption processes (Tullo et al. 2016). Sulfidic conditions could lead to complete removal of Se from solution by forming insoluble or volatile Se(0), metal Se(-II), or other Se(-II) species (Lenz and Lens 2009).

6.5 Material and Methods

6.5.1 Sample Collection and Storage

Wells were selected for sample collection based on historical Se concentrations and their location along previously determined past and current flow paths of the contaminant plumes (Figure 6.2, 6.3). Samples were collected from these wells in 2013, filtered (0.45 μm), and refrigerated prior to transport. Samples were shipped in one-gallon plastic bottles inside a chilled sample container, and promptly refrigerated upon arrival at the University of Waterloo. The pH, conductivity, total dissolved solids (TDS), and the concentration of Se were determined at the time of sample collection, (Kennecott Utah Copper 2013). The concentration of Se in the samples was confirmed using inductively coupled plasma optical emission spectroscopy (ICP-OES, Thermo ICAP) after the samples arrived at the University of Waterloo. Additional lysimeter samples PM-A and PM-B were collected and sent to the University of Waterloo in 2014. Total Se concentrations and Se isotope ratio measurements were made within 1 month, and 1-6 months of sample collection, respectively.

6.5.2 Sample Purification Method

The method for the purification of samples was similar to that used for previous studies (Shrimpton et al. 2015, 2018). Samples were allowed to warm before the dilution and reduction

steps preceding the purification method. Samples were spiked with ^{77}Se and ^{74}Se prior to purification to account for fractionation during sample preparation and measurement (Zhu et al. 2008). Samples were purified using thiol cotton fiber (TCF) (Rouxel et al. 2002). Enough sample volume was used to load 1.2 µg of Se on the TCF. The extraction steps used were similar to those of others (Elwaer and Hintelmann 2008), with the exception that only 0.1 g of TFC was loaded onto 1 mL columns (Layton-Matthews et al. 2006; Shrimpton et al. 2015). Samples were filtered using 0.45 µm syringe filters before the final reduction step to remove any remnant TCF and thereby prevent Se(IV) from re-adsorbing. Interferences due to sulfur and remaining organic compounds released from the TCF were resolved by using blanks that had been run through TCF columns. Samples were diluted to 2 M HCl and 80 µg L^{-1} Se with ultrapure water then left to sit for at least 18 hours prior to analysis to allow volatile species to degas and Kr levels to reach equilibrium with the atmosphere. Doing so dramatically improved measurements, and decreased the number of corrections required.

6.5.3 Isotope Measurement

Samples were analyzed using a hydride generator (LI-2 system, CETAC) coupled to a Neptune inductively coupled plasma mass spectrometer (Thermo Finnigan, HG-MC-ICP-MS). The use of a hydride generator boosts signal intensities, and reduces interferences caused by chloride ions, among others. Interfering species that must be corrected for include the Ar-Ar dimers, ArCl, Kr, Ge, as well as Ge-, As-, and Se-hydrides (Elwaer and Hintelmann 2007; Stüeken et al. 2013). Delta values are reported relative to the NIST SRM 3149. Details of instrument set up can be found elsewhere (Shrimpton et al. 2015, 2018).

6.5.4 Mass-balance Modeling of Isotopic Fractionation

Mass balance modeling of isotopic fractionation is discussed in Appendix B.

6.6 Results

6.6.1 Groundwater Geochemistry

The concentration of total dissolved solids increases away from 476 mg L^{-1} behind the source (Figure 6.4) to 6910 mg L^{-1} near GSL (not shown). The highest TDS measurements in the source zone area occur in wells associated with the former EP pond (wells 708 13.6 g L^{-1}, 2813A 1140 mg L^{-1} and B 3670 mg L^{-1}), and the wells surrounding the former PM building (wells 2811A 1960 mg L^{-1} and 723 1740 mg L^{-1}). Conductivity is highest in well 708 and low elsewhere in the source areas (Figure 6). The conductivity remains comparatively low in the 2569 well nest (Figure 6).
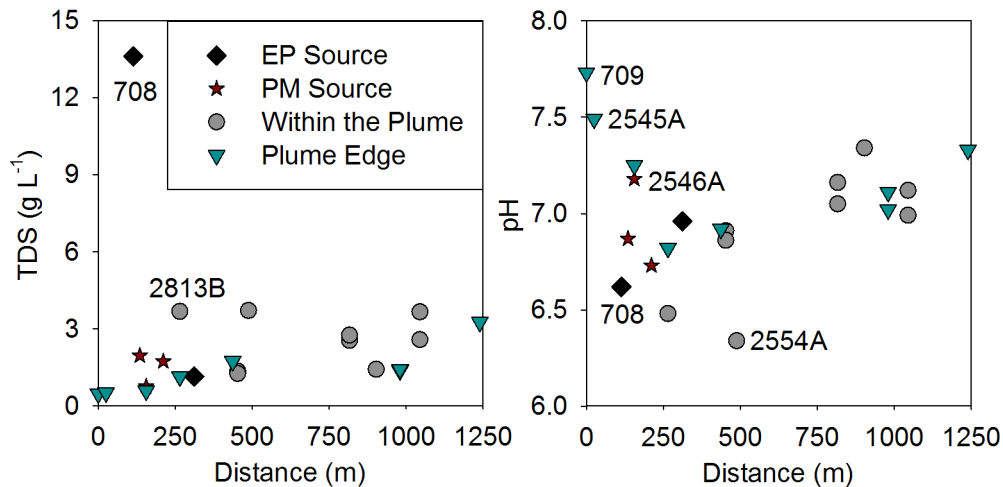
Figure 6.4: The TDS and pH measured in well samples along the length of the plume. The wetlands begin at approximately 900m.

The pH of the ground water is near neutral throughout the plume (Figure 6.4). The pH is higher (7.8 – 7.5) upgradient of the source zone and in the lysimeter samples. In source zone wells, and up to 600 m downgradient, the pH is more variable (7.5 – 6.3). The pH increases (to pH 7 or higher) in wells further downgradient from the source.

89
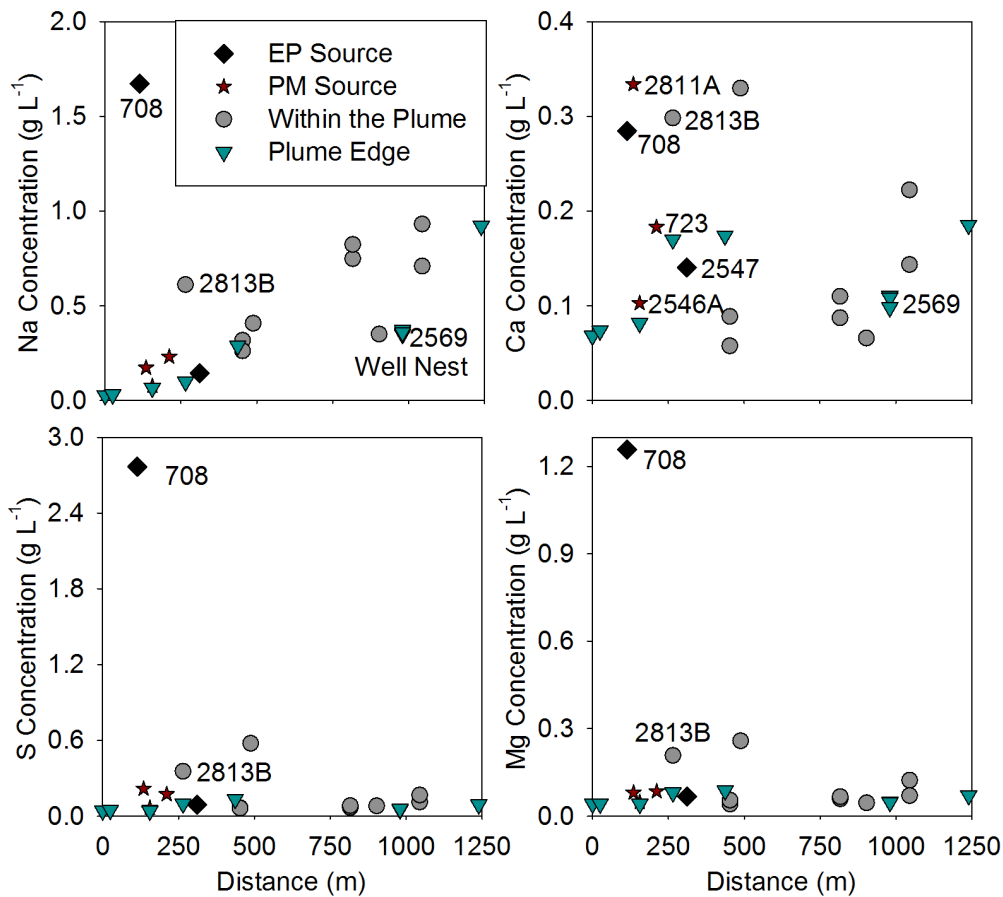
Figure 6.5: Concentration of major cations in wells along the length of the plume.

The groundwater chemistry varies depending on the depth of the well screen, the lithology at the position of the well screen, and proximity to the GSL (Figure 6.5). Similar to the TDS the concentrations of most major ions increase along the flow path after initially decreasing including Na (26 – 2138 mg L^{-1}), Ca (57 – 956 mg L^{-1}), Mg (40 – 1258 mg L^{-1}), and S (123– 8282 mg L^{-1}; as SO$_4^{2-}$) (Figure 6.3-6.5). Minor elements that also follow this trend include K (0 – 64 mg L^{-1}), Si (6.5 – 19 mg L^{-1}) and Sr (0 – 5 mg L^{-1}) (Figure 6.6). The elevated concentrations of Na, S, Mg, Ca, and Sr present in well 708 (EP source area), differ from nearby wells.
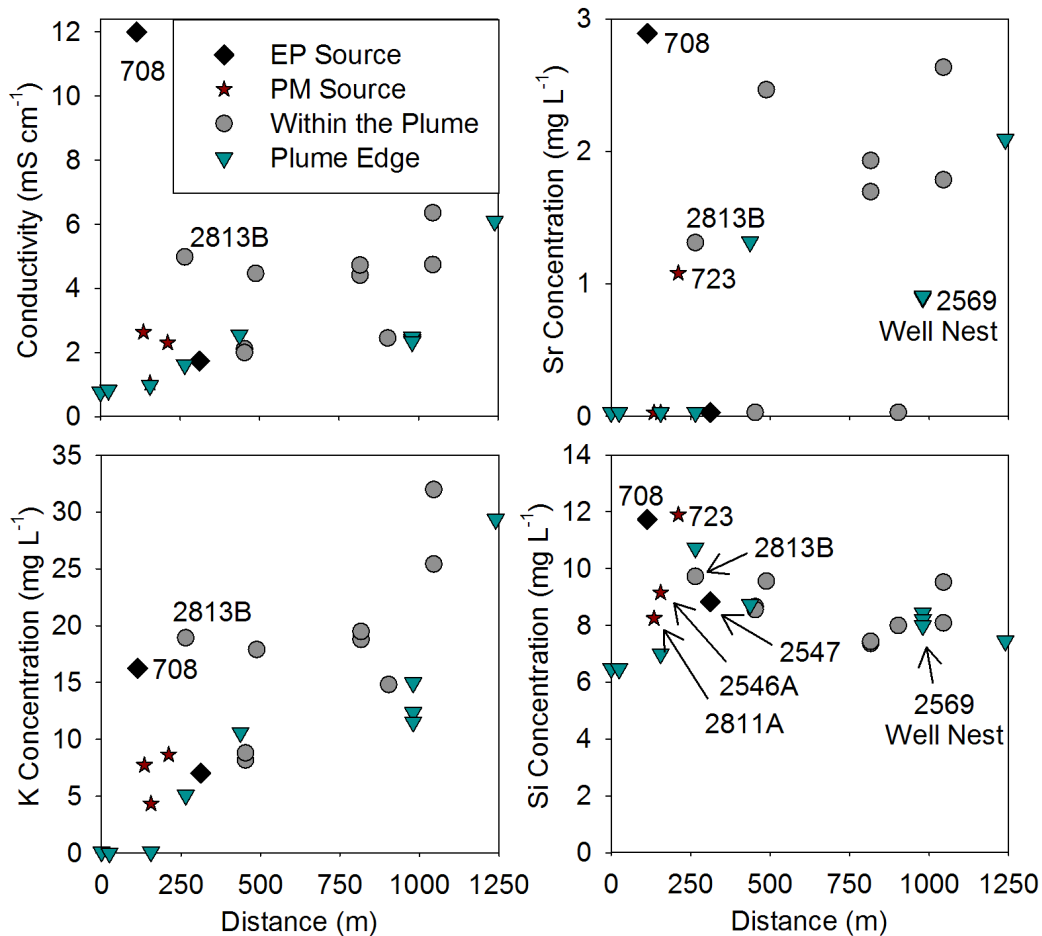
Figure 6.6: Some of the minor elements in well samples taken from along the length of the plume. The wetland area begins at approximately 900m.

Dissolved silica concentrations generally decrease downgradient from the source zone, with the highest concentrations observed at well 708, located in the EP source area, and well 723, in the PM source area (Figure 6.6). Strontium concentrations are highest in the most downgradient wells, and are variable elsewhere (Figure 6.6). Potassium concentrations gradually increase with proximity to the GSL and are also comparatively elevated in wells 708 and 2813B.

The concentration of Se decreases with distance downgradient from the source zones (Figure 6.7). In addition, the concentration of Se in groundwater derived from the source zone has varied over time due to remediation efforts and fluctuations in recharge rates (Kennecott Utah Copper 2013; Golder 2018). Lysimeter samples collected at the time of this study show the Se

concentrations in vadose zone porewater at the PM building location are much higher than normally found in nature (typically < 1 µg L^{-1}), with concentrations of 1.66 g L^{-1}, and 0.090 g L^{-1} at PM-A and PM-B respectively. Wells upgradient of the source zone have lower (103 - 149 µg L^{-1}) concentrations of Se, though they are still more than 100 times higher than Se concentrations in filtered surface water samples from the GSL (0.4 – 1.2 µg L^{-1} between 2002 and 2011) (Adams et al. 2015). Pockets of lower Se concentrations are also observed closer to the source, often where well screens are much deeper in the subsurface (Figure 6.3). Wells on the margin of the plume with shallow well-screens also have lower Se concentrations (≤ 1 mg L^{-1}).
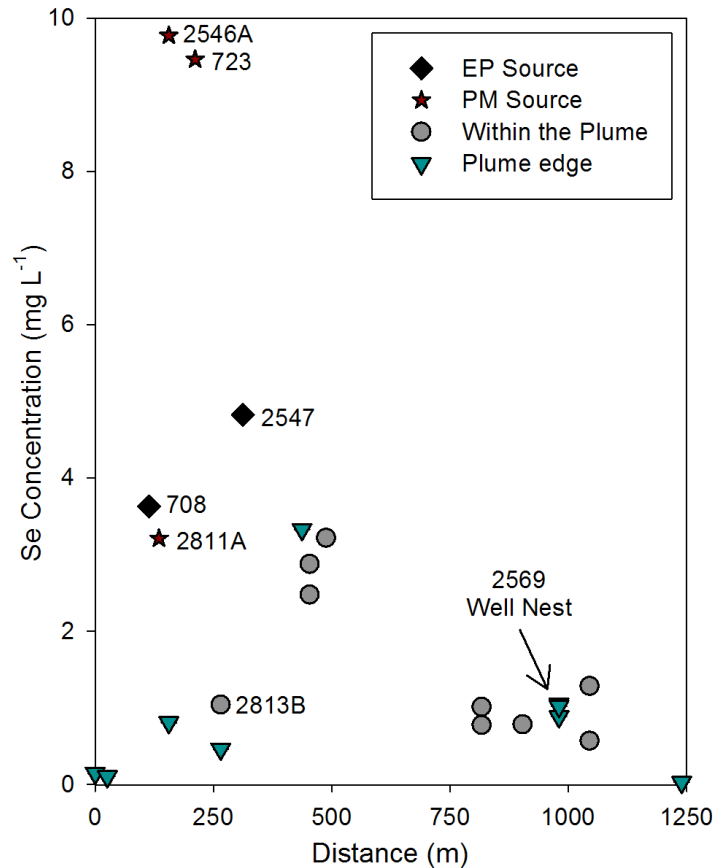
Figure 6.7: Concentration of selenium in groundwater from various depths along a cross-section. The wetlands begin at approximately 900m.

Selenium speciation studies conducted in 1998-2000 and 2010 indicated that most aqueous Se is in the form of Se(VI), with some wells occasionally containing more than 50% Se(IV), likely

coinciding with the presence of more reducing conditions at these locations (Kennecott Utah Copper 2013). Measurements from 2010 indicated that samples from deep groundwater wells in the source zone contained less than 2% Se(IV). Although less than 1% of the dissolved Se from lysimeter samples in the vadose zone occurs as Se(IV), this would be up to 0.897 mg L^{-1} of Se(IV) at PM-B. High masses of Se are also associated with the soils at the former PM building (1.99 – 14.90 g kg^{-1}; Kennecott Utah Copper, 2013).

Significant concentrations of Se(IV) are present at the 2569 well nest (Figure 6.3) located underneath the wetland area, with Se(IV) representing between 0.47% and 83% of the total Se at well 2569A (17-23 m bgs) and to 5.6% to 99% at 2569C (71-77 m bgs), and between 0.11% and 11% in 2569B (34-40 m bgs) (Kennecott Utah Copper 2013). These measurements from 2010 are inconsistent with the redox measurements from the 2569 well nest, which had an oxic classification in 2016 (Table 6.1), suggesting redox conditions have changed with time.

6.6.2 Selenium Isotope Results

Upgradient of the source area where conditions are oxic, the δ^{82}Se values are highly variable, ranging from around 0 ‰ (Well 709, total Se: 149 μg L^{-1}; Figure 6.8, 6.9) to extremely negative (Well 2545A -26 ‰, total Se: 103 μg L^{-1}; Figure 6.9).
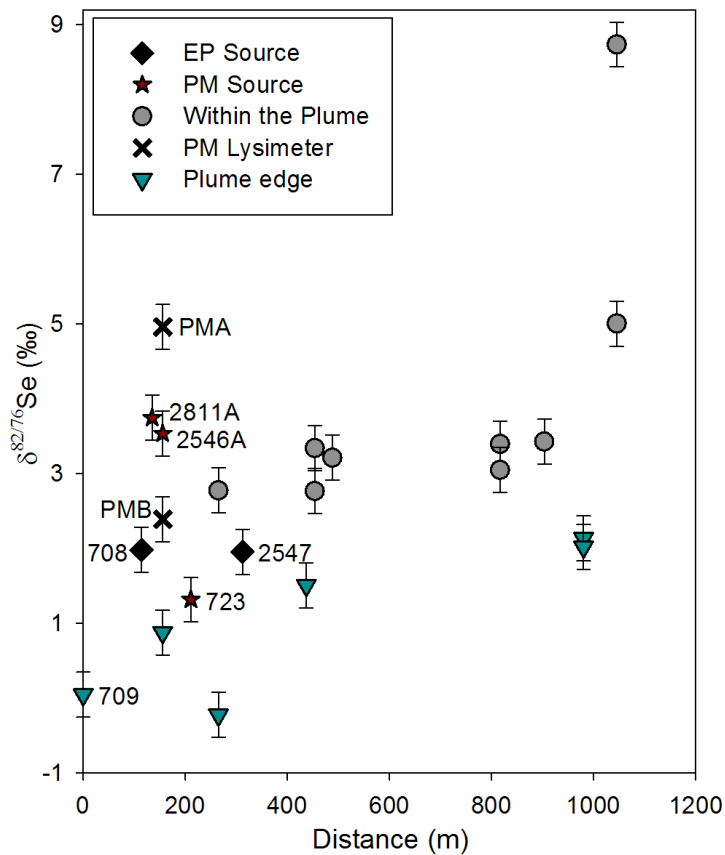
Figure 6.8: Se stable isotope ratios in solution along the flow path. The wetlands begin at approximately 900 m.

There is a large variability in δ^{82}Se values within the source zone area (Figure 6.8), where conditions range from oxic to sulfidic. In general, the Se concentrations are greatest (3.2 – 9.77 mg L^{-1}) and δ^{82}Se values are lower (1.3 – 3.8 ‰) near the source area. Higher concentrations are not directly linked in this area to lower δ^{82}Se values; instead, the δ^{82}Se values are similar for the wells near the former EP pond (Wells 708 and 2547, 2.0 ‰) and the former PM building (Wells 2811A and 2546A, 3.8 ‰ and 3.5 ‰; Figures 6.8, 6.9).
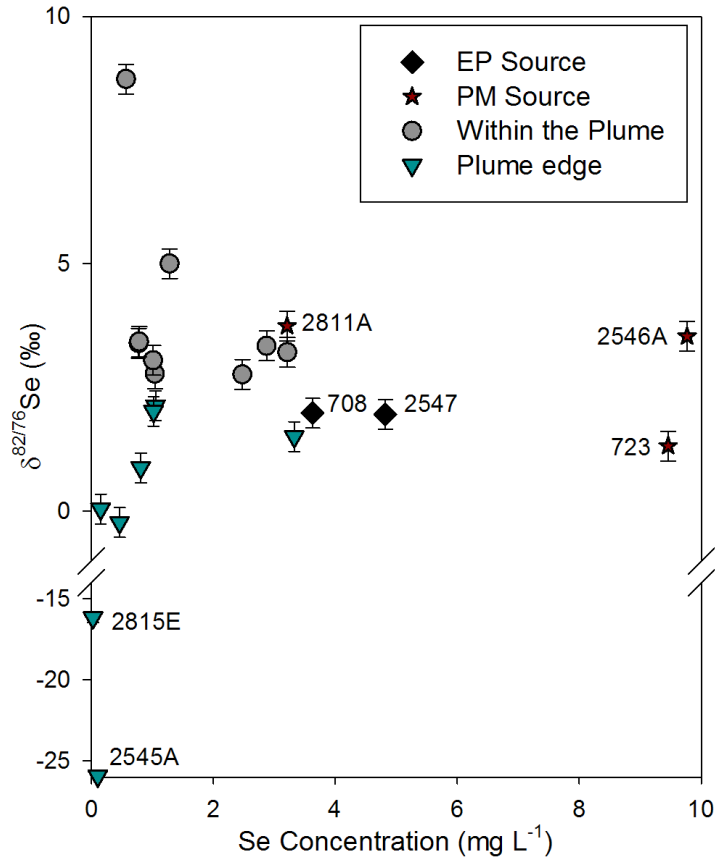
Figure 6.9: Se isotope ratios in solution. Values are plotted relative to Se concentration.

Moving downgradient, the Se concentrations decrease and the δ^{82}Se values are between those of the PM building and former EP pond areas (Figure 6.8, 6.9). Most of the wells in this region do not have strongly reducing conditions (Table 6.1). In areas where local reducing conditions exist, an increase in the δ^{82}Se values is observed; there is an increase in δ^{82}Se between wells 708 and 2813B (2.0 and 2.8 ‰ respectively) accompanied by a decrease in dissolved Se concentration from 3.6 to 1.0 mg L^{-1}, for instance.

As conditions become more reducing under the wetlands, we observe increasing δ^{82}Se as well as the highest measured δ^{82}Se of 8.7‰ within the plume (Wells 2814A: 567 µg L^{-1}, 2814B: 1282 µg L^{-1}; Figure 6.8, 6.9). Once past the sulfidic zone under the wetlands, the δ^{82}Se again declines and the Se concentration further decreases, with an observed δ^{82}Se of -16‰ (Total Se concentration 27 µg L^{-1} (Figure 6.9).

6.7 Discussion

6.7.1 Groundwater Geochemistry and Isotopes

The relatively elevated TDS in well 708 is likely due to evaporation in the former EP pond storage of electrolytes at this location. The shallow well screen spans the water table, resulting in limited local dispersive dilution (Golder 2018). Other source wells may have high TDS due to higher concentrations of dissolved constituents derived from the process waters. Lower TDS measurements throughout the plume suggest dispersive mixing of the plume water with fresher groundwater. The increase in TDS at the distal end of the flow path (Maximum TDS 3660 mg L^{-1}) is associated with proximity to the GSL, and likely indicates a mixing of plume waters with intruding saline water from the GSL, dissolution of salt beds, and possibly other unknown and unaccounted for anthropogenic contributions.

The leak from the former PM building was highly acidic (process water pH < 0.5) resulting in dissolution of acid-consuming minerals in the vadose zone, and slightly lower pH values in groundwater wells affected by the process water (Golder 2018). The relative stability of the pH values downgradient of the PM Building (Figure 6.4) is likely due to groundwater contributions from fractured limestone and $CaCO_3$-cemented quartzite located deeper in the subsurface and further from the source area (Figure 6.3). The pH affects the potential for Se(IV) and Se(VI) to be attenuated via adsorption on $CaCO_3$ surfaces (Neal et al. 1987) soils (Goh and Lim 2004) and Fe-oxide minerals (Rovira et al. 2008), as there is increased adsorption at lower pH, especially below a pH of 7 in the case of Se(VI) up to a pH of 5 (Goldberg and Glaubig 1988). Adsorbed Se(IV) is inferred to be present in areas where dissolved Se(IV) occurs, because the pH range and presence of $CaCO_3$ is favorable for Se(IV) adsorption (Neal et al. 1987; Chakraborty et al. 2010). The pH can also affect Se isotopic fractionation due to adsorption onto Fe (0.67 – 0.87 ‰ for Se(IV) at pH 7 – 5) or Mn oxide minerals (0 – 1.24 ‰ for Se(IV) at pH 8 – 5) (Xu et al. 2020).

The dissolved concentrations of major elements decrease, then increase over the length of the plume (Figure 6.5). Concentrations are high in well 708, reflecting the location of the well

screen, which spans the water table, resulting in minimal dispersive dilution. The S concentration is highest at well 708 compared to anywhere else in the plume. The initial decrease in concentration of most elements along the flow path is likely due to dispersion along the groundwater flow path. Increasing Na and K concentrations with increased proximity to the GSL are likely a result of remnant salt wedges or lake water intrusion. The Ca and Mg concentrations likely reflect changes in local geology, which can be predominantly limestone or quartzite. The dissolved concentrations of other minor elements present in the source zone increase together with the increasing major elements (Sr), or remain largely the same as the source area (Si) (Figure 6.6). The trend of the minor elements is similar to the major elements, suggesting that increase in concentration is also due to the intrusion of underlying saline GSL waters, and water/rock interactions along the flow path.

Although the solid Se was removed from the upper region of the contaminated areas during remediation, some residual Se remained in the deeper region of the vadose zone, beneath the reclamation cap. The Se retained in the vadose zone, above the fractured bedrock, provided an ongoing source of the Se to the groundwater system. It is likely that the transport of dissolved Se was associated with recharge water derived from ponding due to storm events, which passed vertically through the vadose zone upgradient of the source area, and then flowed laterally through the source area. This dissolved Se was displaced into the underlying aquifer (Golder 2018).

Samples of vadose-zone water obtained from two lysimeters (PM-A: 4.9 m; PM-B: 7.6 m) contained elevated concentrations of Se, but the δ^{82}Se values are significantly different. The δ^{82}Se of the pore water from PM-B (2.4 ‰) is similar to source wells 708 (2.0 ‰) and 2547 (2.0 ‰), suggesting that modest differences in Se concentrations between samples collected from PM-B and wells 708 and 2547 are due to dispersive mixing (Figure 6.10). The similarity in δ^{82}Se values between PM-B and these EP source wells supports that a large portion of Se in the ground water originated from the PM building area (Kennecott Utah Copper 2013). The δ^{82}Se of the pore water from PM-A has a higher δ^{82}Se (5 ‰), suggesting that reduction has impacted Se concentrations at this location, and that this water does not contribute significantly to the plume.
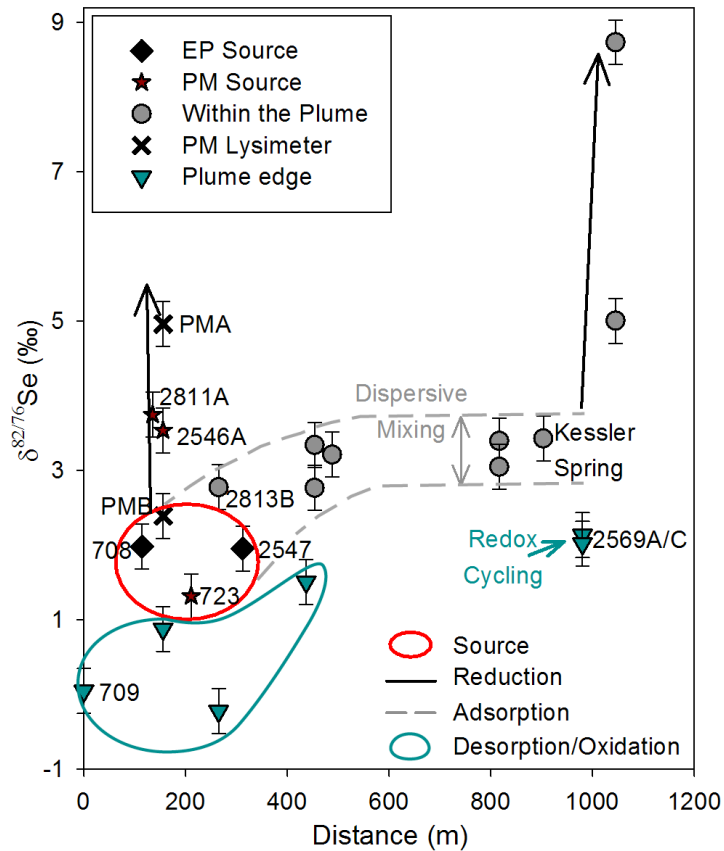
Figure 6.10: Conceptual model of probable processes occurring throughout the plume, based on isotope mixing and fractionation calculations.

The higher $\delta^{82}Se$ value observed at PM-A lysimeter $\delta^{82}Se$ suggests lighter Se was removed while the heavier Se remained in solution. The difference in $\delta^{82}Se$ values makes it unlikely that Se from this location makes a significant contribution to the dissolved Se in the groundwater plume; this observation is consistent with the GMC, which indicated that the PM-A area contributes only a small amount of Se (~1%) for well 2546A (Kennecott Utah Copper 2013). Higher $\delta^{82}Se$ values (3.5 – 3.8 ‰) at 2811A and 2546A are consistent with the Fe-reducing conditions at these wells (Table 6.1), which indicates local Se reduction and removal is thermodynamically possible.

Local reduction, adsorption, and mixing processes result in a large range of $\delta^{82}Se$ values within the source region due to localized redox conditions (Table 6.1, Figures 6.10, 6.11). For

example, the decrease in concentration and increase in δ^{82}Se between well 708 and the downgradient well 2813B is enough to indicate either adsorption, or reductive processes coupled with dispersive dilution (See appendix B). Wells 2811A and 2546A have similar δ^{82}Se values that are much higher than surrounding or downgradient wells and likely indicate localized reduction (Figure 6.10, 6.11).
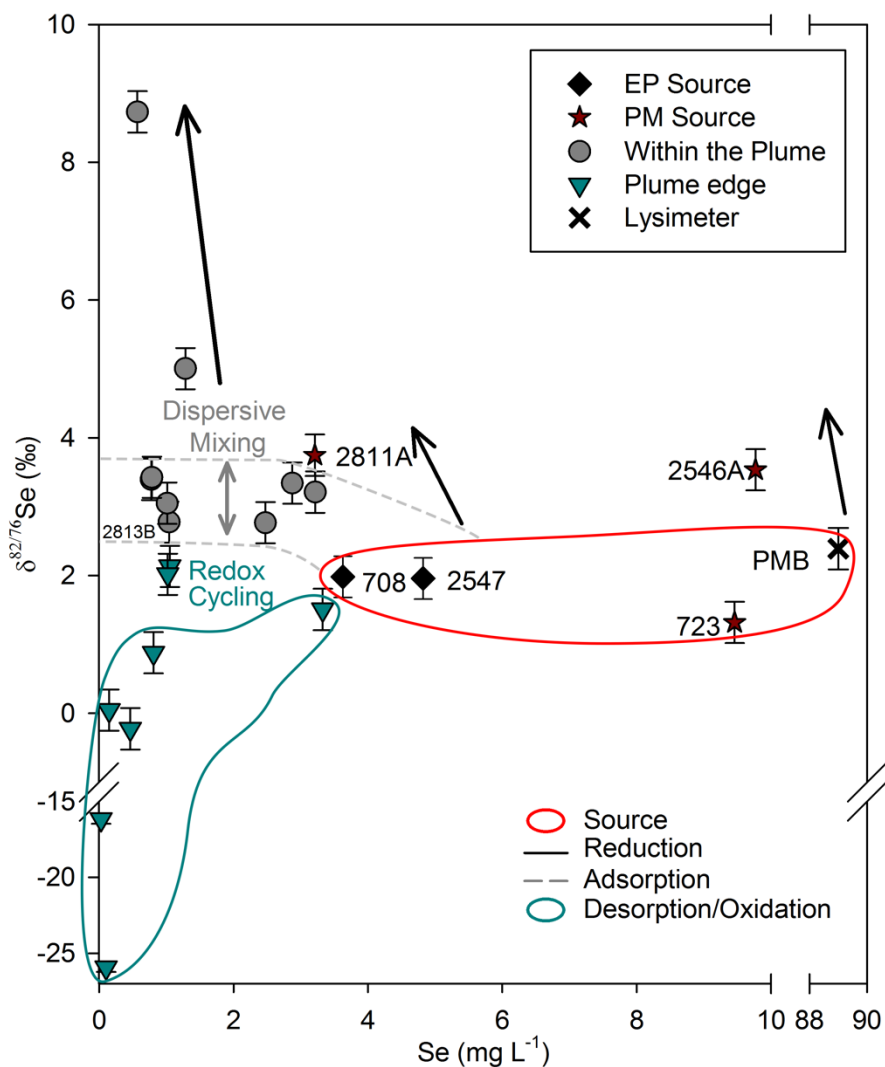
Figure 6.11: Conceptual model of processes occurring throughout the plume, based on modeling results and plotted with respect to concentration.

Selenium concentrations decrease along the length of the plume, whereas δ^{82}Se values remain relatively constant (Figure 6.8, 6.9). Dispersive mixing with water containing much lower concentrations of Se causes a decrease in Se concentrations without altering the Se stable isotope ratios. Most δ^{82}Se values within the plume could have been influenced by adsorption over the transport distance from around wells 723 and 2547, or dispersive dilution and mixing of waters from well 2546A (Figure 6.10). Variations in the concentrations of other dissolved constituents along the length of the plume are consistent with dispersive mixing of plume water with background groundwater geochemistry (Kennecott Utah Copper 2013).

The δ^{82}Se values increase sharply at the extreme downstream margin of the active plume (wells 2577, 2569A-C, and 2814A-B; Figure 6.10). This region of the plume is beneath the wetland complex and has been classified as more reducing at depth (Table 6.1). Adsorptive processes ($\varepsilon < 1.0$ ‰; Johnson 2012; Xu et al. 2020) cannot explain the higher δ^{82}Se values in deeper downgradient wells 2814A and B, suggesting that reduction reactions affected these concentrations. A larger effective fractionation would need to be invoked to produce the same δ^{82}Se value with a smaller decrease in Se concentration ($\varepsilon > 3.7$ ‰). Reduction at this location has been corroborated by recent updates to the site conceptual model (Golder 2018). The variable presence of Se(IV) has been reported in the 2569 well nest, located 18 – 76 m under the wetland complex (Kennecott Utah Copper 2013), requiring either the release of Se through desorption, or reduction of Se(VI). Additionally, Se(IV) in the 2569 well-nest samples could have lowered the measured δ^{82}Se values (2569A: 2.16 ‰, 2569B: 0.76 ‰, 2569C: 2.02 ‰), because Se(IV) and Se(VI) were not separated during isotope measurements due to the sample age and preservation method. The variable abundance of Se(IV) at this location (Kennecott Utah Copper 2013)suggest redox conditions change seasonally, resulting in overall lower δ^{82}Se values at the time samples were collected..

The very low Se concentrations in water samples obtained from wells located near the source-zone boundaries, with well screens completed in the shallower horizons of the bedrock aquifer, or below or downgradient of the Se plume, also have lower or very negative δ^{82}Se values. These values can only be explained by oxidation or desorption releasing Se with lower δ^{82}Se values,

previously accumulated on the solid materials if within the relict plume path, or weathered from native shales. Shales often have negative δ^{82}Se values (Layton-Matthews et al. 2006; Wen and Carignan 2011; Wen et al. 2014), and have been measured as low as -14.2 ‰ (Zhu et al. 2014).Water samples from wells near the plume margin fit within the mixing model for plume Se combined with oxidized Se. Extremely negative δ^{82}Se values located upgradient and downgradient of the plume represent areas where the dissolved Se was derived from oxidation or desorption of low δ^{82}Se from solids. Alternatively, low δ^{82}Se downgradient of the plume could come from the volatilization of reduced Se phases (e.g. methyl selenides, or $H_2Se_{(g)}$) (see Chapter 4, (Schilling et al. 2011b)). These locations are beyond the boundaries of the current plume.

6.7.2 Isotope Mass-Balance Modeling Discussion

A thorough description and discussion of the isotope mass-balance modelling results can be found in the supplementary material. Isotope mass-balance calculations using an ε value of 1.0‰ provided a reasonable description for the maximum change in Se concentrations and δ^{82}Se moving from the source to the wetland. An ε value of 0.9 ‰ is the currently known maximum fractionation caused by adsorption onto Fe oxides (Mitchell et al. 2013; Xu et al. 2020) (Figure B1). An ε value greatly exceeding 1.0‰ is required to explain the shift in the Se concentrations and δ^{82}Se under the wetland area, suggesting the greater degree of isotopic fractionation that would accompany a reductive removal process (Johnson 2012).

6.8 Conclusions

Identification of a single representative δ^{82}Se value for the source zone for dissolved Se at the site is challenging. There are several potential source areas and variable source-zone concentrations. It is likely that Se was released as meteoric water percolates through fine-grained, Se-bearing sediments, after lateral flow had occurred, and recharges the upper shallow gravel aquifer, eventually migrating into the underlying fractured bedrock aquifer. Localized reduction and adsorption were occurring in the source area, especially directly under the former PM building and between wells 708 and 2813b. Within the core of the plume downgradient of

the source area dissolved Se concentrations decline, whereas the δ^{82}Se values remain relatively constant, suggesting the decline in Se concentrations is due to dispersive mixing within the aquifer. A sharp decline in dissolved Se concentrations, associated with a sharp increase in δ^{82}Se values indicates reductive processes in the aquifer beneath the wetland result in Se removal. Upgradient and on the outer fringes of the main flow path of the plume, δ^{82}Se values are low or extremely negative, suggesting the presence of low concentrations of background Se, or remobilization of a very small quantity of Se that was previously attenuated by reduction and precipitation processes. This Se could be from the Se plume's relict flow path.

Selenium isotopes can be used to interpret the main source of Se in a groundwater system. They also provide a tool for defining the extent of a plume, as well as the location of the main plume body. Used in conjunction with the delineation of groundwater flow system, Se isotope ratio values can provide insight into the processes occurring in the subsurface, and to identify mechanisms causing variations in the Se concentrations.

Chapter 7: Conclusions

7.1 Summary of Findings

Computational and analytical methods were used to link changes in Se isotope ratios to specific removal mechanisms. These findings were then combined with data from previous literature to interpret Se isotope ratio measurements at a contaminated field site. The theoretical fractionation of Se isotopes between different Se-bearing molecules (SeO_4^{2-}, $CaSeO_4$, SeO_3^{2-}, $HSeO_3^-$, $CaSeO_3$) were calculated using *ab initio* methods in Chapter Two. First, the molecules of interest were modeled using Gaussian 09, and their geometries optimized using Hartree Fock (HF) and density functional theory (DFT) methods, sequentially. The vibrational energies of these molecules were then used to compute β values. The β value of a reactant molecule divided by the β value of the product molecule yields the equilibrium fractionation factor. The DFT method provided fractionation factors that were similar to another *ab initio* study (Li and Liu 2011), and were the same magnitude as experimentally derived fractionation factors.

In the third chapter, Se(IV) was reduced abiotically by $H_2S_{(g)}$. The $H_2S_{(g)}$ was generated by neutralizing a basic (pH > 11) Na_2S solution. First, different volumes of a Na_2S solution were added to a Se(IV) solution to remove different quantities of Se, in order to determine the degree of isotopic fractionation. More Se was removed from solution when the concentration of Na_2S was increased. In a second experiment, the solution remained in contact with the product for increasing amounts of time to assess the stability of the reaction product and determine whether contact time affected the fractionation factor. When the solid was left in contact with the solution, the Se concentration decreased further before subsequently increasing. The increase in concentration was linked to signs of oxidation. The reduction products were examined by synchrotron-based PXRD. The isotope fractionation was examined for both the change in S:Se ratio, and the time the product was in contact with solution. An orange precipitate formed instantly upon the addition of Na_2S to solution. Precipitation was complete within three hours. Further contact between the solution and the solid caused the precipitate to change color. Oxidation may have influenced this color change. The PXRD analysis of the orange precipitate is qualitatively similar to $Se_{1.09}S_{6.91}$ and $Se_{3.04}S_{4.96}$ (Geoffroy and Demopoulos 2011). The

fractionation factor for the initial reaction between Se(IV) and $H_2S_{(g)}$ is 7.9 ‰. The fractionation factor increased with the length of time the Se precipitate was in contact with the solution (9.4 – 10.9 ‰ by 24 hours), suggesting that there is initially kinetic fractionation, followed by a shift toward the equilibrium fractionation factor. The change in fractionation factor suggests that a different change in $\delta^{82}Se$ values from the source is expected depending on the length of contact time between the solution and the solid. The implication is that batch treatment systems, or tailing ponds or wetlands that produce $H_2S_{(g)}$ would be expected to have different Se fractionation factors than column treatment systems or groundwater systems. The overall fractionation factor for the reduction of Se(IV) by S(-II) is slightly higher than biotic reduction by SRB ($\varepsilon = 6.2 – 7.8$ ‰; Schilling et al. 2020) and within the same range as reduction by pyrite ($\varepsilon = 9.7$ ‰; Mitchell et al. 2013).

In Chapter Four, Se(IV) was reduced biotically by a natural SRB consortium made from brewer's yeast. Solid samples were collected for SEM imaging, and liquid samples were collected for cation and isotope analysis. The samples required treatment with H_2O_2 in order to measure the Se concentrations, because a brown precipitate (likely humic acid) formed upon the addition of HNO_3, and Se disappeared from solution. After the samples were digested with H_2O_2, Se concentrations were observed to decrease over time, with a brief initial increase in concentration observed in individual samples. Isotope analysis shows an initially rapid increase in $\delta^{82}Se$, with a high fractionation factor ($\varepsilon \approx 19$ ‰), followed by decreasing $\delta^{82}Se$ with decreasing concentration remaining in solution. When $\delta^{82}Se$ are plotted with time, increases in the $\delta^{82}Se$ value are visible, suggesting there are multiple pools of Se in solution, probably organic and/or volatile in nature. Some form of reduced Se, which would have a lower $\delta^{82}Se$ value than oxidized Se, is likely released into solution (possibly associated with the H_2O_2 treatment). As this reduced pool of Se is transformed into another form of Se, the $\delta^{82}Se$ values begin to rise again. The dip and eventual increase in $\delta^{82}Se$ values happens 2-3 times, suggesting there are at least 3-4 forms of Se involved in the process, not including the initial Se(IV).

In Chapter Five, Se(VI) was reduced by zero valent iron (ZVI) in a column experiment. The Se(VI) concentration was periodically increased to obtain different removal ratios in solution, to

make it possible to compute a fractionation factor. The Se(VI) was removed from the input solution at the end of the experiment to test the stability of the Se on the solid phase. XANES were collected throughout the reduction process, as were samples for cation and isotope analysis. The mass of Se(VI) removed from solution was not constant with increasing concentration, possibly due to the higher Ca concentration in some of the input solutions. Otherwise, different removal ratios were obtained throughout the experiment, with the lowest removal observed at the end of the experiment. Analysis of the real-time XANES data revealed that Se was present both on the solid and in solution, and that the reaction product changed with increasing Se(VI) concentrations. Over the first five hours, the most abundant reduced phases present were Se(IV) and Se(0). After this time, Ferroselite was observed, followed by Achávalite at 32 hours. More reduced phases of Se (Ferroselite, Achávalite) were present in the middle of the column and at the effluent end of the column than near the input end. Se(0), which disappeared in the middle and end locations, was present at the influent end throughout the experiment. When Se(VI) was removed from the input solution at the end of the experiment, the abundance of the Na_2SeO_4 phase declined sharply, and the total absorbance decreased. Although it is difficult to determine whether other Se phases were removed after Se(VI) was removed from the input, the more reduced phases seemed persistent over the time frame of the experiment. The $\delta^{82}Se$ values fit a straight line, with an isotopic discrimination (Δ) of 9.6 ‰. When Se(VI) was removed from the input, the Se concentrations gradually decreased in the column effluent, providing another opportunity to determine a fractionation factor. The resulting fractionation factor of 2.4 ‰ falls between the fractionation factor for Se(VI) reduction by ZVI in a $CaCO_3$ rich system (4.3 ‰) and adsorption onto iron oxides (< 1.0 ‰).

In Chapter Six, samples from a Se contaminated groundwater plume were analyzed to assess whether trends in the isotope ratios could be linked to other environmental factors, including total Se concentration and redox zonation. A 65-year-old Se plume is situated between a mountain and wetland area upgradient of a hypersaline lake. The lateral movement of the plume was limited by recharge from a nearby tailings impoundments to the east. The Se originated from pipes leaking underneath a mineral processing facility (PM building), with an additional source

of Se coming from underneath a former electrolyte purification (EP) pond. Both sources of contamination were previously excavated, although Se in solid form persisted in the deep soils below these source areas. Samples were collected for isotope analysis from throughout the source area, extending downgradient. Selenium concentrations are highly variable in the source area, and decrease away from the source. The δ^{82}Se values are somewhat variable in the source area, and are different between the two distinct sources (EP pond $\approx$ 2.0 ‰, PM building $\approx$ 3.6 ‰). Large shifts in δ^{82}Se values within the source area are likely due to local reductive processes. Within the main plume body, δ^{82}Se values are mostly unchanged from source δ^{82}Se values, with the exception of some slight increases, probably due to adsorption processes. Under the wetland, there is a sharp increase in δ^{82}Se values coupled to a decrease in the concentration, indicating reductive processes must be occurring in this region. It is not possible to discern whether if the reduction is due to biotic or abiotic processes. On the periphery of the plume, there are low concentrations of Se and the δ^{82}Se values are either negative or lower than within the plume body or source area. These low δ^{82}Se values indicate either very small quantities of reduced forms of Se that have oxidized, desorbed, or volatilized, or possibly the presence of local background Se.

7.2 Scientific Contributions

The research in this thesis has contributed knowledge of Se isotope fractionation paired to specific removal mechanisms. Selenium remediation methods have also been investigated. The scientific contributions include:

- Using different basis sets to model molecules (SeO_4^{2-}, SeO_3^{2-}, $HSeO_3^-$), independently confirming the results of others.

- Modeling two new molecules ($CaSeO_4$, $CaSeO_3$) using ab initio methods to compute Se stable isotope fractionation.

- Determining the Se isotopic fractionation associated with reduction of Se(IV) by $H_2S_{(g)}$.

- Ascertaining that the fractionation of Se(IV) during reduction by $H_2S_{(g)}$ is linked to contact time in solution, which has implications to the long term stability of this reaction in natural systems.

- Demonstrated the importance of speciation data for interpreting results during the microbial reduction of Se(IV) by a natural SRB consortium.

- Measuring the efficacy of the treatment of Se by ZVI in a column using real-time XANES, by quantifying the solid products and matching them with an associated Se isotope fractionation.

- Determining whether the resulting reduction product was stable under changing conditions, by altering the input solution of the column and observing the absolute intensity decrease and the Se speciation.

- Developed a conceptual model to determine what reactions could cause differences in Se isotope ratios measured at a field site along the length of an Se-bearing groundwater plume.

7.3 Future Work and Recommendations

A comprehensive set of fractionation factors for different reactions involving Se are required to assess Se remediation in the environment. Computational methods can be used to supplement any deficiency in the currently known set of Se isotope fractionation factors. Some Se-bearing molecules of interest that could be modeled include Fe-Se compounds such as $FeSeO_3$, $FeSe_2$, and FeSe, Se-S precipitates (Se_nS_{8-n}), and organic selenium compounds. Knowing at least the magnitude and direction of fractionation associated with a transformation to any of the above compounds would provide an improved foundation for laboratory and environmental measurements.

The precipitation of Se_nS_{8-n} compounds results in both isotopic fractionation, and removal of Se from groundwater when the pH is less than 7. A more detailed examination of whether pH has an effect on fractionation is recommended, because only near-neutral pH conditions were

evaluated, and anthropogenic waste waters can be quite acidic. Additionally, Se removal is likely more efficient and long-term under lower pH. A range of experiments conducted at both different pH and contact durations would allow for a more complete evaluation of the possible extent of fractionation in the environment.

Microbial reduction of Se(IV) results in rapid removal of Se from solution, but seems to result in multiple reduction products, not all of which are stable (e.g., $H_2Se_{(g)}$). Trapping volatile forms of Se and speciating reduced organic Se prior to isotopic analysis would give a better understanding of isotopic fractionation in this system.

Using ZVI to remove Se from solution was demonstrated to result in the precipitation of Se forms that are recalcitrant to remobilization. The flow-through cell study could be extended to examine whether the same range of precipitants are formed in the absence of $CaCO_3$. Additionally, other removal materials could be tested using similar methodology.

For additional laboratory studies, there is still a great deal of experimental work to be done on fractionation factors related to Se adsorption and oxidation; others are only now beginning to examine these aspects of Se isotopes. The presence of Ca seems to play an important role in Se removal, so fractionation in systems with high Ca concentrations, or adsorption onto calcite or $CaCO_3$ coated sands should be examined.

Selenium isotope ratio measurements were applied to a field site to aid in the determination of the processes occurring in the ground water. Other field sites containing Se could also have Se isotope ratio measurements taken to determine whether there are any restrictions to applying the technique. Different source conditions, site pH, and geology could all contribute to a more extensive picture of the applicability of Se isotopes at contaminated sites.

References

Adams WJ, Deforest DK, Tear LM, et al (2015) Long-term monitoring of arsenic, copper, selenium, and other elements in Great Salt Lake (Utah, USA) surface water, brine shrimp, and brine flies. Environ Monit Assess 187:1–13

Amrhein C, Hunt M, Roberson M, et al (1998) The use of XANES, STM, and XPS to identify the precipitation products formed during the reaction of U, Cr, and Se with zero-valent iron. In: Goldschmidt Conference T oulouse. Toulouse, pp 51–52

Bailey RT (2017) Revue: contamination au sélénium, devenir et transport réactif dans les eaux souterraines en relation avec la santé humaine. Hydrogeol J 25:1191–1217

Banuelos GS, Pflaum T (1990) Determining selenium in plant tissue with optimal digestion conditions. Commun Soil Sci Plant Anal 21:1717–1726

Basu A, Schilling K, Brown ST, et al (2016) Se isotopes as groundwater redox indicators: detecting natural attenuation of Se at an in situ recovery U mine. Environ Sci Technol 50:10833–10842

Beauvais J (2016) Aquatic Life Ambient Water Quality Criterion for Selenium in Freshwater 2016 – Fact Sheet. Washington, DC, United States

Bigeleisen J, Mayer MG (1947) Calculation of equilibrium constants for isotopic exchange reactions. J Chem Phys 15:261–267

Black JR, Kavner A, Schauble E a. (2011) Calculation of equilibrium stable isotope partition function ratios for aqueous zinc complexes and metallic zinc. Geochim Cosmochim Acta 75:769–783

Bye R, Lund W (1988) Optimal conditions for the reduction of selenate to selenite by hydrochloric acid. Anal Chemie 332:242–244

Canadian Council of Ministers of the Environment (2016) Canadian Environmental Quality Guidelines. Canadian Council of Ministers of the Environment

Chakraborty S, Bardelli F, Charlet L (2010) Reactivities of Fe(II) on calcite: selenium reduction. Environ Sci Technol 44:1288–94

Charlet L, Scheinost AC, Tournassat C, et al (2007) Electron transfer at the mineral/water interface: Selenium reduction by ferrous iron sorbed on clay. Geochim Cosmochim Acta 71:5731–5749

Clark SK, Johnson T (2008) Effective isotopic fractionation factors for solute removal by reactive sediments: a laboratory microcosm and slurry study. Environ Sci Technol 42:7850–7855

Clark SK, Johnson TM (2010) Selenium stable isotope investigation into selenium biogeochemical cycling in a lacustrine environment: Sweitzer Lake, Colorado. J Environ Qual 39:2200–2210

Cowan CE, Zachara JM, Resch CT (1990) Solution ion effects on the surface exchange of selenite on calcite. Geochim Cosmochim Acta 54:2223–2234

Deen SG, Bondici VF, Essilfie-Dughan J, et al (2018) Biotic and abiotic sequestration of selenium in anoxic coal waste rock. Mine Water Environ 37:825–838

Ellis AS, Johnson TM, Herbel MJ, Bullen TD (2003) Stable isotope fractionation of selenium by natural microbial consortia. Chem Geol 195:119–129

Elwaer N, Hintelmann H (2007) Comparative performance study of different sample introduction techniques for rapid and precise selenium isotope ratio determination using multi-collector inductively coupled plasma mass spectrometry (MC-ICP/MS). Anal Bioanal Chem 389:1889–99

Elwaer N, Hintelmann H (2008) Selective separation of selenium (IV) by thiol cellulose powder and subsequent selenium isotope ratio determination using multicollector inductively coupled plasma. J Anal At Spectrom 23:733–743

EnviroMetal Technologies Inc. (2007) Bench-scale treatability report in support of a granular iron permeable reactive barrier installation at the Pleasant Hill Site , CA. Waterloo, ON,

Canada

Fernández-Martínez A, Charlet L (2009) Selenium environmental cycling and bioavailability: a structural chemist point of view. Rev Environ Sci Biotechnol 8:81–110

Floor GH, Millot R, Iglesias M, Négrel P (2011) Influence of methane addition on selenium isotope sensitivity and their spectral interferences. J Mass Spectrom 46:182–8

Fodje M, Grochulski P, Janzen K, et al (2014) 08B1-1: an automated beamline for macromolecular crystallography experiments at the Canadian Light Source. J Synchrotron Radiat 21:633–637

Fordyce F (2005) Selenium deficiency and toxicity in the environment. In: Selenus. pp 402–415

Frisch MJ, Trucks GW, Schlegel HB, et al (2009) Gaussian 09

Geoffroy N, Demopoulos GP (2011) The elimination of selenium (IV) from aqueous solution by precipitation with sodium sulfide. J Hazard Mater 185:148–154

Gheju M (2011) Hexavalent chromium reduction with zero-valent iron (ZVI) in aquatic systems. Water Air Soil Pollut 222:103–148

Gibson BD, Blowes DW, Lindsay MBJ, Ptacek CJ (2012) Mechanistic investigations of Se(VI) treatment in anoxic groundwater using granular iron and organic carbon: an EXAFS study. J Hazard Mater 241–242:92–100

Gobi N, Vaseeharan B, Rekha R, Vijayakumar S (2018) Cytotoxicity and oxidative stress of the acute exposure selenium in Oreochromis mossambicus. Ecotoxicol Environ Saf 162:147–159

Goff J, Terry L, Mal J, et al (2019) Role of extracellular reactive sulfur metabolites on microbial Se(0) dissolution. Geobiology 17:320–329

Goh K-H, Lim T-T (2004) Geochemistry of inorganic arsenic and selenium in a tropical soil: effect of reaction time, pH, and competitive anions on arsenic and selenium adsorption. Chemosphere 55:849–59

Goldberg S (2013) Modeling selenite adsorption envelopes on oxides, clay minerals, and soils using the triple layer model. Soil Sci Soc Am J 77:64–71

Goldberg S, Glaubig R (1988) Anion sorption on a calcareous, montmorillonitic soil – Selenium. Soil Sci Soc Am J 52:954–958

Goldberg S, Martens D a., Forster HS, Herbel MJ (2006) Speciation of selenium(IV) and selenium(VI) using coupled ion chromatography—hydride generation atomic absorption spectrometry. Soil Sci Soc Am J 70:41

Golder (2018) Final north zone groundwater (OU23) focused feasibility study: 2018 updated conceptual site model, Kennecott North Zone Site

Gustafsson JP, Johnssont L (1994) The association between selenium and humic substances in forested ecosystems – laboratory evidence. Appl Organomet Chem 8:141–147

Hagiwara Y (2000) Selenium isotope ratios in marine sediments and algae – a reconaissance study. University of Illinois at Urbana-Champaign

Hamilton SJ (2004) Review of selenium toxicity in the aquatic food chain. Sci Total Environ 326:1–31

Hayes JM (2004) An introduction to isotopic calculations. 1–10

Henderson AD (2010) Solids formation and permeability reduction in zero-valent iron and iron sulfide media for permeable reactive barriers. University of Michigan

Herbel MJ, Johnson TM, Oremland RS, Bullen TD (2000) Fractionation of selenium isotopes during bacterial respiratory reduction of selenium oxyanions. Geochim Cosmochim Acta 64:3701–3709

Herbel MJ, Johnson TM, Tanji KK, et al (2002) Selenium stable isotope ratios in california agricultural drainage water management systems. J Environ Qual 31:1146–1156

Jamieson-Hanes JH, Lentz AM, Amos RT, et al (2014) Examination of Cr(VI) treatment by zero-valent iron using in situ, real-time X-ray absorption spectroscopy and Cr isotope measurements. Geochim Cosmochim Acta 142:299–313

Jamieson-Hanes JH, Shrimpton HK, Veeramani H, et al (2017) Evaluating zinc isotope fractionation under sulfate reducing conditions using a flow-through cell and in situ XAS analysis. Geochim Cosmochim Acta 203:1–14

Janz DM, Deforest DK, Brooks ML, et al (2010) Selenium toxicity to aquatic organisms. In: Chapman PM, Adams WJ, Brooks ML, et al. (eds) Ecological Assessment of Selenium in the Aquatic Environment. Society of Environmental Toxicology and Chemistry, Pensacola

Jeen S, Blowes DW, Gillham RW (2008) Performance evaluation of granular iron for removing hexavalent chromium under different geochemical conditions. J Contam Hydrol 95:76–91

Johnson T (2004) A review of mass-dependent fractionation of selenium isotopes and implications for other heavy stable isotopes. Chem Geol 204:201–214

Johnson TM (2012) Stable isotopes of Cr and Se as tracers of redox processes in earth surface environments. In: Baskaran M (ed) Handbook of Environmental Isotope Geochemistry. Springer Berlin Heidelberg, Berlin, Heidelberg, pp 155–175

Johnson TM, Bullen TD (2003) Selenium isotope fractionation during reduction by Fe (II)-Fe (III) hydroxide-sulfate (green rust). Geochim Cosmochim Acta 67:413–419

Johnson TM, Bullen TD (2004) Mass-dependent fractionation of selenium and chromium isotopes in low-temperature environments. Rev Mineral Geochemistry 55:289–317

Johnson TM, Herbel MJ, Bullen TD, Zawislanski PT (1999) Selenium isotope ratios as indicators of selenium sources and oxyanion reduction. Geochim Cosmochim Acta 63:2775–2783

Jung B, Safan A, Batchelor B, Abdel-Wahab A (2016) Spectroscopic study of Se (IV) removal from water by reductive precipitation using sulfide. Chemosphere 163:351–358

Kang M, Ma B, Bardelli F, et al (2013) Interaction of aqueous Se(IV)/Se(VI) with FeSe/FeSe$_2$: Implication to Se redox process. J Hazard Mater 248–249:20–28

Kaplan IR (1975) Stable isotopes as a guide to biogeochemical processes. In: Proceedings of the Royal Society of London. Series B., Biological Sciences. Royal Society, pp 183–211

Kennecott Utah Copper (2013) North zone groundwater (OU23) remedial investigation update report Kennecott north zone site

Kipp MA, Algeo TJ, Stüeken EE, Buick R (2020) Basinal hydrographic and redox controls on selenium enrichment and isotopic composition in Paleozoic black shales. Geochim Cosmochim Acta 287:229–250

Kneteman JG (2016) Resilient space: bighorn sheep (Ovis canadensis) ecological resilience in the northern Rocky Mountains. University of Alberta

König S, Eickmann B, Zack T, et al (2019) Redox induced sulfur-selenium isotope decoupling recorded in pyrite. Geochim Cosmochim Acta 244:24–39

Krouse H, Thode H (1962) Thermodynamic properties and geochemistry of isotopic compounds of selenium. Can J Chem 40:367–375

Kurzawa T, König S, Labidi J, et al (2017) A method for Se isotope analysis of low ng-level geological samples via double spike and hydride generation MC-ICP-MS. Chem Geol 466:219–228

Layton-Matthews D, Leybourne MI, Peter JM, Scott SD (2006) Determination of selenium isotopic ratios by continuous-hydride-generation dynamic-reaction-cell inductively coupled plasma-mass spectrometry. J Anal At Spectrom 21:41–49

Lemly AD (2002) Symptoms and implications of selenium toxicity in fish: the Belews Lake case example. Aquat Toxicol 57:39–49

Lemly AD (2004) Aquatic selenium pollution is a global environmental safety issue. Ecotoxicol Environ Saf 59:44–56

Lenz M, Lens PNL (2009) The essential toxin: the changing perception of selenium in environmental sciences. Sci Total Environ 407:3620–33

Levander OA, Burk RF (2006) Update of human dietary standards for selenium. In: Hatfield DL, Berry MJ, Gladyshev VN (eds) Selenium: Its Molecular Biology and Role in Human Health, Second Edi. Springer, New York, pp 399–410

Li X, Liu Y (2011) Equilibrium Se isotope fractionation parameters: a first-principles study. Earth Planet Sci Lett 304:113–120

Liang L, Yang W, Guan X, et al (2013) Kinetics and mechanisms of pH-dependent selenite removal by zero valent iron. Water Res. https://doi.org/10.1016/j.watres.2013.07.011

Lindberg RD, Runnells DD (1984) Ground water redox reactions: an analysis of equilibrium state applied to eh measurements and geochemical modeling. Science (80-) 225:925–927

Loyo RLDA, Nikitenko SI, Scheinost AC, Simonoff M (2008) Immobilization of selenite on Fe_3O_4 and Fe/Fe_3C ultrasmall particles. Environ Sci Technol 42:2451–6

Martens D, Suarez D (1997) Selenium speciation of soil/sediment determined with sequential extractions and hydride generation atomic absorption spectrophotometry. Environ Sci Technol 31:133–139

Mills TJ (2016) Water chemistry under a changing hydrologic regime: investigations into the interplay between hydrology and water-quality in arid and semi-aridwatersheds in Colorado, USA. University of Colorado

Misoka MJ (2012) A column experiment for groundwater remediation post-mine closure at the Wolverine Mine, Yukon. Royal Roads University

Missana T, Alonso U, Scheinost AC, et al (2009) Selenite retention by nanocrystalline magnetite: Role of adsorption, reduction and dissolution/co-precipitation processes. Geochim Cosmochim Acta 73:6205–6217

Mitchell K, Couture R-M, Johnson TM, et al (2013) Selenium sorption and isotope fractionation: Iron(III) oxides versus iron(II) sulfides. Chem Geol 342:21–28

Mondal K, Jegadeesan G, Lalvani SB (2004) Removal of selenate by Fe and NiFe nanosized particles. Ind Eng Chem Res 43:4922–4934

Morrison SJ, Goodknight CS, Tigar AD, et al (2012) Naturally occurring contamination in the Mancos Shale. Environ Sci Technol 46:1379–87

Morrison SJ, Metzler DR, Dwyer BP (2002) Removal of As, Mn, Mo, Se, U, V and Zn from

groundwater by zero-valent iron in a passive treatment cell: reaction progress modeling. J Contam Hydrol 56:99–116

Nancharaiah Y V, Lens PNL (2015) Ecology and biotechnology of selenium-respiring bacteria. Microbiol Mol Biol Rev 79:61–80

Neal RH, Sposito G, Holtzclaw K, Traina S (1987) Selenite adsorption on alluvial soils: I. Soil composition and pH effects. Soil Sci Soc Am J 51:1161–1165

Pettine M, Gennari F, Campanella L, et al (2012) The reduction of selenium(IV) by hydrogen sulfide in aqueous solutions. Geochim Cosmochim Acta 83:37–47

Pettine M, Mcdonald TJ, Sohn M, et al (2015) A critical review of selenium analysis in natural water samples. Trends Environ Anal Chem 5:1–7

Plant J, Kinniburgh D, Smedley P, et al (2003) Arsenic and selenium. In: Treatise on Geochemistry, Plan. Elsevier Ltd, Keyworth, Nottingham, UK, pp 17–66

Qiu SR, Lai H-F, Roberson MJ, et al (2000) Removal of contaminants from aqueous solution by reaction with iron surfaces. Langmuir 16:2230–2236

Rashid K, Krouse HR (1985) Selenium isotopic fractionation during SeO_3^{-2} reduction to Se(0) and H2Se. Can J Chem 63:3195–3199

Ravel B, Newville M (2005) ATHENA, ARTEMIS, HEPHAESTUS: data analysis for X-ray absorption spectroscopy using IFEFFIT. J Synchrotron Radiat 12:537–41

Rees CE, Thode HG (1966) Selenium isotope effects in the reduction of sodium selenite and of sodium selenate. Can J Chem 44:419–427

Reyes HL, García-Ruiz S, Tonietto BG, et al (2009) Quantification of selenium species in petroleum refinery wastewaters using ion chromatography coupled to post-column isotope dilution analysis ICP-MS. J Braz Chem Soc 20:1878–1886

Rigby MC, Dennis A, Gerads R (2014) Fish toxicity testing with selenomethionine spiked feed – what's the real question being asked? Environ Sci Process Impacts 16:511–517

Roe JH, Hopkins WA, Baionno JA, et al (2004) Maternal transfer of selenium in Alligator mississippiensis nesting downstream from a coal-burning power plant. Environ Toxicol Chem 23:1969–1972

Rossberg A, Scheinost AC, Schmeisser N, et al (2014) AcReDaS, an actinide reference database for XAS, EELS, IR, raman, and NMR spectroscopy. https://www.hzdr.de/acredas

Rouxel O, Ludden J, Carignan J, et al (2000) Natural variations of selenium isotopes determined by multicollector plasma source mass spectrometry. In: Geoanalysis 2000. pp 43–44

Rouxel O, Ludden J, Carignan J, et al (2002) Natural variations of Se isotopic composition determined by hydride generation multiple collector inductively coupled plasma mass spectrometry. Geochim Cosmochim Acta 66:3191–3199

Rovira M, Giménez J, Martínez M, et al (2008) Sorption of selenium(IV) and selenium(VI) onto natural iron oxides: goethite and hematite. J Hazard Mater 150:279–84

Sasaki K, Blowes DW, Ptacek CJ, Gould WD (2008) Immobilization of Se(VI) in mine drainage by permeable reactive barriers: column performance. Appl Geochemistry 23:1012–1022

Schauble E, Rossman GR, Taylor HP (2004) Theoretical estimates of equilibrium chromium-isotope fractionations. Chem Geol 205:99–114

Schauble EA (2007) Role of nuclear volume in driving equilibrium stable isotope fractionation of mercury, thallium, and other very heavy elements. Geochim Cosmochim Acta 71:2170–2189

Schauble EA, Rossman GR, Taylor HP (2001) Theoretical estimates of equilibrium Fe-isotope fractionations from vibrational spectroscopy. Geochim Cosmochim Acta 65:2487–2497

Scheinost AC, Charlet L (2008) Selenite reduction by mackinawite, magnetite and siderite: XAS characterization of nanosized redox products. Environ Sci Technol 42:1984–9

Scheinost AC, Kirsch R, Banerjee D, et al (2008) X-ray absorption and photoelectron spectroscopy investigation of selenite reduction by FeII-bearing minerals. J Contam Hydrol 102:228–45

Schilling K, Basu A, Wanner C, et al (2020) Mass-dependent selenium isotopic fractionation during microbial reduction of seleno-oxyanions by phylogenetically diverse bacteria. Geochim Cosmochim Acta 276:274–288

Schilling K, Johnson TM, Dhillon KS, Mason PRD (2015) Fate of selenium in soils at a seleniferous site recorded by high precision Se isotope measurements. Environ Sci Technol 49:9690–9698

Schilling K, Johnson TM, Mason PRD (2014) A sequential extraction technique for mass-balanced stable selenium isotope analysis of soil samples. Chem Geol 381:125–130

Schilling K, Johnson TM, Wilcke W (2011a) Selenium partitioning and stable isotope ratios in urban topsoils. Soil Sci Soc Am J 75:1354

Schilling K, Johnson TM, Wilcke W (2011b) Isotope fractionation of selenium during fungal biomethylation by Alternaria alternata. Environ Sci Technol 45:2670–2676

Scott AP, Radom L (1996) Harmonic vibrational frequencies: an evaluation of Hartree-Fock, Møller-Plesset, quadratic configuration interaction, density functional theory, and semiempirical scale factors. J Phys Chem 100:16502–16513

Shrimpton HK, Blowes DW, Ptacek CJ (2015) Fractionation of selenium during selenate reduction by granular zerovalent iron. Environ Sci Technol 49:11688–11696

Shrimpton HK, Jamieson-Hanes JH, Ptacek CJ, Blowes DW (2018) Real-time XANES measurement of Se reduction by zero-valent iron in a flow-through cell, and accompanying Se isotope measurements. Environ Sci Technol 52:9304–9310

Siebert C, Nägler TF, Kramers JD (2001) Determination of molybdenum isotope fractionation by double-spike multicollector inductively coupled plasma mass spectrometry. Geochemistry Geophys Geosystems 2:2000GC000124

Spallholz JE, Hoffman DJ (2002) Selenium toxicity: cause and effects in aquatic birds. Aquat Toxicol 57:27–37

Stevenson FJ (1994) Humus chemistry: genesis, composition, reactions, 2nd edn. Wiley, New

York

Stolz JF, Basu P, Santini JM, Oremland RS (2006) Arsenic and selenium in microbial metabolism. Annu Rev Microbiol 60:107–130

Stüeken EE, Foriel J, Nelson BK, et al (2013) Selenium isotope analysis of organic-rich shales: advances in sample preparation and isobaric interference correction. J Anal At Spectrom 28:1734

Su C, Suarez DL (2000) Selenate and selenite sorption on iron oxides. Soil Sci Soc Am J 64:101–111

Tan D, Zhu J, Wang X, et al (2020) Equilibrium fractionation and isotope exchange kinetics between aqueous Se(IV) and Se(VI). Geochim Cosmochim Acta 277:21–36

Tang Y, Werth CJ, Sanford RA, et al (2015) Immobilization of selenite via two parallel pathways during in situ bioremediation. Environ Sci Technol 49:4543–4550

Teng F-Z, Watkins JM, Dauphas N (eds) (2017) Non-traditional stable isotopes. Mineralogical Society of America, Geochemical Society

Toby BH, Von Dreele RB (2013) GSAS-II: the genesis of a modern open-source all purpose crystallography software package. J Appl Crystallogr 46:544–549

Tullo P Di, Pannier F, Thiry Y, et al (2016) Field study of time-dependent selenium partitioning in soils using isotopically enriched stable selenite tracer. Sci Total Environ 562:280–288

Urey HC (1947) The thermodynamic properties of isotopic substances. J Chem Soc 562–581

US EPA (2002) Five-year review report Kennecott North Zone superfund site: appendix J: background/remedial actions

Van Dyke JU, Hopkins WA, Jackson BP (2013) Influence of relative trophic position and carbon source on selenium bioaccumulation in turtles from a coal fly-ash spill site. Environ Pollut 182C:45–52

von Strandmann PAEP, Coath CD, Catling DC, et al (2014) Analysis of mass dependent and

mass independent selenium isotope variability in black shales. J Anal At Spectrom 29:1648–1659

Wachsmann M, Heumann KG (1992) Negative thermal ionization mass spectrometry of main group elements Part 2. 6th group: sulfur, selenium and tellurium. Int J Mass Spectrom Ion Process 114:209–220

Wasserman NL, Schilling K, Johnson TM, Pallud C (2021) Selenium isotope shifts during the oxidation of selenide-bearing minerals. ACS Earth Sp Chem 5:1140–1149

Wayland M, Kneteman J, Crosley R (2006) The American dipper as a bioindicator of selenium contamination in a coal mine-affected stream in West-Central Alberta, Canada. Environ Monit Assess 123:285–298

Wells M, Stolz JF (2020) Microbial selenium metabolism: a brief history, biogeochemistry and ecophysiology. FEMS Microbiol Ecol 96:1–16

Wen H, Carignan J (2011) Selenium isotopes trace the source and redox processes in the black shale-hosted Se-rich deposits in China. Geochim Cosmochim Acta 75:1411–1427

Wen H, Carignan J, Chu X, et al (2014) Selenium isotopes trace anoxic and ferruginous seawater conditions in the Early Cambrian. Chem Geol 390:164–172

Wiederhold JG (2015) Metal stable isotope signatures as tracers in environmental geochemistry. Environ Sci Technol 49:2606–2624

Williams KH, Wilkins MJ, N'Guessan AL, et al (2013) Field evidence of selenium bioreduction in a uranium-contaminated aquifer. Environ Microbiol Rep 5:444–452

Winkel LHE, Johnson CA, Lenz M, et al (2012) Environmental selenium research: from microscopic processes to global understanding. Environ Sci Technol 46:571–9

Winkel LHE, Vriens B, Jones GD, et al (2015) Selenium cycling across soil-plant-atmosphere interfaces: A critical review

Xu W, Qin H-B, Zhu J-M, et al (2021) Selenium isotope fractionation during adsorption onto montmorillonite and kaolinite. Appl Clay Sci 211:106189

Xu W, Zhu J, Johnson TM, et al (2020) Selenium isotope fractionation during adsorption by Fe, Mn and Al oxides. Geochim Cosmochim Acta 272:121–136

Yierpan A, König S, Labidi J, et al (2018) Chemical sample processing for combined selenium isotope and selenium-tellurium elemental investigation of the earth's igneous reservoirs. Geochemistry, Geophys Geosystems 19:516–533

Young TF, Finley K, Adams WJ, et al (2010) What you need to know about selenium. In: Chapman P (ed) Ecological Assessment of Selenium in the Aquatic Environment. SETAC Press, Pensacola, pp 7–45

Yu M, Tian W, Sun D, et al (2001) Systematic studies on adsorption of 11 trace heavy metals on thiol cotton fiber. Anal Chim Acta 428:209–218

Zhang P, Sparks D (1990) Kinetics of selenate and selenite adsorption/desorption at the goethite/water interface. Environ Sci Technol 24:1848–1856

Zhang Y, Moore JN (1996) Selenium fractionation and speciation in a wetland system. Environ Sci Technol 30:2613–2619

Zhu J-MM, Johnson TM, Clark SK, et al (2014) Selenium redox cycling during weathering of Se-rich shales: a selenium isotope study. Geochim Cosmochim Acta 126:228–249

Zhu J, Johnson T, Clark S, Zhu X (2008) High precision measurement of selenium isotopic composition by hydride generation multiple collector inductively coupled plasma mass spectrometry with a 74Se-77Se double spike. Chinese J Anal Chem 36:1385–1390

Appendices

Appendix A: Supporting information for real-time XANES measurement of Se reduction by zero-valent iron in a flow-through cell, and accompanying Se isotope measurements

The zero valent iron (ZVI) used in this study was Connelly GMP ZVI. Individual iron grains are long, thin, and narrow, with lengths in the range of 2-5mm. The iron was sieved to select a particle range of 0.25–1 mm. The surface area of Connelly ZVI is typically 1.8 ± 0.4 m^2 g^{-1} (EnviroMetal Technologies Inc. 2007; Jeen et al. 2008; Henderson 2010; Gheju 2011). The acid-washed iron (100 g) was carefully packed with a random-orientation of the iron grains into the flow-through cell to avoid creating preferential flow-paths. The iron was packed slightly above the cut out in the cell to account for bulging of the Kapton™ film window during flow. The porosity was close to 0.50.

The concentration of Se flowing through the cell was increased over time by changing the composition of the input solution (Table A1).

Table A1: The composition of the input solution over time.

Time Started	Input Concentration (mg L^{-1})				
(Hr)	Se	Na	Ca	Ionic Strength	pH
0	15.31	8.67	29.69	1.51×10^{-3}	8.42
8	27.47	15.22	30.58	2.40×10^{-3}	8.32
16	44.09	24.82	39.01	3.76×10^{-3}	8.78
24	62.5	34.55	53.75	5.26×10^{-3}	8.41
32	72.89	40.87	30.53	5.78×10^{-3}	8.66
40	95.21	52.39	34.58	7.40×10^{-3}	8.53
48	0	0	48.78	6.09×10^{-4}	8.78

The sample flow rate started at 50 mL hr^{-1} and gradually decreased to 44 mL hr-1 over time (Figure A1). Flow rate was calculated by subtracting the mass of the collected samples from the mass of the pre-weighed collection tubes.
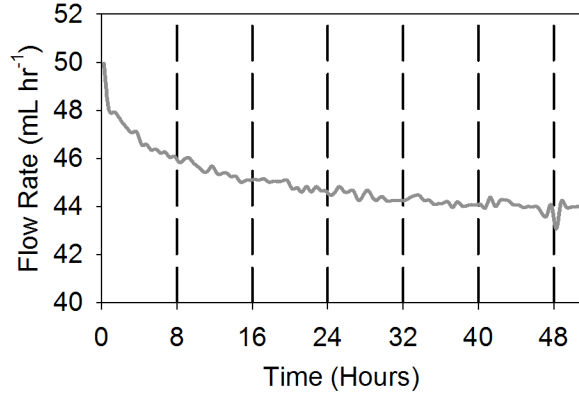

Figure A1: Flow rate over the course of the experiment.

Removal rate per hour was calculated as:

$$\sum_{t=0}^{1hr} Sample\ Mass\ Collected\ per\ 15\ min\ \times\ ([Se]_{INP} - [Se]_{OUT}) \qquad \text{Eq. A1}$$

The sampling interval was 15 minutes, and the mass of each sample was recorded, making the sum of the masses over the hour equal to the mass removed from solution for that hour (Figure A2). If the increased removal rate between 24 and 32 hours (Se input = 60 mg L^{-1}) is considered the beginning of a change in removal rates, linear regression for a fit of the early data yields an R^2 of 0.895. If all data are included in the fit, assuming a constantly increasing removal rate, the R^2 value is 0.783. An R^2 value of 0.945 can be obtained if the elevated removal rate between 24 and 32 hours is ignored from the single rate fit.
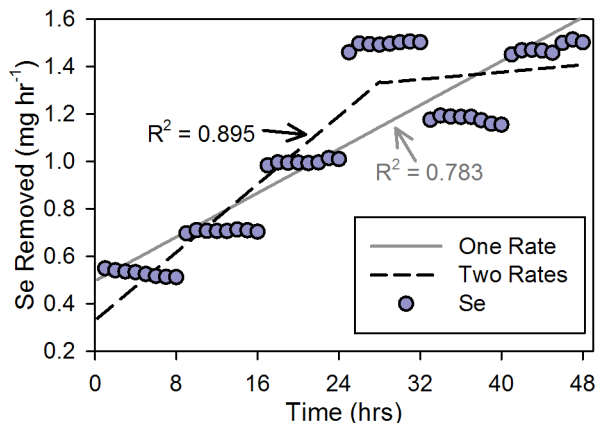
Figure A2: Removal rate of Se from solution, normalized to sample mass, and fit with a single and two rate removal model.

The percentage of Se removed relative to the input concentration was not constant throughout the experiment (Figure A3). The largest variation in removal percentage is observed in the 15 mg L^{-1} input solution.
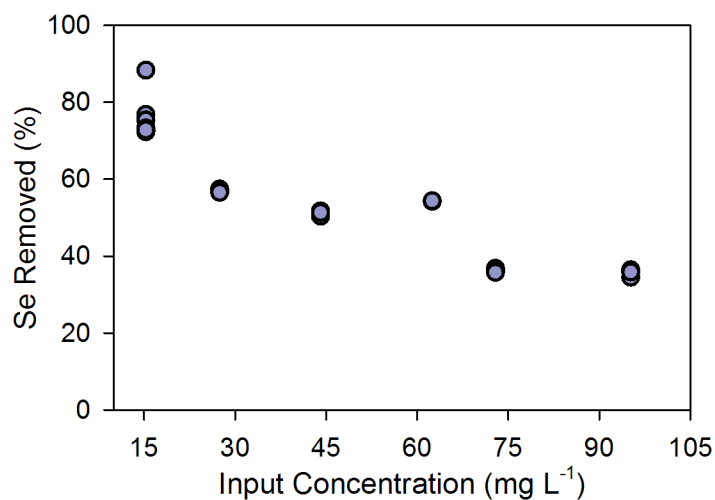

Figure A3: The removal percentage for a given input Se(VI) concentration.

Selenium isotopes have multiple interferences on MC-ICP-MS (Elwaer and Hintelmann 2007). Transition metals and nitric acid interfere with hydride generation, krypton, which may be present in the Ar gas and atmosphere, is an isobaric interference, and As, Ge, and Br produce hydrides with the same mass as Se isotopes. The Ar gas itself forms three dimers, $^{40}Ar^{36}Ar$,

124

$^{40}Ar^{38}Ar$, and $^{40}Ar^{40}Ar$, which interfere on ^{76}Se, ^{78}Se, and ^{80}Se. Argon-chloride dimers also interfere on ^{74}Se and ^{77}Se. Many of these interferences can be removed by sample purification. Blank subtraction was used to eliminate interferences caused by ArCl. Sample purification blanks with carefully matched acid matrixes were run as blanks in the isotope measurement sequence, as they were found to provide more reliable results for on-peak blank subtraction than running blanks with an equivalent HCl concentration alone. Argon interferences on Se, and Se hydrides were calculated by monitoring mass 83, with the Kr determined using a blank measurement. While Br was not found to be present in any of our samples, allowing purified Se samples to equilibrate overnight improved results, likely due to gas-based interferences.
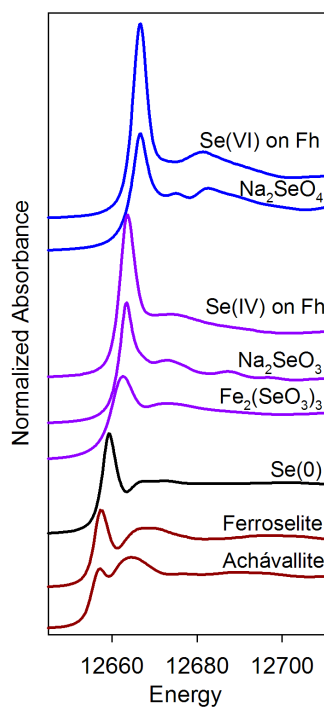

Figure A4: Normalized XANES spectra of several selenium standards used in the fitting process.

Standards used included selenate adsorbed on ferrihydrite (Se(VI) on Fh), sodium selenate (Na_2SeO_4), selenite adsorbed on ferrihydrite (Se(IV) on Fh), sodium selenite (Na_2SeO_3), ferric selenite ($Fe_2(SeO_3)_3$), elemental Se, ferroselite ($FeSe_2$) and achávalite (FeSe) (Figure A4)(Rossberg et al. 2014).

Three scans were taken at each location in the flow through cell before moving on to the next location. These three scans were then merged to reduce noise (Figure A5). Scans with excessive noise or glitches were discarded. For linear combination fitting (LCF), standards making up less than 1% of the composition were excluded. Standards that made up greater than 1% but less than 10% of the total composition were included in the fit in order to identify trends in components over time.
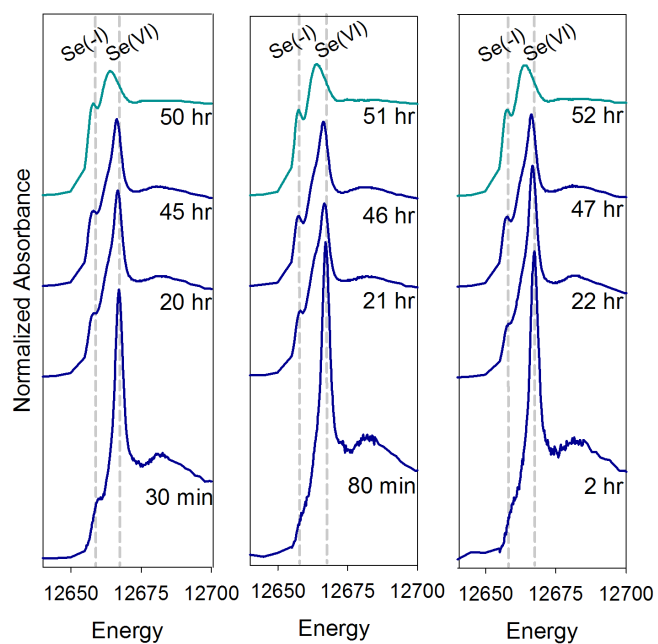

Figure A5: Normalized Se absorbance spectra from the influent (left), middle (center), and effluent (right) ends of the flow through cell.

Appendix B: Supplementary materials for selenium isotope fractionation in groundwater: a field study of a 65-year-old selenium plume

Mixing Calculations

Previous investigations at the site included the development of geochemical mixing calculations (GMC) for the source zone, based on the major ion chemistry, TDS, and Se concentrations of the wells in the source zone area (Kennecott Utah Copper 2013). The GMC determined the proportion of Se the vadose zone contributed to the groundwater for wells within the two source zones. The original GMC were used in combination with the 2013 sample Se concentrations and measured Se isotope ratios to determine whether the isotope ratios in and downgradient of the groundwater wells within the source zones could result from mixing of waters with different isotopic signatures, as opposed to fractionating processes. The following relationship was used (modified from (Schilling et al. 2015)):

$$\delta^{82}Se_{mix} = \frac{\sum_{i=1}^{n} \delta^{82}Se_i \times M_i}{\sum_{i-1}^{n} M_i}$$

Eq. B1

Where δ^{82}Se is the isotope ratio expressed in delta notation, and M is the mass contribution from each component i in the mixture, up to component n, calculated by:

$$M_i = C_i F_i$$

Eq. B2

Where C is the concentration of the component, and F is the fraction of that component in the mixture.

Mass-balance Modeling of Isotopic Fractionation

Decreasing Se concentrations could be due to processes with known effective fractionation (ε) values. In order to conduct mass–balance calculations, the expected decrease in concentration with distance from the source zones was first determined using linear regression. The expected δ^{82}Se for a given concentration decrease can be determined using the following equation:

$$\delta_{calc} = \left((\delta_0 + 1000) \left(\frac{C_{calc}}{C_0} \right)^{\left(\frac{-\varepsilon}{1000} \right)} \right) - 1000 \qquad \text{Eq. B3}$$

Where δ_0 and C_0 are the $\delta^{82}Se$ value and concentration of the source, δ_{calc} and C_{calc} are the expected concentration and calculated $\delta^{82}Se$ value for a given distance along the flow path and ε is the effective fractionation. Note that in this case, a positive ε value indicates that the product is enriched in the lighter isotope, relative to the reactant (Shrimpton et al. 2015), hence a negative sign is required to result in positive fractionation in the calculations.

These calculations assume that the decrease in concentration is due to a single process. Many processes could simultaneously affect the $\delta^{82}Se$ value of downgradient wells, including mixing between multiple sources of Se; especially if the $\delta^{82}Se$ values of Se from the former EP pond area, the former PM building footprint, and background Se are all different. Multiple possible upgradient groundwater wells within the source zone were tested as model origins based on the fit of the linear regression of distance versus concentration, and the fit of the modeled $\delta^{86}Se$ values to the data. Doing so helped account for mixing between sources and removal processes within the source zone. The final model uses the wells that best described the breadth of the isotope ratios within the plume.

Isotope Mass-Balance Modeling Results and Discussion

There was insufficient isotopic data available to model the contribution of pore water in the vadose zone to the groundwater composition at the wells located in the source zone using isotopes, so these calculations were not attempted. The PM-A and PM-B samples were collected one year after the samples for isotopic analysis, and no samples for isotopes were collected from the former EP pond vadose zone or the well used to determine the 'background' Se concentrations. Hence, isotopic mixing calculations were performed using the groundwater isotope samples in the source zones, and nearby low-concentration background wells.

The water in the Se plume at the time of sampling is likely derived from temporally variable contributions within the source area, including the deep vadose zones of the former PM building

and the former EP Pond areas. As a consequence, the concentration and isotopic signature of Se in the source area groundwater is a highly variable mix of Se derived from these sources.

Dispersive dilution, adsorption, and possibly a small amount of reduction can account for isotopic changes between wells 708 and 2813B ($\varepsilon = 0.6‰$ if no dispersive dilution has occurred between both wells). Wells slightly downgradient from the source areas represent the entire plume more accurately than wells directly associated with the former EP pond and PM building areas. Of the near-source groundwater wells, well 2547 was selected to represent a lower Se concentration (4.821mg L^{-1}), higher $\delta^{82}Se$ value (2.0 ± 0.3 ‰) associated with the source area, whereas well 723 was selected to represent a much higher Se concentration (9.459 mg L^{-1}), but lower initial $\delta^{82}Se$ value (1.3 ± 0.3 ‰). Linear regression was used to determine the appropriateness of these source terms for calculations. An R^2 value of 0.898 was obtained when well 2547 was used as the source, whereas well 723 yielded an R^2 value of 0.880.

Some wells downgradient exhibit similar $\delta^{82}Se$ values to a source well with lower Se concentrations, suggesting that these samples were affected by dispersive dilution, or possibly adsorption onto clay minerals (Xu et al. 2021). Isotopic mixing calculations were used to assess the potential impacts of the release of Se previously retained on the solid material, through reduction or adsorption, on the $\delta^{82}Se$ value when re-mobilized. Oxidation was not known to cause significant fractionation (Johnson 2012), but Se that had previously been reduced and precipitated in a reduced form would be relatively enriched in the lighter isotopes, provided subsequent re-adsorption of Se(IV) does not occur (Wasserman et al. 2021). The lower dashed line (Figure B1) indicates that low $\delta^{82}Se$ values are often paired with low concentrations, and do not significantly decrease the $\delta^{82}Se$ value unless Se concentrations are already low. The isotope mass-balance model describes the maximum Se concentration associated with a $\delta^{82}Se$ value created by a single process. Thus, locations with lower Se concentrations than expected for a given range of $\delta^{82}Se$ values can be used to identify a combination of the processes (e.g., adsorption and dispersive dilution).
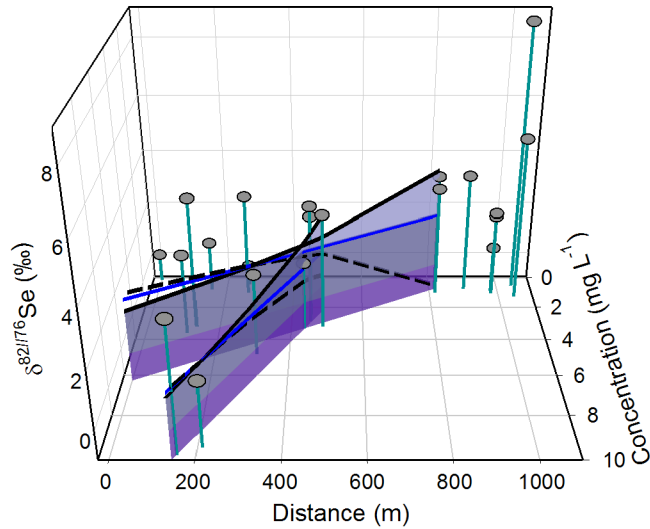
Figure B1: Positive δ⁸²Se values plotted versus distance and concentration along the flow path, fit with two models for expected changes to the delta value for a particular process. The upper black line represents expected change due to adsorption, the middle blue line is the change due to dilution from dispersive mixing, the lower dashed black line is the change in δ^{82}Se value due to mixing with waters characterized by low concentrations of Se with an isotopically light δ^{82}Se signatures that may have oxidized or desorbed from the solid phase.

The concentrations from the lysimeter samples exceed concentrations that are consistent with the source term assumed in the mixing model (PM-B is 9 times greater than the highest groundwater concentration), which suggests significant dilution of Se occurred when it percolated from the vadose to the groundwater. Although the area around PM-B could contribute Se to the underlying area without undergoing any significant reactions, the δ^{82}Se value of PM-A is much higher than any source area sample, suggesting reduction occurred in the vadose zone at this location.

The wells in the source zone show a large variation in δ^{82}Se values and Se concentrations which are difficult to account for by a single process, suggesting a combination of processes affected Se concentrations and δ^{82}Se ratios in this area. Trends in the Se concentrations and δ^{82}Se values in samples from wells within the plume can be accounted for by combinations of dispersion, adsorption or mixing with water impacted by the oxidation of secondary reduced Se-bearing

phases. Samples from the vicinity of the wetland at the end of the flow path contain low Se concentrations coupled with high δ^{82}Se values. The change in δ^{82}Se observed in these samples is beyond the maximum degree of fractionation that could be caused by adsorption. Reduction is the only process known to result in this magnitude of isotopic fractionation (Johnson 2012).

Well nests with Se(IV) present are more likely to have lower δ^{82}Se values (e.g. well nest 2569A/B/C). Additionally, water samples from the wells at the fringes of the plume tend to have low total Se concentrations and lower δ^{82}Se ratio values compared to water samples from the source area, where Se concentrations are much higher.